Interaction Forces, Deformation and Nano - Rheology of Emulsion Droplets as Determined by Colloid Probe AFM

Graeme Gillies BSc. (Hons)

Ian Wark Research Institute

University of South Australia

Submitted for the degree of Doctor of Philosophy

June 2003

UNIVERSITY OF
SOUTH AUSTRALIA
28 JAN 2005
jwr LIBRARY

Table of Contents

Table of Contents ii
Table of Figures iii
Tables iv
Abstract v
Acknowledgements vii
1. Introduction 1
2. Underlying Principles and Literature Critique 3
2.1 Surface Forces Pertaining to Colloids In Electrolyte Solution 3
2.1.1 The Electrical Double Layer and the Force Arising from Two Overlapping Double Layers 3
2.1.2 The van der Waals Force 4
2.1.3 The Hydrophobic Force 6
2.1.4 Forces arising from Adsorbing (and Non Adsorbing) Species 6
2.1.5 Hydrodynamic Force 9
2.1.6 Hydration Force 9
2.2 Deformation of Colloidal Bodies 10
2.2.1 Deformation of Elastic and Viscoelastic Particles 10
2.2.2 Deformation of liquid droplets 13
2.3 Surface Force Measurement Techniques and their Application to Deformable Systems 15
2.3.1 Surface Force Apparatus 15
2.3.2 Thin Film Balance 16
2.3.3 Measurement and Analysis of Surface and Interaction Forces (MASIF) 17
2.3.4 The Johnson Kendall Roberts (JKR) Device 18
2.3.5 Total Internal Reflection Microscopy 18
2.3.6 Atomic Force Microscopy 19
3 Materials and Methods 24
3.1 Materials 24
3.1.1 Reagents 24
3.1.2 Preparation of PDMS emulsions 24
3.2 Experimental Procedures 25
3.2.1 Determination of Bulk Rheology 25
3.2.2 Droplet Sizing by Dynamic Light Scattering 25
3.2.3 Determination of Zeta Potential 25
3.2.4 Determination of the Interfacial Tension and Contact Angle 26
3.2.5 Procedures Relating to Atomic Force Microscopy 26
Chapter 4. Results and Discussion 34
Preamble 34
4.1 Characterisation of PDMS Droplets 36
4.1.1 Rheology of Bulk PDMS Material from Droplets 36
4.1.2 Droplet Size 39
4.1.3 Interfacial Tension and Contact Angle 40
4.1.4 Surface Electrical Properties of PDMS Droplets and the Colloid Probe 41
4.2 Interaction Forces and Deformation of PDMS Droplets 45
4.2.1 Highly Cross-Linked Droplets 45
4.2.2 Liquid Droplets of Newtonian PDMS 54
4.2.3 The Influence of Bulk Rheology, pH and Radius on Droplet Deformation 57

4.2.4 Interactions Forces and Deformation in the Presence of SDS 66
4.2.5 Interaction Forces of Droplets with Adsorbed Nano-Particles 71
5. Conclusions and Perspectives 78
References: 81

Table of Figures

Figure 2.1 7
Figure 2.2 12
Figure 3.1a 31
Figure 3.2a 32
Figure 4.1 34
Figure 4.2 35
Figure 4.3 36
Figure 4.4 39
Figure 4.5 39
Figure 4.6 41
Figure 4.7 43
Figure 4.8 44
Figure 4.9 45
Figure 4.10 47
Figure 4.11 48
Figure 4.12 50
Figure 4.13 51
Figure 4.14 52
Figure 4.15 54
Figure 4.16 56
Figure 4.17 57
Figure 4.18 58
Figure 4.19 59
Figure 4.20 61
Figure 4.21a 62
Figure 4.21b 63
Figure 4.22a 63
Figure 4.22b 64
Figure 4.23 65
Figure 4.24 66
Figure 4.25 67
Figure 4.26 68
Figure 4.27 69
Figure 4.28 70
Figure 4.29 70
Figure 4.30 71
Figure 4.31 72
Figure 4.32 73
Figure 4.33 74
Figure 4.34 75
Figure 4.35 75
Figure 4.36 77

Figure 4.37 77

Tables

Table 3.1 32
Table 4.1 35
Table 4.2 40
Table 4.3 59
Table 4.4 67
Table 4.5 73

Abstract

Atomic force microscopy (AFM) has been used to determine the interaction forces between a spherical silica probe and immobilised colloidal droplets of polydimethylsiloxane (PDMS) in aqueous solution. Between pH 4.5 and 9.5 where PDMS droplets and the silica probe are both negatively charged, a repulsive force is evident that increases less rapidly on surface approach than expected for electrical double layer interaction of rigid particles. The departure from hard-sphere behaviour, i.e. the deformation, has been determined and by varying the extent of internal cross-linking within the PDMS droplets, the influence of bulk rheology and interfacial properties on droplet deformation and nano-rheology has been isolated.

For highly cross-linked droplets, the extent of deformation is controlled by the bulk rheology rather than the droplet's interfacial properties. Upon retraction of the surfaces, force curve hysteresis is observed and is due to the viscoelastic response of the PDMS. The extent of hysteresis is dependent on the rate of approach/retraction and the loading force, and has been theoretically fitted to obtain nano-rheological parameters, which describe the droplet relaxation processes.

For liquid-like droplets, with a low level of cross-linking, no force curve hysteresis is observed and the elastic deformation may be described by a single spring constant. The spring constant is proportional to the surface tension (as controlled by surfactant adsorption) and the reciprocal of the droplet radius, i.e. deformation is controlled by the Laplace pressure. Furthermore, droplet deformation is altered by the presence of adsorbed nano-particles.

These colloid probe AFM studies offer due insight into the deformation and interaction of emulsion droplets and have implications when considering the stability, adhesion and processing of emulsions.

I declare that this thesis does not incorporate without acknowledgement any material previously submitted for a degree or diploma in any university and that to the best of my knowledge it does not contain any materials previously published or written by another person except where due reference is made in the text.

Graeme Gillies

Acknowledgements

Over the past three and a half years I have been fortunate to receive assistance, comments, and insights from many fellow scientists. All of the following people have in some way contributed to the production of this thesis.

First, I would to acknowledge Professors John Ralston and Roger Horn. Both these people have often provided intelligent comments and useful insights by means of the occasional discussions near the Photocopier and/or in the IWRI kitchen. The value of such coincidental conversations are often undervalued by many. Furthermore, I'd like to thank Dr. Jason Connor for his knowledgeable insights and giving me access to his very useful library of papers.

I'd also like to thank the following PhD students: Jingwu Yang for helping me with my sometimes-lacking mathematics. Spomenka Simovic for continual explanations about the adsorption of nano-particles. Tim Barnes for discussions helpful to characterisation and synthesis of PDMS droplets. Nate Stevens for his assistance in determining interfacial tension values as well as contact angles of PDMS samples.

I am also indebted to Dr. Ian Larson for teaching me how to use the AFM and prepping me for the anguish it was going to cause me. Further to this, I'd like to thank Dr Kristen Bremmell, as it seems I spent at least one day a week in her office with complaints of AFM related software and hardware problems, all of which were resolved with time.

I'm deeply grateful for the time I was able to spend with Assoc. Prof. Phil Attard. Phil supplied me with the programs that allowed me to determine nano-rheological parameters. Phil also provided some fundamental and crucial insights relating to the AFM, surface forces and deformation for which I am most grateful.

Finally I'd like to thank my primary supervisor Dr Clive Prestidge. Over the last three and a half years Clive has constantly inspired professionalism and encouraged me to achieve a quality of work that was better than 'just good enough', unlike many answers to scientific questions, such advice is invaluable and not found within the literature. I am also fortunate to have received most of Clive's time over the last few months for which I am most grateful.

The research conducted in this thesis was entirely funded by the Australian Research Council through the Ian Wark Research Institute's Special Research Centre for Particle and Material Interfaces.

1. Introduction

An understanding of emulsion droplet interaction is critical when considering emulsion stability and emulsion droplet adhesion. For non-deformable particles the theories for colloid stability are well advanced and the subject of many texts. Furthermore, for particle systems there are extensive reports in the literature of direct force measurements using colloid probe atomic force microscope (AFM); and electrostatic,[1-3] hydration,[2] van der Waals,[4] steric[2,3] and hydrophobic forces,[5] as well as forces introduced due to both adsorbing and non-adsorbing polymer molecules,[6,7] have been quantitatively determined. For emulsion droplets, where deformation complicates the interaction behaviour, i.e. when in close proximity, droplets may deform as result of interaction forces; the theories to describe droplet interaction and stability are less well developed. Additionally, droplet deformation is not easily measured nor described trivially. With respect to coalescence of deformable droplets, Danov et al[8] have suggested that droplets flatten on approach and a film is formed between them, the thickness of this film then decreases before it ruptures and the two droplets coalesce. Where the two droplets are sufficiently large, hydrodynamic forces result in the formation of a dimple that flattens prior to film thinning. Clearly, the rate at which this process occurs and thus the stability of the emulsion will depend on how easily the droplet is deformed.

The colloid probe AFM technique, originally developed for hard particles,[1,9] has recently been applied to bubbles[10-12] and soft polymer microspheres,[13] and is proving to be a valuable tool in characterising droplet deformation.[14-19] For large liquid drops,[15,16] the level of deformation has been shown to be strongly influenced by interfacial effects and no evidence of hydrodynamic forces was observed for the size of probe investigated and at the range of drive velocities at which the loading and unloading cycles were undertaken. Interaction studies on droplets are still in their infancy and further work is required prior to the development of a fully quantitative description of the interplay between emulsion droplet deformation and interaction.

This thesis is a study of the deformation of colloidal silicone [polydimethylsiloxane (PDMS)] droplets in aqueous solution using colloid probe AFM, motivated from the observation that emulsions of deformable droplets are more stable than emulsions of non – deformable droplets.[20] A particular feature of this model droplet system is that

the degree of internal cross-linking within the PDMS droplets may be altered and therefore deformability may be systematically controlled.[20] Therefore, investigations may be performed on a range of equivalent droplets with various internal rheological properties, i.e. from Newtonian fluids to viscoelastic semi-solids. Where droplets are "liquid-like", deformation is described by a spring constant, and we pay particular attention to interfacial effects and droplet size. For the viscoelastic droplets, we pay particular attention to the time-dependent behaviour, i.e. dynamic deformation effects, and analyse the deformation using a relatively sophisticated viscoelastic theory.[21,22]

2. Underlying Principles and Literature Critique

In this chapter the underlying principles relevant to this thesis are discussed. Current literature relevant to the deformation of colloidal bodies is examined and discussed in depth, whilst instrumentation and surface forces are only discussed briefly as such information can be found in a number of texts[23-25] and review articles.[26-28]

2.1 Surface Forces Pertaining to Colloids In Electrolyte Solution

2.1.1 The Electrical Double Layer and the Force Arising from Two Overlapping Double Layers

When a body is immersed in an electrolyte solution, the adsorption or desorption of ions will generally take place at the interface resulting in a surface charge or potential. This surface charge causes the attraction of oppositely charged ions and repulsion of like-charged ions. Ions from the electrolyte solution distribute themselves in proximity of the charged surface according to the Boltzmann equation and form a diffuse layer. This diffuse layer, comprising of mainly oppositely charged ions, and the charged interface are collectively known as the electrical double layer.

In a two phase dispersion, dispersed particles, (or similarly, liquid droplets and gas bubbles), will acquire the same charge and therefore repel one another. The force associated with the overlap of two electrical double layers is derived from combining Poisson's equation relating charge density and electric potential with Boltzmann's equation describing the distribution of ions around each surface. The result is a partial differential equation that must be solved analytically. To date, numerous authors have published algorithms to do this, for example Chan and co-workers give solutions for symmetric and asymmetric interactions in references 29 and 30 respectively. In general, these calculations impose boundary conditions, assuming each surface will maintain a constant charge or potential. Whilst both conditions result in agreement at relatively large separations, the constant charge analysis results in larger forces than the constant potential analysis at close separations. The constant potential analysis assumes the potential of surfaces remains constant whilst the surface charge density varies with separation, a classic example of a constant potential system is a dispersion of AgI particles, where I^- ions dissociate on close approach resulting in a smaller

surface charge. Similarly the constant charge condition assumes no net change in surface charge density with the potential varying, a typical of constant charge system is an oil water interface. However, if $|e\psi_0| << k_BT$ i.e. $|\psi_0| \leq 25$ mV, then a simplified solution exists[24], where e is the charge of an electron, ψ_0 is the surface potential, k_B is Boltzmann's constant, and T is the absolute temperature. This solution is referred to as the linear Poisson – Boltzmann equation (the above analysis is refereed to as non-linear) and can be further extended[31] to account for larger (and asymmetric) potentials giving the renormalised linear Poisson – Boltzmann equation:

$$F = 32\pi\varepsilon_0\varepsilon_r R\left(\frac{k_BT}{ze}\right)^2 \gamma_1\gamma_2\kappa e^{-\kappa h} \qquad 2.1$$

Here, F is the force between two spheres of radius R, ε_0 is the permittivity of free space, ε_r is the relative dielectric constant of the aqueous medium, z is valency of the ions, of the electrolyte solution, and h is the separation. The renormalised potential, γ, and the reciprocal Debye length κ, are defined as follows:

$$\gamma = \tanh(ze\psi_0/4k_BT) \qquad 2.2$$

$$\kappa = \sqrt{2n_0e^2/\varepsilon_0\varepsilon_r k_BT} \qquad 2.3$$

where n_0 is the volume concentration of the salt.

The renormalised linear Poisson – Boltzmann equation is a good approximation of the full non-linear Poisson – Boltzmann equation for separations greater than a Debye length, however, within this distance equation 2.1 may be less accurate. There currently exist numerous approximations for the interaction of two overlapping double layers, (e.g. Gregory[32] and Hogg et al[33]) each derived for greater accuracy under specific conditions.

2.1.2 The van der Waals Force

The van der Waals force between two like bodies in an aqueous continuous phase is an attractive short ranged force. Generally the term van der Waals force refers to London interactions, but can also refer to Keesom and Debye interactions.[23] London

interactions arise from an oscillating or rotating dipole inducing similar oscillating or rotating dipoles in surrounding atoms in such a way that they are attracted to the first one. Keesom and Debye interactions are similar to London interactions but arise from the orientation of permanent dipoles, and permanent dipoles inducing dipoles in polarisable atoms respectively. Clearly, if there are no permanent dipoles within a system then the associated van der Waals forces can only refer to London interactions.

A method for calculating van der Waals forces was first proposed by Hamaker[34] in 1937. The 'microscopic approach' suggested that the van der Waals force between two bodies can be calculated by integrating the interaction between an atom from each body for over the shape of each body. This approach incorrectly assumes that the interactions between atoms can be directly added, when it is more likely that the interaction between two atoms is likely to be changed in the presence of third. Lifshitz[35] theory (also called the macroscopic theory) overcomes this problem by assuming the dipole fluctuations are correlated. In doing so, each body can be treated as a continuous medium. This approach calculates the Hamaker constant differently but results in the same expression describing interactions.

For two interacting spheres of radius R the van der Waals force (F_{vdW}) between two spheres of radius R is given by equation 2.4

$$F_{vdW} = -\frac{A_h R}{12h^2} \qquad 2.4$$

Where A_h is the Hamaker constant and h is the separation between the two spheres. The Hamaker constant characterises the resonance interactions between electronic orbitals in two particles and the intervening medium. In terms of colloidal dispersions, in electrolyte solution, colloids experience weaker attractions when the dielectric properties of the colloid are similar to that of the solution.[24] For the asymmetric PDMS – water – borosilica interactions studied within this thesis, an approximate Hamaker constant of 1.27 10^{-20} J can be calculated from the respective refractive indices, dielectric permittivities and mean ionisation frequencies, given in reference 25.

2.1.3 The Hydrophobic Force

The hydrophobic force is an attractive force between two hydrophobic surfaces in water. Evidence for hydrophobic interaction has existed for decades, for example Blake and Kitchener[36] report the collapse aqueous films between hydrophobic silica and an air bubble at separations of 65nm. However, the hydrophobic force wasn't quantified until 1984,[37] in this initial work Israelachvili and Pashley determined forces between two mica surfaces in aqueous solution prior to and subsequent to the adsorption of CTAB ($CH_3(CH_2)_{15}N(CH_3)_3^+Br^-$). The adsorption of CTAB resulted in an attractive force with a range of 10nm well described by an exponential force law. Israelachvili and Pashley suggested the origin of this force was a result of a deficiency of hydrogen bonding near the surfaces compared with bulk water. Such behaviour is now referred to as the 'short ranged' hydrophobic force. Whilst solvent structure mechanisms[37,38] may well describe short ranged attractions, it is not clear how such an effect could extend to ranges up to 300nm as reported by Carambassis et al.[5] Other mechanisms used to describe the 'long range' hydrophobic force include unusual electrostatic mechanisms[39,40] and cavitation or nano-bubbles[41]. The conceptual basis for long ranged electrostatic mechanisms resulting from patches of charge or diapoles[40] arise from observations that the hydrophobic force has dependency on the concentration of electrolyte. Also Podgornik[39] suggests that specific ion adsorption would lead to a large correlation force due to the lateral mobility the adsorbed ions. The primary shortcoming of these above theories is that there is no exact dependence on the concentration of salt and that the presence of salt may only be reducing the hydrophobicity of the surfaces.

Parker[41] et al attributed the long range attraction due to the bridging of submicroscopic cavities or bubbles between surfaces. This theory accounts for the random nature of hydrophobic force[41] and the dependence on dissolved gas.[42,43] Whilst thermodynamic calculations would suggest these bubbles are unstable, recently published images of small bubbles[44,45] favour this last theory.

2.1.4 Forces arising from Adsorbing (and Non Adsorbing) Species

The presence of adsorbed species such as polymers or nano-particles may result in one of several distinct behaviours including steric repulsion, bridging flocculation, depletion flocculation or depletion stabilisation. Steric repulsion occurs when solid

particles or a compact polymer layer adsorbs to a surface creating a layer that physically prevents surfaces from coming into close contact. However if the physical properties of the adsorbed layer are similar to that of the dispersed phase then the dispersed particles (or droplets) will act as larger particles. The adsorption of solid particles may rigidify an oil/water interface,[46-48] preventing droplet deformation, however this is an indirect effect and not a surface force. In general, the adsorption of polymer does not usually result in an adsorbed layer that is sufficiently dense to form a hard layer at the interface. It is more likely that polymers will adsorb at the surface and extend out into the continuous phase creating adsorbed trains, loops, and tail conformations, see Figure 2.1. In order for another colloidal body to approach this

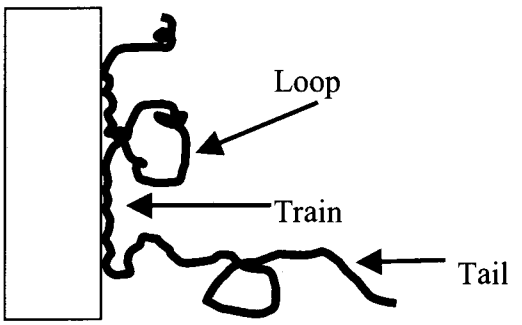


Figure 2.1 Schematic outlining the configuration of one adsorbed polymer.

polymer-coated surface, the polymer layer must compress. The force associated with this compression has been studied by many, specifically De Gennes[49] gives equation 2.5 for the compression of 'brush like' polymer layer with a high surface coverage.

$$f \approx k_b T \Gamma^{3/2} \left[\left(\frac{2L_0}{h} \right)^{9/4} - \left(\frac{h}{2L_0} \right)^{3/4} \right] \qquad 2.5$$

where f is the force per unit area, Γ is the adsorption density and L_0 is the equilibrium thickness of the polymer brush.

In the case where high molecular weight polymers are adsorbed at only partial coverages, attraction has been observed.[50] This attraction is referred to as bridging flocculation where polymer molecules adsorb onto both surfaces causing them to be drawn together.

Non-adsorbed polymers may also influence colloid stability through depletion flocculation or depletion stabilisation. For low concentrations of a non-adsorbing polymer with a radius of gyration much smaller than that of the dispersed particles depletion interactions are generally described using the model of Asakura and Oosawa.[51] When two particles approach to within separations smaller than twice the radius of gyration of the non-adsorbing polymer the region between particles will be 'depleted' of polymer molecules. This results in an imbalance of osmotic pressure, which consequently drives solution from this region creating an effective attraction between the particles.

Alternatively the approach of two particles within separations smaller than twice the radius of gyration will be unfavourable if polymers are highly soluble, and concentrated in solution. This depletion stabilisation arises from large amounts of free energy required to exclude polymers from this region between particles. Furthermore oscillatory effects that decay with separation have been reported for these systems correspond to the layering of the dispersed polymers molecules around surfaces. Theoeretical[52] and experimental[53] studies have shown the force law (equation 2.6) given by Asakura and Oosawa[51] to be valid for low micellar concentrations of polymers but invalid at greater concentrations. It follows that the exact nature of depletion interactions will depend on the chemical nature of the polymer, the solvent and the surfaces as well as the molecular weight of the polymer, temperature and polymer concentration. For instance depletion interactions were subject of a recent colloid probe AFM investigation,[54,55] in which the transition from repulsive to attractive interactions with varying polymer concentration and molecular weight.

$$F = \pi\Pi\left(\left(\frac{R+r}{2}\right)^2 - \left(\frac{h+r}{2}\right)^2\right) \qquad 2.6$$

where $h < R$.

Here Π is the osmotic pressure of the polymer solution, R is the radius of curvature of interacting surfaces not to be confused with r, the radius of gyration of the polymer

molecules. Note that $\Pi = \rho k_B T$ where ρ is the bulk density of dispersed polymer molecules (which are assumed to act as hard spheres).

2.1.5 Hydrodynamic Force

The hydrodynamic force is not actually a surface force, rather a dynamic effect observed when two surfaces (in liquid) are brought together. That is, the liquid separating these surfaces must either be displaced (drained) or compressed. Thus there exists a force opposing the approach of two surfaces associated with the drainage of water. Surface Force Apparatus (SFA) studies[56] and later, AFM studies[57] have confirmed equation 2.7 approximating the hydrodynamic force (F_H).

$$F_H = 6\pi\eta b U \frac{b}{a} \qquad 2.7$$

where η is the viscosity of the continuous phase, b is the radius of curvature of the surface approaching a wall at a velocity of U and a is the surface separation between surfaces.

2.1.6 Hydration Force

Hydrophilic surfaces in electrolyte solution are known to be surrounded by a layer of structured water. Thus there exists a short ranged repulsive force between hydrophilic surfaces associated with dehydrating these surfaces. Hydration forces have been observed between mica[58] and silica[59] surfaces and are known to depend on both how well surfaces and adsorbed counter ions hydrate.[60] Intuitively hydration forces are repulsive, however, the hydration force is not always monotonic, i.e. Pashley and Israelachivili[58] observed oscillatory behaviour between two mica sheets where the periodicity of oscillations was found to be similar to the diameter of a water molecule (~0.25 nm).

Often discussed in connection with the hydration force is the protrusion force, which exists between amphiphilic surfaces such as soap films and lipid bilayers. These forces typically decay exponentially over a range of 1 - 2 nm and are akin to steric forces between polymer covered interfaces already discussed.

2.2 Deformation of Colloidal Bodies

2.2.1 Deformation of Elastic and Viscoelastic Particles

Traditionally the deformation of elastic particles (both macroscopic and microscopic) has been described by the Hertz and Johnson, Kendall and Roberts (JKR)[61] theories (see references 28 and 61 for a detailed description of Hertz theory). Hertz theory considers two perfectly elastic spheres with no mutual attraction forced into contact. This approach assumes a zero contact area when the applied load is zero and thus no adhesion. JKR theory extends Hertz theory to include the effects of adhesion, attributing the observed, finite contact area, under zero load, to the minimisation of surface free energy of each sphere. It was established by Tabor[62] that JKR theory is appropriate for investigations of soft materials such as elastomers particles whilst a variant theory,[63] by Derjaguin, Muller and Toporov (DMT), is more applicable to harder materials such as glass. In general Hertz theory is used to predict the contact area as a function of the applied load[64,65] whilst JKR theory is used to relate the adhesion (of both elastic[66-76]and viscoelastic particles[72]) to the surface energy.

These approaches assume that particles only interact when in contact and ignore the extended range of the interactions that may occur. For example, deformation of rubber and polymethylmethacrylate has been reported to occur prior to contact due to van der Waals[77] and electrical double layer[65] forces, respectively. Beyond Hertz and JKR contact theories are the soft contact approaches, which take into account these extended interactions. In a similar manner to Hertz and JKR theories, the soft contact approaches[78-83] are based on linear elasticity. However, the contact theories assume particular analytic expressions for the pressure profile, namely those necessary to give a flat contact region. In contrast soft contact theories calculate the pressure profile, local separation and deformation, self-consistently using a prescribed force law.

In soft contact theory the pressure profile $p(s)$ is related to the given formulae for the pressure between flat surfaces $p_\infty(h)$ separated by h:

$$p(s) = p_\infty(h(s)) \qquad 2.8$$

The local separation between the surfaces at a distance s from the axis of symmetry is given by:

$$h(s) = h_0(s) - U(s) \qquad 2.9$$

Where $h_0(s)$ is the local separation between the undeformed surfaces and U(s) is the local deformation. For two elastic bodies the local deformation is given by equation 2.10.[22] The complexity of equation 2.10 is a result of the deformation at any one point being dependent on the entire interaction profile. That is when a point force is applied to an elastic solid the resultant deformation will decay away from the point of contact, with the amount of deformation inversely proportional to the distance away from this point.[82] Thus the deformation at a point s must be calculated by summing the entire pressure profile. In equation 2.10 it is essential here to define the pressure profile with p(r) as opposed to p(s) because in this instance s relates to a specific point within the profile where as r relates to any point within the entire pressure profile.

$$U(s) = \frac{-2}{\pi E} \int d\mathbf{r} \frac{p(r)}{|\mathbf{s} - \mathbf{r}|} \qquad 2.10$$

Here the elasticity parameter (E) is related to the Young's modulus (E_Y) and Poisson's ratio (ν) of each material by $2/E = (1-\nu_1^2)/E_{Y1} + (1-\nu_2^2)/E_{Y2}$.

These expressions assume that the two interacting particles are cylindrically symmetric. Theoretical force plots for a given trajectory can be calculated by solving equations 2.10 - 2.12 by iteration to self-consistency.

Of particular interest, is Attard's treatment of viscoelastic deformation by soft contact.[21,22] The approach considers simple viscoelastic materials with two elastic limits; these represent short term, E_0, and long term, E_∞, elastic behaviour as well as a characteristic relaxation time, τ.

$$\frac{1}{E(t)} = \frac{1}{E_\infty} + \frac{E_\infty - E_0}{E_0 E_\infty} e^{-t/\tau} \qquad 2.11$$

where t is the interaction time and E(t) is the effective viscoelastic parameter (its reciprocal is often called the creep compliance function). From equation 2.11 it follows that at relatively fast interactions i.e. $t<<\tau$, $E(t) \longrightarrow E_0$; whereas for relatively slow interactions where $t>>\tau$, $E(t) \longrightarrow E_\infty$ as demonstrated in Figure 2.2. This approach shows a reasonable comparison with behaviour to the Kelvin - Voigt model, a mechanical analogue that describes viscoelastic solids with a spring and a dashpot in parallel. In the Kelvin - Voigt model the spring element relates to the elastic component and is assumed to respond instantaneously and reversibly to applied loads and deformations. The dashpot element describes the viscous component, in which the stress is assumed to be proportional to the strain rate, not the strain. It follows that, at relatively slow interactions the dashpot resistance is small, and the overall behaviour is characterised by the spring constant. At relatively fast interactions the dashpot response is dominant and the viscosity governs the amount of deformation. Thus it follows that E_∞ relates to the spring constant, i.e. the elastic modulus, and is equal to E (defined on the previous page) in experiments where no time dependence is assumed and E_0 relates to the additional rigidity from the viscous contribution at fast interactions. If E_0:E_∞ is small then the contribution of the viscous modulus is small, whereas when E_0:E_∞ is large then the viscous contribution is large. Comparing E_0:E_∞ is akin to the relaxation time in a Kelvin-Voigt body where the relaxation time is controlled by the relative value of the viscous and elastic moduli. It is also worth

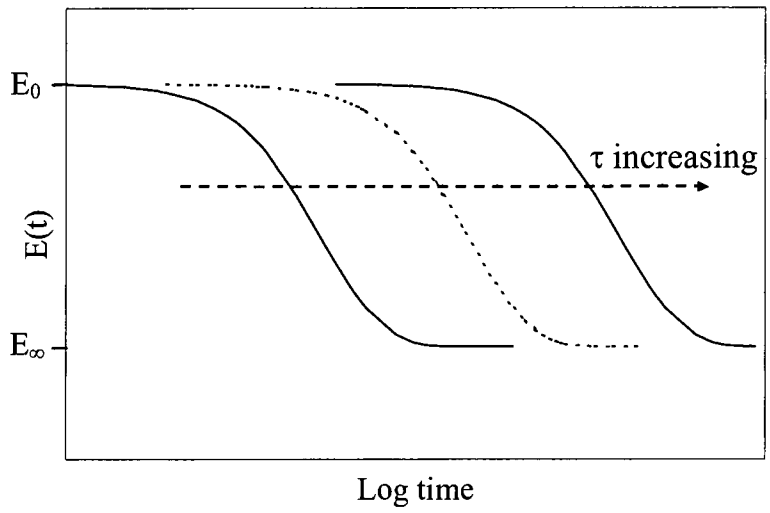


Figure 2.2 Schematic representation of the effective viscoelastic parameter for viscoelastic deformation, i.e. E(t) as a function of t for differing relaxation times, τ.

noting that in both models the rate at which the behaviour decays to the long term behaviour is given by $e^{-t/\tau}$ where τ is the relaxation time in both models. This would suggest that the relaxation times in both models are approximately equivalent. The essential difference between the Kelvin Voigt model and that of Attards is that for infinitely fast interaction the Kelvin-Voigt body doesn't deform, as the dashpot has not had time to respond, whereas Attard's model predicts a finite amount of deformation. In practice infinitely fast interaction times are not possible and such differences are of little concern.

The incorporation of equation 2.11 into equation 2.10 leads to

$$U(r,t)-U(r,t_0)=\int_{t_0}^{t} dt' \frac{-2}{\pi E(t-t')} \int d\mathbf{s} \frac{\dot{p}_{\infty}(h(s,t'))}{|\mathbf{r}-\mathbf{s}|} \qquad 2.12$$

Here $\dot{p}_{\infty}(h(r,t))=p'_{\infty}(h(r,t))\dot{h}(r,t)$ is the time rate of change of the pressure, and $\dot{h}(r,t)$ is the time rate of change of the local separation.

This approach is not unlike the time dependence introduced into JKR theory, which was shown by Tirrell[72] to give reasonable surface energies when investigating the adhesion of viscoelastic PDMS 'caps'.

2.2.2 Deformation of liquid droplets

Theoretical treatments relating to the deformation of liquid droplets (and bubbles) are somewhat more complex than those based on elasticity. Furthermore, experimental studies of droplet deformation are still in their infancy, with the observed results specific to the chosen methodology. That is, investigations using surface force apparatus (SFA) report an equilibrium film thickness[84-87] and considerable hydrodynamic forces,[85,86] whereas investigations involving the colloid probe AFM technique generally report no hydrodynamic effects[16] and express deformability in terms of a spring constant.[10-12,15,17] To date, all soft contact analyses calculate droplet profiles by incorporating the effects of gravity and a disjoining pressure into the Young-Laplace equation. A common finding in SFA related analyses[88,89] is the presence of a thin film preventing droplets from approaching beyond a critical separation. This critical, or equilibrium, separation is dependent on the magnitude of

surface forces and internal pressure of the droplet. Furthermore, theoretical predictions suggest that this minimum separation will be smaller in colloid probe experiments where larger internal droplet pressures are achieved due to smaller radii.[88]

In colloid probe AFM studies, droplet deformation is usually expressed in terms of a spring constant relating to a linear region in the determined force-separation relationhsip. In general these analyses report the spring constant of droplets to be strongly dependent on the interfacial tension,[18,19,90-92] radius[90-92] and the contact angle the droplet forms with the AFM stage.[90-93] However, these studies all focus on relatively large macroscopic droplets with radii much greater than that of the probe with little attention having been given to smaller colloidal sized droplets. This is considered to be due to the lack of suitable experimental systems and experimental difficulties. Of particular interest is a series of investigations reported by Attard and Miklavic,[90-92] specific attention is paid to these studies as the authors derive, from the augmented Young – Laplace equation, a simple easily treatable analysis for a colloid probe approaching a large droplet where interactions are dominated by the electrical double layer. Relatively weak interactions can be solved using the equations 2.13 to 2.15.

$$h - h_0 = \frac{F}{k_{cant}} \qquad 2.13$$

$$F = 64\pi\varepsilon_0\varepsilon_r \frac{R_p R_w}{R_w - R_p}\left(\frac{k_B T}{ze}\right)^2 \gamma_1\gamma_2\kappa e^{-\kappa h} \qquad 2.14$$

where

$$R_w = R_o \frac{F\kappa R_p + 4\pi\gamma R_p}{F\kappa R_o - 4\pi\gamma R_p} \qquad 2.15$$

where F is the determined force between the colloid probe with radius R_p and the droplet with radius R_o.

Denkov and co-workers[8,94] also examine droplet deformation using the augmented Young-Laplace equation. However, these investigations do not consider the

applicability to force measurement techniques, but rather discuss the role of deformation on emulsion stability. These studies report deformation in terms of droplet flattening or film flattening between two attractive, colliding droplets. For weak attractions droplets were reported to act as undeformed spheres, whereas when attractive forces were larger, or the interfacial tension was smaller, an equilibrium plane parallel film is formed, separating droplets, corresponding to a minimum in free energy.

2.3 Surface Force Measurement Techniques and their Application to Deformable Systems

Throughout the force measurement literature, the Derjaguin approximation[95] is used to compare interactions between colloidal bodies of different shape and size. The Derjaguin approximation relates the force F and the interaction energy V between two spherical particles of radius R at separation d to the energy of flat plates per unit area V^A as follows:

$$F(d) = -\frac{dV}{dd} = \pi R V^A(d) \qquad 2.16$$

The Derjaguin approximation is valid where the range of interaction forces is much smaller than the radius of curvature and can be further extended[96] to give the interaction between a sphere and a flat plate ($F(d) = 2\pi R V^A(d)$) or two dissimilar spheres of radius R_1 and R_2 respectively

$$F(d) = \pi \frac{2R_1R_2}{R_1 + R_2} V^A(d) \qquad 2.17$$

2.3.1 Surface Force Apparatus

The surface force apparatus (SFA) was developed by Isrealchvili and Adams[97] in the late 70's based on an earlier apparatus developed by Tabor and Winterton.[98] Substrate surfaces (generally mica or coated mica) are mounted onto two crossed cylinders, which is geometrically equivalent to a sphere - flat plate interaction. One of these cylinders is mounted on a cantilever, whilst the other cylinder can be displaced via a piezoelectric translator or stepper motor. The force acting between the two surfaces is determined from the cantilever's deflection using Hooke's law. Cantilever deflection

is ascertained by subtracting the separation of surfaces, determined by white light interferometry, from the applied displacement in the absence of surface forces. Whilst the use of interferometry gives a greater resolution than the atomic force microscope, at least one surface must be semitransparent, thus restricting the choice of sample substrates.

SFA studies have resolved electrical double layer forces,[97] hydrophobic,[37] hydrodynamic[56] and hydration[99] forces. The SFA has also proved useful for studies of deformation and adhesion[64,100,101] asserting good comparison with JKR and Hertz theories[64] as well as establishing time-dependent behaviour not adequately accounted for by these theories.[100,101] The SFA investigations most relevant to this thesis are those of Horn and co-workers[84-87] where the SFA was further developed to investigate a mercury droplet approaching a flat surface. This recent application of the SFA is essentially an advancement of earlier interference and ellipsometric investigations of oil – water interfaces approaching a silica surface.[102-104] This new methodology reports good comparisons with theoretical studies where droplet deformation results from electrical double layer and hydrodynamic forces. However the real advantage of this system is in its ability to determine the droplet profile and thus confirm the applicability of the augmented Young-Laplace equation. Interestingly, Horn et al[86] describe the deformation with a spring constant comparable to the interfacial tension; a result reported in several AFM studies (see section 2.3.6).

2.3.2 Thin Film Balance

Another interferometric technique is the Thin Film Balance (TFB). Pioneered by Scheludko and Exerowa[105], it is used to determine the disjoining pressure in liquid film as a function of film thickness. The primary difference between the TFB and the SFA is that in a TFB the liquid film separates two air-water interfaces and thus can only support small pressures. The so-called Scheludko cell consisted of a capillary tube (~3mm) with a small hole in the side to withdraw liquid, adjusting the capillary pressure on the applied film. Current TFBs resemble the designs of Mysels[106] and Exerowa and Scheludko[107] and consist of a porous glass plate welded to a glass capillary. This capillary feeds liquid film (via gravity) across the plate applying a constant pressure at the same time. For foam films, a pressure is applied to the

interfaces by placing the plate – capillary assembly in a cell with a regulated syringe pump. Changing the gas pressure varies the pressure inside the film as well as the interfacial separation. Disjoining pressure is determined from the pressure in the cell, pressure from the capillary and the interfacial tension and curvature of the interfaces.

The TFB has been used to investigate the influence of both non-ionic[108] and ionic[109] ionic surfactants on foal film stability. Notably Bergeron and Radke[109] suggest bilayer-like domains existed near the air water interface for concentrated solutions of anionic surfactant. More recent studies have focused on film drainage[110] and hydrophobic forces.[111] Asymmetric films can also be used to infer emulsion stability, that is where the liquid film separates an air – liquid (water or oil) and an oil – water interface.

2.3.3 Measurement and Analysis of Surface and Interaction Forces (MASIF)

Sometimes referred to as a bimorph surface forces apparatus, the MASIF instrument, developed in 1992,[112,113] was derived from the surface force apparatus. The technique determines interaction forces between millimetre-sized spheres (or their adsorbed layers) one of which is mounted on a bimorph sensor, whilst the other remains stationary. Sample separation is controlled via a piezoelectric translator or stepper motor, and is calculated from the point at which hard-wall contact is first observed. Interaction forces are quantified from the deflection of the bimorph sensor, and / or a force feedback loop.[112] The distinct advantage of the MASIF over the SFA is that samples need not be transparent and thus a wider range of samples can be used. Throughout current literature, the MASIF has been used to determine surface forces including oscillatory forces in oil,[112] hydrophobic interactions,[114-117] electrical double layer interactions,[114,115] van der Waals forces[113,116] as well as adhesion.[114,115] Specifically, Fröberg and Ederth[117] employed the MASIF to show that contamination from the presence of Epikote resin 1004 (used in this study to mount colloid probes to AFM cantilevers) is not sufficient to influence surface forces.

Literature reports of deformation include studies of elastic vibration of elastic lenses.[118] Furthermore, Parker and Stewart[114] account for deformation in calculating

the separation in mica - mica studies and Ederth et al[115] used JKR theory to account for the plastic deformation of gold films on glass spheres in studies of adhesion.

2.3.4 The Johnson Kendall Roberts (JKR) Device

The JKR device describes a number of apparatuses used to study deformation of soft polymers, the label 'JKR device' originates from their original specific design to investigate the JKR theory.[61] In general, a JKR device consists of a micrometer screw used to press an elastomer sphere or hemisphere into a rigid surface. However, an instrument that presses a hard sphere into polymer ribbons has also been reported.[66] Force and position sensors are used to quantify the load and deformation, whilst *in-situ* optical microscopy is used to determine the contact area. Whilst the JKR device cannot be used to determine surface forces, specific interest arises from the numerous investigations on the deformation of PDMS,[66-72] however studies have also examined polyurethane[74,75] and block co-polymers.[76]

2.3.5 Total Internal Reflection Microscopy

The Total Internal Reflection Microscope (TIRM) is contrasting to most other surface force measurement techniques in the sense that surface forces are determined indirectly rather than through a measuring spring or cantilever. Furthermore, TIRM determines the force between a flat surface and a dispersed particle. This gives the TIRM instrument a distinct advantage over the SFA and the MASIF, as interacting surfaces in these instruments are large, millimetres in size, and required to be very smooth. In TIRM, an evanescent wave is formed at a plate/fluid interface using a visible laser beam, and a nearby particle will then scatter this light. The intensity of this scattered light decays exponentially with separation, allowing the particle - plate separations to be determined accurately. By monitoring the scattering intensity for a sufficiently long period of time, a probability distribution of separation distances can be constructed and can then be converted into a potential energy profile using Boltzmann's equation. To date, TIRM has been used to determine interactions between both polystyrene latex[119-121] and biological colloids,[122] and a flat glass plates with various coatings. The gravitation force[121] and depletion forces caused by the exclusion of surfactant micelles[123] have been reported. Prieve[124] and Bevan and Prieve[125] further developed the technique by investigating the time dependence of

separations for the quantification of particle diffusion and hydrodynamics respectively.

Whilst TIRM determines forces with one to two orders of magnitude greater resolution than AFM and SFA, the technique is limited to only relatively small forces. That is, where interactions are repulsive and relatively long ranged, the determined light intensity is small and more susceptible to noise. Typically the range of forces capable of being determined by TIRM compares with the noise detected in AFM studies. This relatively small range of forces prevents any direct quantification of deformation; furthermore, TIRM is also limited to only larger (microscopically visible), spherical, non-adsorbing particles.

2.3.6 Atomic Force Microscopy

The AFM was developed in 1986[126,127] for imaging non-conductive surfaces, however, it soon became apparent that one could measure forces between the imaging tip and the surface. In a similar manner to the MASIF instrument, a piezoelectric translator controls the separation between the sample and the tip with the force determined from cantilever deflection. The difficulty in determining forces with an imaging tip is that the geometry of the interaction is non trivial, i.e. see reference 128. Such difficulties are overcome by attaching a microsphere to the end of the cantilever.[1,9]

Colloid probe AFM is now a widely adopted technique and with numerous reports of surface forces,[6,7,129-131] capillary forces,[132,133] adhesion,[6,134-136] steric forces,[6,137-139] friction,[140,141] deformation,[10,15,16,142-144] and nano-rheology[145-148] within current literature. The main disadvantage of AFM, like the MASIF, is that separation is calculated relative to hard body contact. Upon interaction of the colloid probe with either another colloidal particle or a surface, any deformation will result in additional variation of the surface separation and/or contact area and it is inappropriate to describe interaction behaviour as for rigid bodies. In considering colloid probe AFM studies on deformable systems, i.e. bubbles, droplets, biological cells and soft polymer materials there are two major difficulties that need be addressed

- There is no sharp transition between contact and non-contact, because deformation occurs prior to contact due to the extended range of surface forces. Therefore, the zero of separation cannot be determined in the same way as for rigid bodies.
- The increasing deformation with load means that even when in contact the cantilever does not move the drive distance. Although the force may appear linear (with respect to piezo drive) at high loads, this should not be mistaken for rigid substrate compliance since deformation is still occurring. Thus, the resultant slope in this region should not be used to calibrate the photo-diode.

Any quantitative AFM force measurement should address both issues. One way to calibrate the photo-diode is to press against a hard surface prior to measuring the deformable object. Throughout the literature, one can identify six methods that have been used in an attempt to resolve these difficulties. (i) The piezo drive distance is used as the abscissa and all separations are reported as relative to an arbitrary zero.[149,150] This approach simply ignores the problem. (ii) The deformation is modelled as a Hookean spring and the zero of separation is taken to be the point at which the linear compliance line reaches zero force.[10-12] This approach is only valid if the surfaces come into intimate contact in the constant compliance region. In the case of bubbles and droplets often a liquid film remains between the surfaces and the zero is displaced by the thickness of the film, as was originally recognised by Ducker et al.[10] (iii) A related method assumes the zero to be where deformed surfaces in contact have zero force.[77,151,152] Since "zero force" generally occurs due to the balance of van der Waals attraction and steric repulsions, the amount of flattening can be substantial, and errors arise from ignoring this effect. (iv) The zero of separation is taken to be the separation corresponding to the maximum force.[17,114,153] This approach also ignores the flattening of a deformable body and can be in serious error for compliant bodies. (v) The zero of separation is taken to occur at the point of the first measurable force.[17] This approach is appropriate for contact forces of zero range, but is evidently incorrect for forces of extended range. A related method fixes the zero of relative separation at an arbitrary small force,[15] which allows comparison of data with the same force law but not if the forces are of different magnitude or type. (vi) Mulvaney et al[14] have fitted the non-linear Poisson-Boltzmann equation for rigid bodies by adjusting both the zero of the experimental separation and the surface potential. The

problem with this approach is that it ignores the deformation at small separations, and at large separations an arbitrary change in surface potential can be compensated by a change in separation. In other words, one cannot determine unique values for the potential and the zero of separation simultaneously.

Despite problems in calculating the zero, examining the literature reveals only a few studies that report or consider soft contact deformation in solid materials. This is largely because surface forces are not usually sufficient to result in significant deformation. However, deformation prior to contact has been considered in studies of rubber[77] and polymer microspheres.[65] Vakarelski et al[65] examine differences between a rigid poly(methyl methacrylate) (PMMA) particle and a deformable poly(acryl methacrylate) (PAMA) particle coated in PMMA to confirm the soft contact theory by Hughes and White.[78] The Hughes and White approach discusses deformability in terms of a unitless term λ, where particles are Hertzian when $\lambda >> 1$ and completely rigid when $\lambda << 1$. The calculated λ values for PMMA coated PAMA particles varied between 5 and 12, suggesting that particles were deformable but do not acquire the specific profile predicted by Hertz. These predictions were then confirmed by observing non-Hertzian behaviour in deformation and adhesion measurements.

Considine et al[144] examined interactions of a silica probe interacting with a *Cryptosporidium parvum*oocysts. Interactions were described by electrical double layer theory at large separations and polyelectrolyte 'brush' behaviour at intermediate separations. Unfortunately this analysis results in large discrepancies at relatively small separations. In addition to this analysis, deformation of these oocysts was discussed in terms of the spring constant, using the analysis of Ducker et al.[10] Interestingly, force interactions show behaviour typical of electrical double layer interactions for rigid bodies at large separations as well as repulsive, monotonically increasing forces not unlike the interactions presented throughout this thesis.

To date the vast majority of AFM soft contact studies examine the interactions of a colloid probe interacting with a macroscopic bubble or droplet. Perhaps the most reviewed article within the literature is the particle – bubble analysis reported by Ducker et al,[10] this investigation postulated that:

- Force versus nominal separation relationships tend to a linear regime where interactions can be described using Hooke's law. This finding was reproduced in practice[11,12,15,16] but questioned in subsequent analyses.[86,154]
- By modelling deformation as a Hookean spring, the zero of separation can be established by extrapolating the linear compliance to zero force. Despite separations being offset by the film thickness, this method was used in subsequent studies.[11,12] Within this postulate there is an implicit assumption that the thickness of the film remains constant. It follows that if the thickness of the film is not constant in the region of compliance then the deformation is not proportional to the applied load. These postulates were then clarified by Dagastine and co-workers[18,19] using the augmented Young-Laplace equation. Dagastine and co-workers suggest that there exists a film between the colloid probe and the bubble (or droplet) as observed in SFA studies,[84-89] however film thinning will occur at weak interactions, with a minimum thickness observed at relatively large forces. These studies also confirmed that interactions obey Hooke's law up to moderate forces.

Another significant finding was observed by Hartley et al,[15] who examined particle – drop interactions. The spring constant describing the interaction of a 300 μm droplet was shown to be proportional to the interfacial tension; this finding was then reproduced in subsequent theoretical investigations.[18,19,90,92] Additionally, at relatively large separations, interaction forces were well described by the Poisson-Boltzmann equation for rigid bodies regardless of the surfactant concentration, a finding reproduced in particle – bubble[12] and particle – oocysts investigations.[144]

Within the literature, the majority of droplet deformation studies do not mention the influence of hydrodynamics. From equations 2.1 and 2.7 it follows that these studies employed experimental conditions where the hydrodynamic interactions are insignificant. Previously, Aston and Berg[17] reported small changes in interaction forces due to hydrodynamics, however these results were not observed by Nespolo et al,[16] this difference is likely to be a result of different sized colloid probes. That is, Aston and Berg use a relatively large colloid probe with a 10 μm radius compared with the 2.5 μm radius used by Nespolo et al. Given that the hydrodynamic force is

proportional to the square of the radius (see equation 2.7) it is not surprising these differences were reported. Both these studies are of additional interest as they are the only studies comparing soft contact theory with colloid probe investigations on droplets or bubbles. Aston and Berg[17] use soft contact theory to show droplet deformation doesn't obey Hooke's law, however, they do report interactions characterised by a spring constant. This observation is consistent with predictions by Dagastine and co-workers.[18,19] Nespolo et al validate the use of the algorithm developed by Dagastine and co-workers[18,19] by reporting good comparisons between experimental findings and those predicted by this algorithm. This study also confirms that the force versus separation (not deformation) obeys Hooke's law.

3 Materials and Methods

3.1 Materials

3.1.1 Reagents

Demineralised water was further purified using a Milli-Q water filtration system and used exclusively throughout. Dimethyldiethoxysilane (DMDES), methyltriethoxysilane (MTES) and a 28% ammonia solution were supplied by Aldrich (Milwaukee, USA). Both DMDES and MTES were redistilled under nitrogen prior to use. Analytical grade potassium hydroxide, nitric acid, potassium nitrate and sodium dodecylsulphate (SDS) were supplied by BDH (Poole, England).

Hydrophilic silica nano-particles (fumed silica particles (Aerosil 380)) were kindly supplied by Degussa and reported[155] to have a BET surface area of 380±30 m^2g^{-1}, 2.5 Si-OH groups nm^{-2} and an average primary particle size of 7 nm. The water/air contact angle of the particles was estimated to be 14°.[156] Hydrophobic silica nano-particles (fumed silica particles (Aerosil R 974)) were kindly supplied by Degussa. Particles were reported[155] to have a BET surface area of 170±20 m^2g^{-1}, 0.39 Si-OH groups nm^{-2} and an average primary particle size of 12 nm. The water/air contact angle of the particles was estimated to be 117±4°.[156]

3.1.2 Preparation of PDMS emulsions

Emulsions of PDMS droplets were prepared by the base catalysed polymerisation of DMDES and MTES using a method adapted from Obey, Vincent and co-workers.[157,158] 4 mls of a DMDES - MTES mixture was added to a solution consisting of 178 mls of water and 18 mls of ammonia solution (28%). Cross-linking within droplets arises from the tri-functionality of MTES, thus the ratio of MTES to DMDES was varied to achieve a desired level of cross-linking within the PDMS droplets. The mixture was shaken vigorously for 30 seconds and left on a rotating frame for 5 hours. The resultant emulsion was then dialysed against Milli-Q water for 24 hours to remove ammonia and any unreacted monomer.

3.2 Experimental Procedures

3.2.1 Determination of Bulk Rheology

Bulk samples of the liquid-like droplets were sourced through centrifugation of coalesced emulsion samples. Bulk samples of the viscoelastic droplets were also separated by centrifugation, but did not coalesce. The semi-solid sediment was collected and pressed into a disc (diameter ~ 25 mm) at a pressure of 1.3×10^5 Nm^{-2} prior to rheological measurement. The dynamic rheological parameters of the bulk PDMS samples were determined using a stress-controlled rheometer (Rheometrics Scientific SR 5000) with parallel plate geometry and a 1mm gap. The viscosity of liquid-like droplets was determined from oscillation measurements at 1 Hz over a stress range of 1 to 1000 Nm^{-2}. The rheology of bulk viscoelastic samples was characterised in terms of frequency and stress. Dynamic frequency sweeps were determined at an applied stress of 10 Nm^{-2} from 0.1 Hz to 1000 Hz, dynamic stress sweeps were determined from 0.4 Nm^{-2} to 400 Nm^{-2} at a frequency of 10 Hz.

3.2.2 Droplet Sizing by Dynamic Light Scattering

Droplet diameters were determined by dynamic light scattering[159] using a Brookhaven light scattering instrument (BI-2030 correlator and BI-200SM stepper-motor controlled goniometer) with a water-cooled Lexel argon laser (λ = 488 nm). The glass sample vial was immersed in a decalin (BDH) bath to match the refractive index. Light scattering data were determined at a scattering angle of 90° with the laser power varied between 50 and 150 mW in order to maximise the signal to noise ratio. The sample temperature was equilibrated at 25.0 ± 0.1 °C using a decalin bath. The average size was determined using Cumulants[159] analysis. The auto-correlation function was then converted to a droplet size distribution using non-negative least squares analysis.[159]

3.2.3 Determination of Zeta Potential

Droplet zeta-potentials were calculated from the Smoluchowski equation using electrophoretic mobilities determined by phase angle light scattering (PALS).[160] The PALS technique is based upon LASER Doppler electrophoresis[161] but analyses the phase, rather than frequency, of a moving interference pattern observed from two crossed laser beams. This technique is reported[162] to calculate the velocity of

droplets, and thus their electrophoretic mobility, with greater accuracy than conventional LASER Doppler electrophoresis. The PALS system uses a helium-neon LASER (5mW, $\lambda = 632.8$ nm), a UV quartz glass cell and palladium electrodes with a nominal separation of 2 mm. Electric field strengths of approximately 5 V/cm were used in each instance.

3.2.4 Determination of the Interfacial Tension and Contact Angle

The interfacial tension of PDMS oil from coalesced emulsion droplets was determined using the drop weight method.[163] Bulk samples of PDMS oil were slowly expelled through a syringe directly into a 1.0×10^{-3} M KNO_3 solution at pH 9.5 with varying concentrations of SDS. The interfacial tension is determined from the weight of the droplet, that is, the force supporting the droplet to the syringe tip is equal to the weight of the droplet via equation 3.1

$$\gamma = \frac{V(\Delta\rho)g}{2\pi r\psi\left(r/V^{1/3}\right)} \qquad 3.1$$

Where γ is the interfacial tension, V is the volume of the droplet, $\Delta\rho$ is the density difference between the PDMS oil and the electrolyte solution, g is acceleration due to gravity, r is the outer radius of the syringe tip and $\psi(r/V^{1/3})$ is the correction factor given by Wilkinson and Aronson.[164]

Advancing contact angles of coalesced PDMS emulsion droplets on of AFM glass substrates were determined by optical microscopy using a CCD camera and SMC Pentax-M lens (Japan) (maximum aperture ratio 1:1.4, 50 mm focal length). Samples were prepared via sedimentation onto glass substrates, similar to the preparation of AFM substrates in section 3.2.5.3.

3.2.5 Procedures Relating to Atomic Force Microscopy

In order to reduce contamination, all procedures relevant to AFM were performed in a class 100 clean room. Samples were stored in airtight containers and cantilevers were stored in closed containers, both samples and cantilevers were handled with tweezers cleaned in analytical grade methanol (BDH) prior to use. All workspaces were cleaned with water, prior to their use.

3.2.5.1 The Characterisation of Cantilevers

Cantilevers are generally characterised by their spring constant as well as their shape. Throughout this thesis, gold coated, silicon nitride tipless 'V' shaped cantilevers (Digital Instruments, Santa Barbara, USA) were used exclusively. These cantilevers were 200 μm in length and possessed spring constants between 180 and 250 mNm^{-1}. Cantilever spring constants were determined by the added mass method described by Cleveland et al.[165] The added mass method involves determining the resonant frequency before and after attaching a known mass to the cantilever. Here, five different tungsten spheres were mounted separately on the cantilever, as described below, using negligible mass of Vaseline to immobilise the spheres. The spring constant of the cantilever was determined using equation 3.2

$$f \approx \frac{1}{2\pi}\sqrt{\frac{k_c}{M+m}} \qquad 3.2$$

Where f is the determined resonant frequency, M is the mass of the cantilever (unknown) and m is the mass of the tungsten sphere determined from the density and the radius determined using optical microscopy. This approach is widely used throughout the literature and determines the spring constant within an error < ±10%.[166]

3.2.5.2 Mounting of Colloid Probes

Colloid probes were attached to the apex of a cantilever using the method reported by Ducker et al[1,9] at least 24 hours prior to use. In this instance colloid probes were borosilicate glass spheres (Polysciences) containing 4% sodium, 2% fluorine, 0.7% calcium and trace amounts of magnesium (as determined by surface analysis using X-ray Photon Spectroscopy).[167] Colloid probes were bound to the apex of a cantilever using a resin (Epikote 1004, Shell) that melts at elevated temperatures (104 °C). Two etched tungsten wires, are placed on the end of a micromanipulation arm (Narishige MN-151) attached to a microscope (Olympus BH2). Tungsten wires were etched electrochemically, with the tungsten as the cathode, stainless steel as the anode in a 1M KOH solution. One wire was used to deposit molten resin whilst the second was used to manipulate glass spheres. Attractive capillary forces keep the glass spheres attached to the wire until the sphere is placed on the glue coated cantilever apex. The

cantilever was then removed from the heat source and the colloid probe was sized by optical microscopy using a CCD camera (SONY, M-852) and image analysis software (Galai-Cue 3).

Silica surfaces (and thus presumably borosilicate particles) are known to readily adsorb airborne contaminants,[129] thus immediately prior to their use, colloid probe modified cantilevers were thoroughly cleaned by repeatedly washing in a 5M KOH solution and rinsing in copious amounts of Milli-Q water. Exposing silica to concentrated alkaline conditions will, with time, roughen the surface. The peak – to - trough roughness of borosilicate probes after this cleaning process was found to be 1.2 nm. This value is relatively small and thus not believed to influence determined interactions.

3.2.5.3 Immobilisation of PDMS Droplets

PDMS droplets were immobilised onto 13 mm round glass substrates (Menzel-Glaser, Frieberg, Germany) by sedimentation from aqueous solution. The glass substrate was cleaned by repeatedly washing in a 5M KOH solution then water, until a zero contact angle with water was observed. Glass substrates were immediately placed in a 25 ml vial filled with emulsion and equilibrated for three days. After this time several droplets could be observed on the glass surface by AFM imaging.

3.2.5.4 Determination of Interaction Forces

A Nanoscope IIIa (Digital Instruments, Santa Barbara) was used to locate surface immobilised PDMS droplets and determine the forces between PDMS droplets and a colloid probe. After sufficient equilibration time (45 minutes) immobilised droplets were located by soft contact imaging.[168] Once imaged, droplets were centred beneath the colloid probe using inbuilt software, great care was taken to align the centres. Any deviation from centre – centre compression was evident when a lateral deflection was observed, such data was discarded and the colloid probe was realigned. Loading (extend) and unloading (retract) force cycles were determined at 0.25, 1.0 and 4.0 μms^{-1} over trajectories of 500 nm in each direction, with two minutes between cycles, allowing complete relaxation to occur (see section 4.2.3). All force plots shown in this thesis were determined at 1 μms^{-1} unless otherwise stated.

3.2.5.5 Analysis of Interaction Forces

To quantify the force, the AFM photodiode was calibrated from the constant compliance region of force curves between the glass probe and the glass substrate in a region free from immobilized PDMS droplets. The force (F) acting between the glass probe and PDMS droplet was determined from the cantilevers deflection using Hooke's Law, $F=k_c x$, where k_c represents the spring constant and x the deflection of the cantilever. The determined force is then normalised by the droplet's radius, according to the Derjaguin approximation,[95,96] however, when a droplet deforms, its radius increases perpendicular to the loading force resulting in a different interaction geometry. This implies, at large loads where droplets are significantly deformed, the force normalised by the undeformed radius does not accurately represent the interaction energy. The effect of ignoring the change in radius has been reported[19] to results in errors of up 15% for a colloid probe approaching a macroscopic droplet. Calculating the effective radius of a deformed droplet is not trivial and likely to be different for viscoelastic cross-linked droplets than for liquid droplets. Thus this effect was minimised by examining only relatively small amounts of deformation, i.e. < 100 nm.

Interactions between silica probes and PDMS droplets exhibited one of two distinct behaviours depending on the level of cross-linking. Droplets were either

- Highly cross-linked, viscoelastic and showed hysteresis and drive-rate dependence. These interactions were analysed using Attard's theory for viscoelastic particles.[21,22]
- Liquid-like, showed no drive-rate dependence and tended to linear elastic behaviour, this behaviour was analysed as a Hookean spring similar to that described by Attard and Miklavcic[90-92] and confirmed with the analysis of Ducker et al.[10]

Determination of the Nano-Rheological Properties of Highly Cross-Linked Droplets.

Theoretical force plots were generated using a computer program written and generously supplied by Phil Attard. This program generated force plots between two

hemispheres (one of which is deformable) based on the soft contact viscoelastic theory outlined in section 2.2.1. These calculations assumed only electrical double layer interactions were present, but included an exceptionally short ranged force (decay length 1 nm) used to prevent bodies from interpenetrating. This short ranged force is similar to 'the "additional" repulsion' between silica surfaces reported by Grabbe and Horn.[169] van der Waals forces were not incorporated into the theoretical force plots presented. The presence of a van der Waals force with Hamaker constants covering a wide range values observed in colloidal systems[170] (0.5 to 10 $\times 10^{-20}$J) resulted in large adhesions not observed experimentally. It is believed that the van der Waals forces are masked due to the presence of a hydration layer on the silica and possibly on the PDMS. This adsorbed water layer prevents surfaces from approaching to separations where van der Waals forces are detectable. Previously, a notable absence of detectable van der Waals forces observed in silica – silica systems was attributed to such short range forces[169]. In each theoretical force plot, electrical double layer parameters (Debye Length, zeta-potentials) were those of the experimental conditions. Thus, for example, the same parameters were used to calculate force plots of varying approach velocities but were changed for droplets of different cross-linking or when surfactant was added. Throughout this thesis zeta-potentials were used to approximate surface potentials as surface potentials were not easily accessible. The difference between determined zeta potentials and surface potentials is not thought to be sufficient to significantly vary determined nominal separations.

Approximate values for E_0 and E_∞ were first obtained from fitting an elastic deformation[82] to the approach force. By systematically varying values for E_0, E_∞ and τ, determined nano-rheological parameters were those which resulted in the smallest variation between experimental and theoretical force plots. That is, a three-dimensional table containing values for E_0, E_∞ and τ was constructed with each series of values evaluated. The variation between values was initially 20%, however the process was then repeated using the refined values with variations of only 10%. The 'error' between experimental and theoretical force plots was determined using a least squares analysis for a series of four force plots determined at different drive velocities and maximum loading forces, naturally drive velocities used in determining

theoretical force plots were equal to that of the relevant experimental force plots. In general, the uncertainty in determining theoretical values of the nano-rheological parameters for a particular droplet was limited to <10%.

In section 2.2.1, the effective viscoelastic parameter variation as a function of elastic limits, characteristic relaxation time and interaction time was discussed. Figure 3.1a and 3.1b shows the effect of the nano-rheological parameters on theoretical force plots and exemplify the fitting process. Figure 3.1a shows the effect of E_0:E_∞ variation; this figure compares interactions where E_0:E_∞ = 2 (series a) with interactions with E_0:E_∞ = 1.5(series b), when t is comparable to τ (see Table 3.1 for details). The force plot shows increasing E_0 results in larger forces, and more hysteresis (energy dissipation). The increase in observed forces can be directly rationalised from equation 2.11 which shows that the magnitude of E(t) is related to the magnitude of both E_0 and E_∞. In terms of the Kelvin Voigt model, the increased E_0 is equivalent to larger viscosity in the dashpot. This increase in viscosity results in greater resistance to deformation and relaxation, thus resulting in larger forces on approach and more hysteresis on retraction. Figure 3.1b shows the effect of t:τ variation, here τ is varied such that interactions occur over time scales where behaviour is strongly influenced by short term (series a), and long term behaviour (series b), as well as behaviour where t is comparable to τ (series c). The force plot shows the amount of hysteresis is

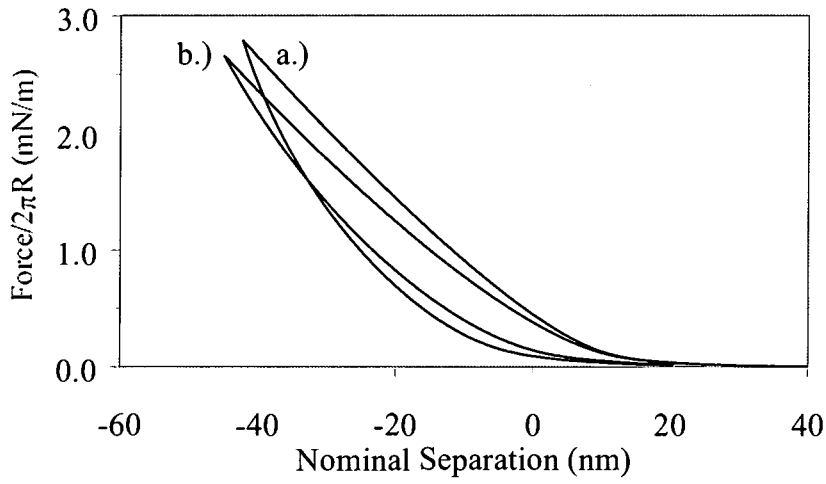


Figure 3.1a Theoretical force plots from Attard's theory,[21,22] for two colloids (R_{eff} = 0.3 μm) interacting at 1.0 μm/s, with a Debye length of 9.6 nm, and surface potentials of 70 and 40 mV. Nano-rheological parameters are given in Table 3.1.

small where interactions are relatively fast or slow. This result is observed because behaviour is dominated by either the short-term or long-term elastic limit. In terms of the Kelvin Voigt model, where interactions are relatively fast, deformation in the dashpot is small; consequently hysteresis resulting from the dashpot resisting relaxation is small. Where interactions are relatively slow the dashpot contribution is small i.e. the force is proportional to the strain rate, and interactions are dominated by the elastic modulus.

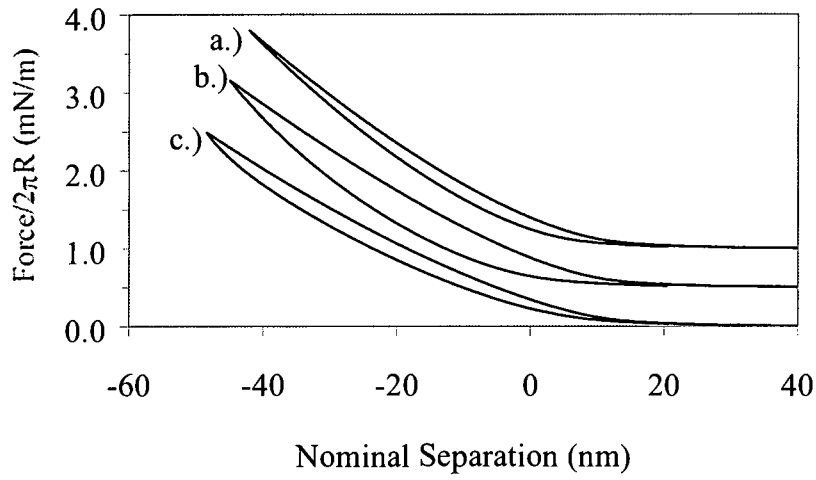


Figure 3.1b Theoretical force plots from Attard's theory,[21,22] for two colloids (R_{eff} = 0.3 μm) interacting at 1.0 μm/s, with a Debye length of 9.6 nm, and surface potentials of 70 and 40 mV Nano-rheological parameters are given in Table 3.1. To improve clairty force plots a and b have been offset by 1 and 0.5 mN/m respectively

Table 3.1 Nano-rheological parameters used in Figure 3.1a and 3.1b

	data	E_0 (MPa)	E_∞ (MPa)	τ (s)	Hysteresis (viscous energy dissipation J)
Figure	a	1.6	0.8	0.09	3.1×10^{-17}
3.1a	b	1.2	0.8	0.09	5.2×10^{-17}
Figure	a	1.2	0.8	0.09	3.1×10^{-17}
3.1b	b	1.2	0.8	0.45	1.4×10^{-17}
	c	1.2	0.8	0.018	1.9×10^{-17}

Hookean Spring Theory for Viscous Droplets

In cases where the force is linear with respect to separation, i.e. for Newtonian, fluid droplet, then the interactions can be characterized using Hooke's law. Throughout

this thesis droplet spring constants were determined using both the analysis used by Ducker et al[10] and an analyses based on the approach given by Attard and Miklavcic.[90-92] Encouragingly, both these approaches calculated the same spring constant.

The approach used by Ducker et al uses equation 3.3 (which is based on Hooke's law for two spring in series) to calculate the spring constant of the interaction.

$$k_{drop} = \frac{k_c}{\left(\frac{D_{rigid}}{D_{drop}} - 1\right)} \qquad 3.3$$

Here k_{drop} is the spring constants of the droplet, D_{rigid} and D_{drop} is the deflection per unit piezo translation against a solid surface and the droplet (in the linear region) respectively. This approach is the most popular throughout the literature but is limited to describing the linear region of the interaction. The approach used by Attard and Miklavcic, uses equations 2.13 to 2.15, to fit the entirety of the interaction, including where droplet surface forces are significant. However this approach is specific to droplets considerably larger than the probe, that is, this approach uses a modified force law, equation 2.14, to account for the dimpling in the droplet. In general, droplets investigated were significantly smaller than the colloid probe and therefore not expected to dimple. Equation 3.4 describes the deformation of smaller droplets by replacing equation 2.14 with the Poisson - Boltzmann equation.

$$h - h_0 = \frac{32\pi\varepsilon_0\varepsilon_r R(k_B T/ze)^2 \gamma_1\gamma_2 \kappa e^{-\kappa h}}{k_{drop}} \qquad 3.4$$

where, h and h_0 are the actual and nominal separations respectively, i.e. h(0) and $h_0(0)$, all other parameters were defined in equations 2.1 and 3.3.

Here k_{drop} is the value that best describes the determined force-separation relationship. This approach is valid for droplets that are not considerably larger than the colloid probe and where the deformation is minimal, i.e. the droplet retains a near spherical profile.

Chapter 4. Results and Discussion

Preamble

This chapter is divided into two major sections. 4.1, Characterisation of PDMS Droplets, and 4.2, Interaction Forces and Deformation of PDMS Droplets. The PDMS system used within this thesis was chosen as it has been well characterised in terms of synthesis and molecular composition,[158] but more importantly the material properties could be altered with little variation in surface chemistry. Recent studies of colloidal stability[160] and adsorption of nano-particles[171] and block copolymers[172] allow interesting comparisons. However, an investigation on adsorbed block copolymers was not pursued as the adsorption of such compounds diminishsd the zeta-potential of the droplets rendering them unsuitable for the analysis used within this study.

Section 4.1 discusses the material properties, size, and surface chemistry of the PDMS droplets under investigation. Concisely, highly cross-linked droplets are viscoelastic, with elastic moduli G' varying from 10^3 to 10^5 Nm^{-2}. These droplets are believed to consist of a cross-linked PDMS network with some low molecular weight (M_w ~500 g mol^{-1}) cyclic and linear oligomeric siloxane molecules.[158] At more moderate levels of cross-linking droplets are composed of Newtonian fluids with viscosities in the range 0.6 to 2.6 $Nm^{-2}s$. The exact size and surface potential of an emulsion droplet sample is dependent on the amount of cross-linking, polymerisation time, and the concentration of ammonium used during synthesis. For the samples investigated over the entire range of cross-linking used droplets were highly monodisperse with average size and zeta-potentials as given in Table 4.1.

Table 4.1 Properties of PDMS emulsion droplets and the glass colloid probe.

Emulsion	MTES - DEDMS ratio	ζ-potential (mV) *1mM KNO_3* *pH 9.5*	*pH 7.0*	*pH 4.5*	*1mM SDS, pH 9.5*	Diameter (nm)
A	50 - 50	-41.3±0.8	-34.0±1.3	-14.1±2.2	-48.4±2.3	600
B	45 – 55	-38.5±1.5	-	-	-	480
C	40 – 60	-37.7±2.5	-	-	-46.5±1.5	450
D	35 – 65	-41.8±1.4	-	-	-	600
E	30 – 70	-38.7±1.8	-29.9±1.9	-13.2±1.5	-50.0±1.3	590
Colloid Probe	-	-70.0±1.7	-64.3±1.9	-24.1±1.2	-70.3±1.4	7000

Section 4.2 examines the interaction forces, determined by colloid probe AFM, between a borosilicate glass probe and PDMS droplets under a variety of conditions.

In analysing determined force versus distance plots for droplet – colloid probe interactions, the zero of separation is an important consideration. In section 4.2 a method for determining the zero of separation is introduced with its applicability rationalised for determined interactions over the entire range of droplets studied. Determined interaction forces showed either: viscoelastic behaviour, where interactions exhibit hysteresis and rate dependence, or Hookean spring behaviour where interactions could be characterised by a single spring constant, these interactions showed no hysteresis nor rate dependence. The viscoelastic behaviour of a highly cross-linked droplet is discussed in depth in section 4.2.1; likewise the 'Hookean' interactions from low or moderately cross-linked liquid droplets is discussed in section 4.2.2. The approaches developed were then used as precedents for analysis of interactions of more complex systems. Section 4.2.3 examines how droplet deformation and relaxation is influenced by bulk material properties, pH and droplet size. Sections 4.2.4 and 4.2.5 explore how droplet deformability can be influenced by interfacial tension, i.e. adsorbed surfactant, and interfacial elasticity, i.e. adsorbed nano-particles.

4.1 Characterisation of PDMS Droplets

4.1.1 Rheology of Bulk PDMS Material from Droplets

Figure 4.1 shows the viscous (G'') and elastic (G') moduli of bulk PDMS samples from emulsions A, B and C as a function of applied stress. For 50% cross-linked droplets (emulsion A) G' is approximately 10^5 Nm^{-2}, which is an order of magnitude greater than G' for the 45% cross-linked droplets and two orders of magnitude greater than G' for the 40% cross-linked droplets. All samples show relatively long linear viscoelastic regions where G' is independent of the applied stress. This is to be expected for cross-linked polymer materials. Samples pertaining to emulsions A and B appear similar with the elastic modulus remaining constant whilst the viscous modulus decreases with stress before reaching a plateau. Rheology data pertaining to droplets from emulsion C differ from those from A and B, that is, the elastic and viscous moduli remain equal and constant, up to relatively high stresses (~1000 Nm^{-2}) where the elastic modulus then decreases. This decrease in elastic modulus is considered to be non-linear viscoelasticity where the relaxation modulus is dependent on the strain.

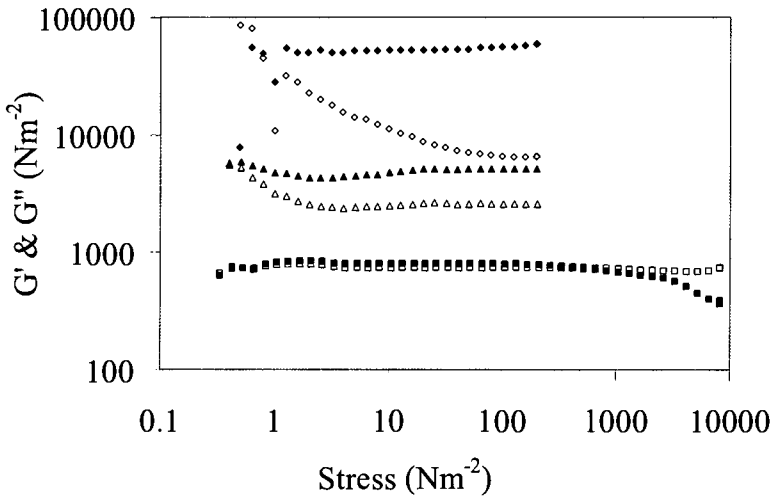


Figure 4.1 Elastic modulus (G') filled symbols and viscous modulus (G") empty symbols of bulk PDMS samples from emulsions A (◆, ◇), B (▲, △) and C (■, □) plotted against applied stress determined at 1 Hz

Viscous and elastic moduli of the bulk PDMS samples from emulsions A, B and C are plotted as a function of frequency determined at a stress in the linear viscoelastic region in Figure 4.2. This data reveals that both the elastic and viscous moduli increase with frequency. However, at relatively large frequencies > 10 Hz the viscous modulus begins to decrease whilst the elastic modulus increases more rapidly with frequency. This behaviour is typical of viscoelastic materials and corresponds to the dashpot not fully recovering from the varying applied strain in a Kelvin-Voigt viscoelastic body.

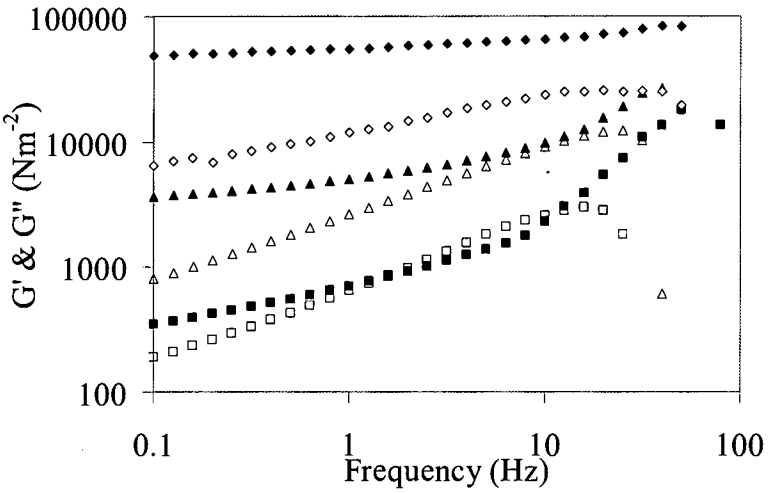


Figure 4.2 Elastic modulus (G') and viscous modulus (G") of bulk PDMS samples from the droplets from emulsions A (◆, ◇), B (▲, △) and C (■, □) plotted against the oscillatory frequency and determined at a stress of 10 Nm^{-2}. Elastic moduli are represented by the filled symbols and viscous moduli are represented by open symbols.

Both Figures 4.1 and 4.2 demonstrate more pronounced differences between the viscous and elastic moduli upon increasing the level of cross-linking. This effect is further demonstrated by plotting G', G" and tan(δ), where tan(δ) = G"/G', against the cross-linking level in Figure 4.3. Here, the elastic and viscous moduli increase exponentially and disproportionately with cross-linking, i.e. tan(δ) decreases with cross-linking confirming the elastic modulus is more dominant in droplets with more cross-linking.

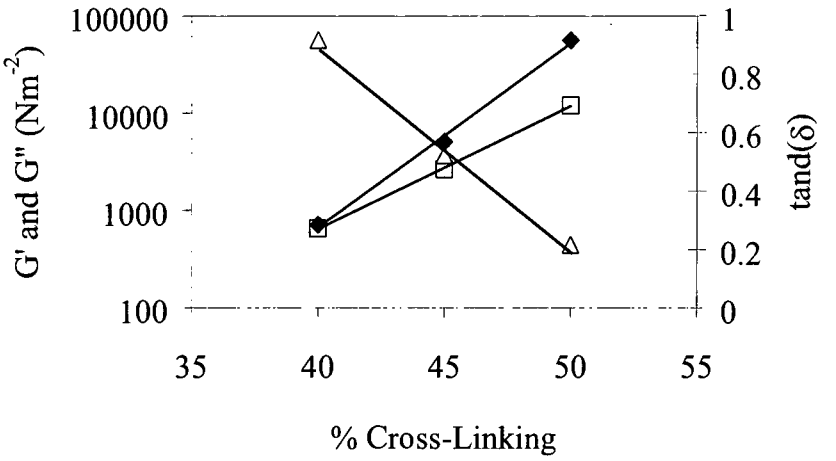


Figure 4.3 elastic (◆) and viscous (□) modulus (left axis) and tan(δ) (△, right axis) plotted against the cross-linking. Determined at a stress of 10 Nm^{-2} and at 1 Hz

Rheological data pertaining to droplets from emulsion A show that the elastic modulus plateaus, with frequency, at approximately 8.5×10^4 Nm^{-2}, which is similar but smaller than a reported value of 1.6×10^5 Nm^{-2} determined for a PDMS network with similar amounts of cross-linking.[173] Furthermore the viscous and elastic moduli of PDMS decreases faster than expected with decreasing cross-linking. That is the elastic modulus of the 40% cross-linked droplets is one to two orders of magnitude smaller than many polymer melts.[174] The sample used to determine rheological data in this present work was prepared from emulsion sediment that was subsequently pressed into a disc. The sample is believed to be semi-particulate in nature; with the possibility that some droplets separate from the bulk sample on application of stress resulting in data that underestimates the true bulk behaviour. This is consistent with the observed stability against coagulation in centrifugation studies.[158]

Figure 4.4 demonstrates that droplets from emulsions D and E are entirely Newtonian by presenting a constant viscosity with varying applied stress or shear rate.

It is clear that the bulk rheological properties from droplets with different degrees of cross-linking vary greatly, with distinct differences in rheological behaviour, i.e. from Newtonian fluid to viscoelastic semi-solid.

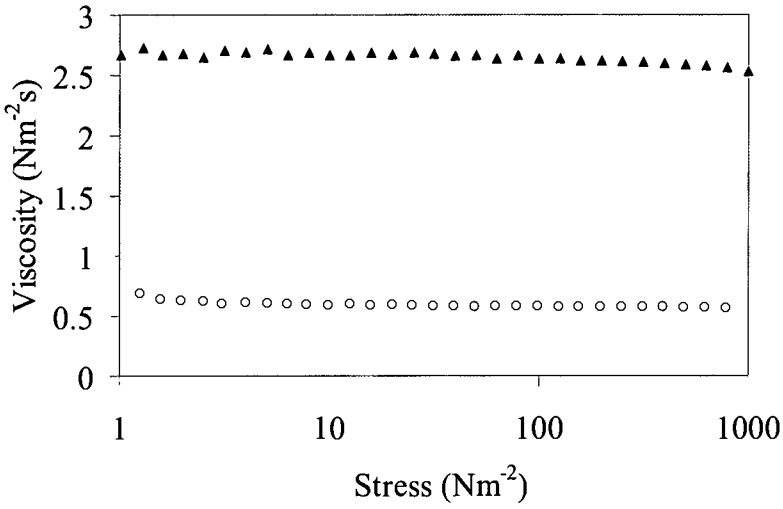


Figure 4.4 Viscosity of coalesced droplets from emulsions D (▲) and E (○) plotted against the applied stress. The corresponding shear rates are in the range of 10^{-3} to 10^{3} s^{-1}

4.1.2 Droplet Size

Figure 4.5 shows the size (diameter) distribution of droplets from emulsions A – E determined by dynamic light scattering. The average size of droplets (Table 4.1) is dependent on the preparation conditions, with subtle batch variations contributing to the average size. The average droplet size is in the range 500 nm ± 100 nm with no general trends in size with cross-linking variation. In all instances, droplets were highly monodisperse in comparison with conventional emulsions.

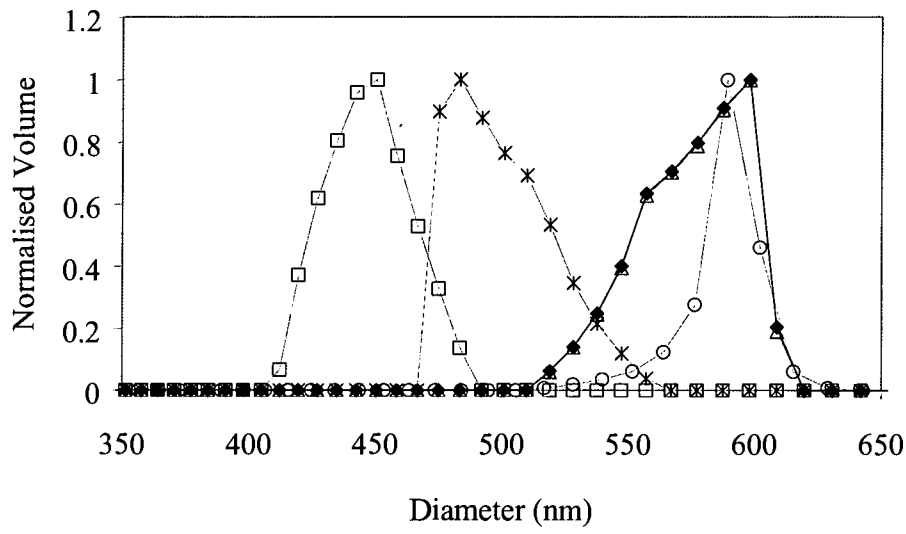


Figure 4.5 Droplet diameter distribution for emulsion A (◆), B (✳), C (□), D (△) and E (○) determined by dynamic light scattering

4.1.3 Interfacial Tension and Contact Angle

The interfacial tension between droplets from emulsion E and a solution of 10^{-3} M KNO_3 at pH 9.5 was determined to be 18 mN/m and at equilibrium after 30 minutes. Section 4.1.4.1 shows subtle differences in the droplet zeta-potential as a result of differences in surface chemistry due to different cross-linking levels. However, it is not believed that these differences in surface chemistry are likely to result in significant differences in interfacial tension. That is, the composition of non cross-linked PDMS droplets was shown by Goller et al[158] to consist of low molecular weight linear and cyclic siloxane oligomers. These low molecular weight species are suspected to be present in all droplets and likely to be the most interfacially active components of the droplets. Therefore not much sample dependency of interfacial tension is anticipated.

The interfacial tension of PDMS oil sourced from emulsion E was also determined as a function SDS concentration. Table 4.2 shows the determined interfacial tension between PDMS oil and a 1.0×10^{-3} M KNO_3 solution at pH 9.5 with varying concentrations of SDS. The interfacial tension significantly decreased with increasing concentrations of SDS.

Table 4.2 Interfacial tension versus SDS concentration

Concentration of SDS (M)	Interfacial Tension (mN/m)
0	18 ±1.0
0.001	12 ±1.0
0.01	10 ±0.7
0.1	5 ±0.8

The contact angle of a 30% cross-linked PDMS droplet (emulsion E) sedimented onto an AFM glass substrate in 1mM KNO_3 at pH 9.5 was determined to be 150 ± 5° from a series of micrographs, as exemplified in Figure 4.6. The figure also shows that droplets retain a sphere-like shape, and thus the average size of immobilised droplets can be approximated with the average size of dispersed droplets.

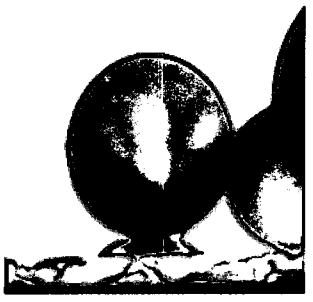


Figure 4.6 Micrograph of coalesced droplet (emulsion E) on an AFM glass substrate in 1mM KNO_3 at pH 9.5 used to determine contact angle.

4.1.4 Surface Electrical Properties of PDMS Droplets and the Colloid Probe

4.1.4.1 In the Absence of Adsorbed Species

The surface electrical properties of PDMS droplets have been studied in detail elsewhere.[158,160] Concisely, the pH dependent behaviour resembles that of silica, i.e. the isoelectric point (iep) ranges between pH 2.5 and 3.5 with droplets possessing a negative surface charge in solutions when the pH is greater than 3. Table 4.1 shows the zeta-potentials of droplets from each emulsion, determined in 1.0×10^{-3} M KNO_3 solutions at pH 9.5, 7.0 and 4.5, precisely replicating conditions at which interaction forces were determined.

The surface active linear oligomers are terminated with hydroxyl groups that assemble at the interface where they can protonate or deprotonate depending on the pH.

$$-[O-Si(CH_3)_2]_n-OH_2^{2+} \xleftrightarrow{pK_{a1}} -[O-Si(CH_3)_2]_n-OH^+ + H^+ \xleftrightarrow{pK_{a2}} -[O-Si(CH_3)_2]_n-O^- + 2H^+$$

Equation 4.1

The values of pK_{a1} and pK_{a2} lead to an iep at pH 3.5. Incorporating MTES into droplets may result in the presence of geminal hydroxyl groups i.e. $-O-Si(CH_3)(OH)_2$,

the presence of which is expected to decrease both the pK_{a1} and pK_{a2}. Thus with cross-linking one would expect a more negative surface charge and potential. However, the surface electrical behaviour of PDMS shows no significant variation with cross-linking. This is because the surface chemistry of PDMS droplets is dominated by low molecular weight species the behaviour of which are not expected to show significant variation with MTES concentration. Thus, considering all the above it is reasonable to suggest the incorporation of MTES results in large variations in material properties such as elastic and viscous moduli, but has little effect on the surface chemistry of droplets.

Zeta-potentials for borosilicate glass spheres used as colloid probes are given as a function of pH in Table 4.1. Determined zeta-potentials are well placed between the values for silica probes by reported by Larson et al[130] and Hartley et al.[175] These studies vigorously investigated the potential of silica probes as a function of pH, whilst determined potentials varied between studies both report relatively large (± 15mV) variation. This observed agreement with literature reports is encouraging and suggests that it is not unreasonable to assume borosilicate glass resembles silica for the pH values investigated.

4.1.4.2 Influence of SDS

Previously, PDMS has been found to remove non-ionic surfactants from solution,[176] however it is not likely that the ionic sulphate head group of SDS is solubilised. Thus the addition of SDS is likely to only affect the surface chemistry (interfacial tension, surface potential) and not material properties such as density or elastic and viscous moduli. Zeta-potentials of droplets from emulsions A, C and E determined in a background solution of 1.0×10^{-3} M KNO_3 and 1.0×10^{-3} M SDS at pH 9.5 are reported in Table 4.1. The presence of SDS increases the magnitude of the zeta-potential by approximately 10 mV. Figure 4.7 shows the zeta-potential of droplets from emulsions A and E as well as the interfacial tension (see 4.1.3) of droplets from emulsion E as a function of time after the addition of SDS. Both the zeta-potential and the interfacial tension data reach a plateau within 90 minutes. At this point the adsorption of SDS to PDMS droplets is considered to have reached equilibrium.

Consequently zeta-potentials, interfacial tensions and relevant force measurements in the presence of SDS are determined after an equilibration time of 90 minutes.

The zeta potential of borosilicate in the presence of SDS did not change significantly suggesting SDS did not adsorb to the glass colloids; this was previously cited by Nespolo et al[16]. This is not surprising when one considers both SDS is an anionic surfactant and borosilicate is both hydrophilic and highly negatively charged in the solutions used, whereas PDMS is negatively charged and hydrophobic in nature, hence SDS tails may adsorb.

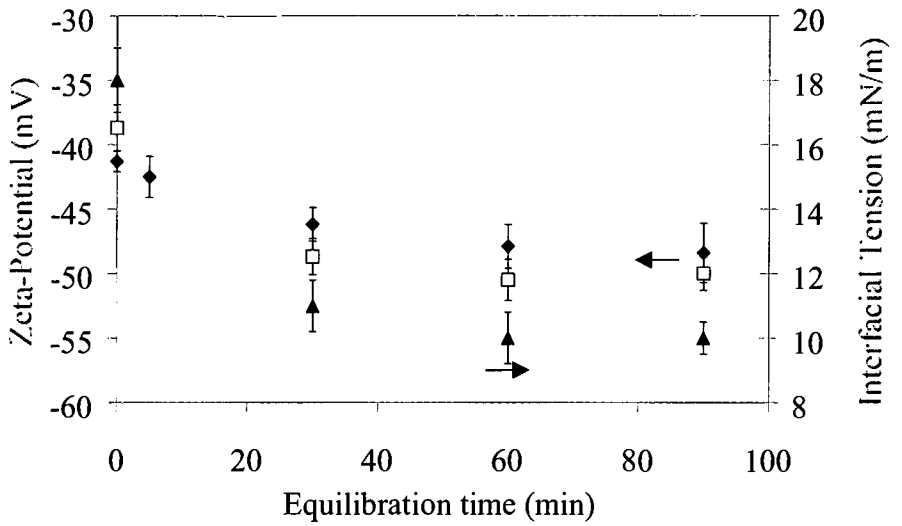


Figure 4.7 The zeta-potentials of droplets from emulsion A (◆) and E(□) and the O/W interfacial tension of bulk PDMS from emulsion E (▲) in 10^{-3} M KNO_3 ,10^{-3} M SDS at pH 9.5 plotted against the equilibration time.

4.1.4.3 Influence of Adsorbed Silica Nano-particles

The zeta-potential of non cross-linked PDMS droplets is plotted against the surface coverage of silica nano-particles in Figure 4.8. In depth discussion of the zeta-potential with adsorbed nano-particles is given in reference 177. Concisely, zeta potentials were determined using PALS, see section 3.2.3, and the surface coverage was determined from the difference in the initial and equilibrium particle concentrations (determined from turbidity) and the interfacial area. The adsorption of both hydrophobic and hydrophilic nano-particles increases the zeta-potential of droplets from ~-65 mV to ~-78 mV. This effect occurs at lower coverages of hydrophilic particles. It is worth noting that this PDMS droplet sample was prepared

under different conditions, i.e. volume fraction, ammonia content and reaction time, which result in a larger zeta-potential than the cross-linked droplets PDMS droplets shown in Figure 4.7 and Table 4.1.

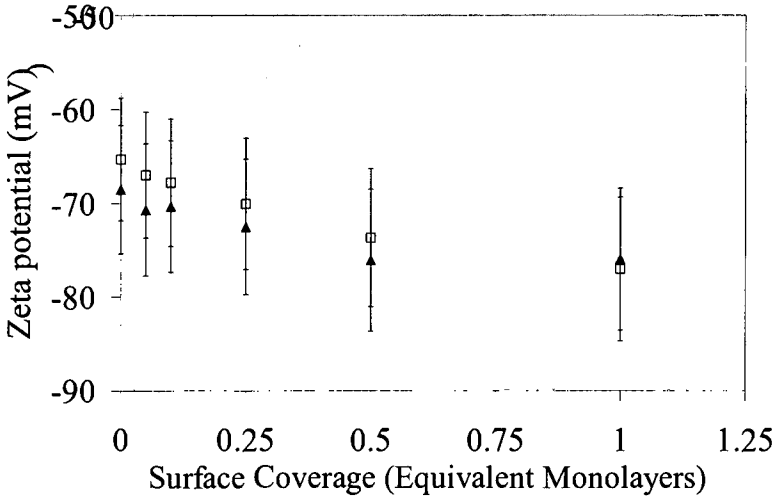


Figure 4.8 Zeta-potential of 0% cross-linked PDMS droplets with adsorbed hydrophobic (□) and hydrophilic (▲) silica nano-particles plotted against adsorbed amount.

4.2 Interaction Forces and Deformation of PDMS Droplets

4.2.1 Highly Cross-Linked Droplets

4.2.1.1 Interactions on Approach, Deformation and the Zero of Separation

Typical interaction force behaviour for a colloid probe approaching a PDMS droplet from emulsion A (50% cross-linking) in a background solution of 1mM KNO_3 at pH 9.5 is shown in Figure 4.9. It should be noted that the force is plotted against arbitrary separation, which in no way represents the actual or nominal separation. Interaction forces are purely repulsive and increase monotonically upon approach. At large separations the decay in the determined force is well described by the (linear) Poisson - Boltzmann (PB) equation (equation 4.2), depicted by the solid black line.

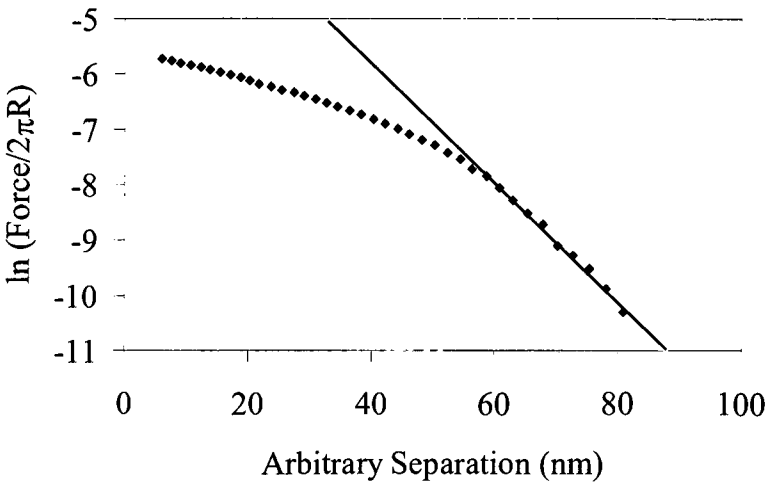


Figure 4.9 Approach force versus arbitrary separation curves determined between a glass probe (R = 3.5 μm) and a droplet from emulsion A (R = 0.3 μm) in a background electrolyte solution of 1 × 10^{-3} M KNO_3 at pH 9.5. Solid line represents the Poisson - Boltzmann equation with a Debye length of 9.6 nm.

$$F = 32\pi\varepsilon_0\varepsilon_r R\left(\frac{k_B T}{ze}\right)^2 \gamma_1\gamma_2\kappa e^{-\kappa h} \qquad \text{Equation 4.2}$$

Equivalent agreement with PB behaviour has also been reported for particle – droplet[15,17] and particle - bubble interactions.[12] This agreement suggests that repulsive electrical double layer forces dominate the interaction. On closer approach deviation is observed at small separations. This deviation is not a result of attractive forces, since these forces generally increase rapidly i.e. the van der Waals force is inversely proportional to the square of the separation, and thus interactions would not be monotonic. It is believed that, the droplet deformation remains insignificant in the

region where PB behaviour is observed and on closer approach the droplet compresses (deforms) resulting in an additional variation in separation unaccounted for and consequently the determined force deviates from the PB equation. Throughout this thesis, it will be shown that all droplets studied can be approximated by a hard sphere until a critical load, F_{crit}, is reached at which point deformation becomes detectable. In this instance (Figure 4.9) the decay of the determined force agrees with the PB equation for rigid bodies up to a load of 550 μN/m.

Clearly, when force is plotted against arbitrary separation, one cannot fully appreciate the range and magnitude of the surface forces, thus it is more desirable to plot force against the actual separation. A major difficulty with AFM measurements on deformable systems is that the zero of separation is ambiguous. For non-deforming bodies, the zero of separation is taken to be the point of constant compliance. However, with the finite range of surface forces, when one or both bodies in an AFM experiment are deformable the point of contact will not be as easily obtained. That is, where a body is deformable, constant compliance will not be observed at the point of first contact. Additionally, if surface forces are sufficiently large, deformation will occur prior to contact. Chapter 2 outlines five methods for determining the zero of separation and associated problems with these approaches. The approach used exclusively throughout this thesis involves applying the linear PB equation (equation 4.2) for rigid bodies to establish the zero of experimental separation. The zero of separation is established by laterally shifting force versus relative separation data such that the weak force tails coincide with the renormalized linear PB theory for rigid bodies. The rationale for such an approach is that rigid body behaviour, i.e. agreement with the PB equation, is observed at relatively large separations, as established in Figure 4.9 and subsequent figures below. Lee and Sigmund[4] recently used a similar approach to determine the separation between a silica colloid probe and a polytetrafluoroethylene surface in cyclohexane. However, in this instance, Lee and Sigmund[4] shifted the separation to coincide with van der Waals forces, rather than electrostatic forces.

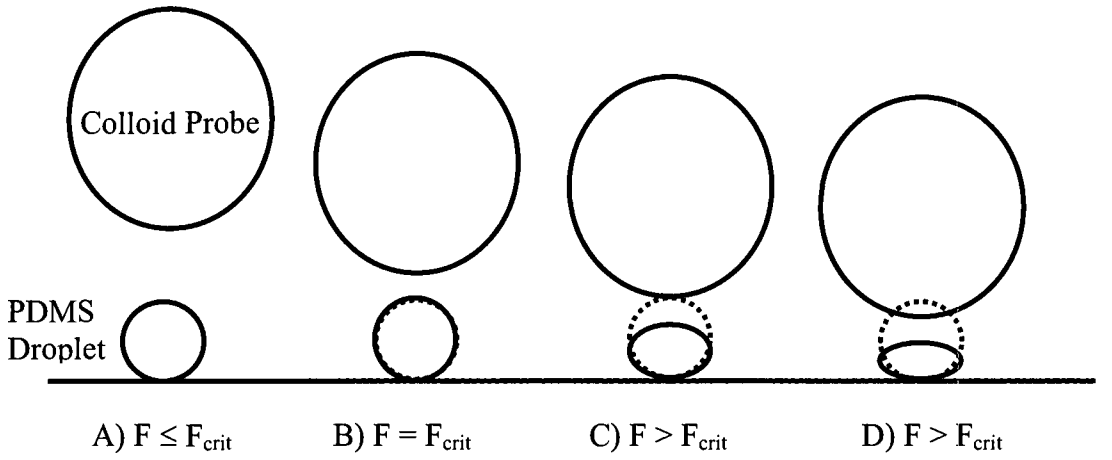


Figure 4.10 Schematic representation of the droplet - probe interaction at different separations. A) Surface forces are less than F_{crit} and the droplet maintains its shape. B) Surface forces are equal to F_{crit}, any subsequent increase in force will result in deviation from hard sphere behaviour. C) Surface forces are larger than F_{crit} and droplet begins to deform significantly, both the undeformed (dotted line) and the deformed (solid line) droplet profiles are shown. Here zero nominal separation is depicted; this is where the colloid probe comes into contact with the droplet in the absence of deformation. D) Surface forces significantly exceed F_{crit} resulting in deformation with a negative nominal separation.

A schematic diagram of droplet deformation at different separations is depicted in Figure 4.10. From this figure F_{crit} can be rationalised and nominal separation is defined as the separation between surfaces as if they remain undeformed. Negative nominal separations correspond to interpenetration of undeformed bodies; the actual separation is always positive. In Figure 4.11 the determined force from Figure 4.9, along with the associated unloading force, are plotted against nominal separation. Significantly Figure 4.11 shows hysteresis between loading and unloading forces, i.e. the force upon retraction is less than that on approach at a given nominal separation. This is considered a viscoelastic effect, and is discussed in greater detail in subsequent sections. Silica – PDMS interactions generally showed no adhesion; although small indiscriminate adhesions were reproduced in loading - unloading cycles for 50% cross-linked droplets, the magnitude of which was comparable to that of a cantilever tip stretching and detaching itself from individual bridged polymer molecules.[137] Adhesion resulting from contamination of the probe is dismissed since no adhesion was observed between the glass probe and the glass substrate both prior and subsequent to force investigations on the PDMS droplet. This observation suggests that the 50% cross-linked droplets may posses a 'hairy' surface, consisting of polymer

molecules extending into solution. However, droplets are believed to be smooth due to the presence of viscous, low molecular weight species at the interface. These small, indiscriminate adhesions were not observed in other droplets. The presence of these adhesions also suggests that the colloid probe contacts the PDMS droplet, however it is not clear, from force plots where this transition occurs. Alternatively, adhesion may result from an asperity on the colloid probe contacting the PDMS surface. It is plausible that the localised pressure on asperity is larger than the average pressure exerted on probe that may result in localised adhesion(s). This would account for both relatively small nature of the adhesion and the lack of adhesion in other droplets. That is, if contact occurs only at an asperity, then the contact area is small and one would expect small adhesions. Furthermore, determined forces are largest in interactions with emulsion A. If contact occurs as a result of the greater pressures at an asperity, it is likely that these pressures are not reached where droplets are more deformable and determined forces are smaller.

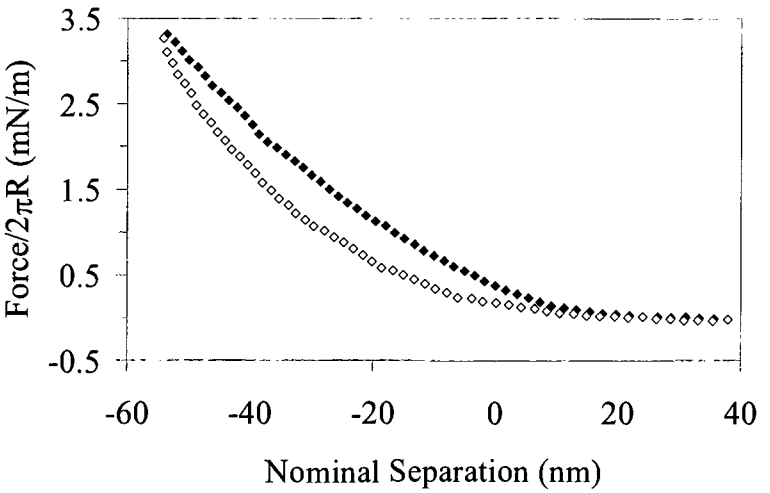


Figure 4.11 Interaction forces, upon approach (◆) and retract (◇), versus nominal separation between a glass probe (R = 3.5 μm) and a droplet from emulsion A (R = 0.3 μm) in a background electrolyte solution of 1×10^{-3} M KNO_3 at pH 9.5.

It should be recognized that the cross-linked PDMS droplets investigated in this study are prepared in batches and that statistical variation in cross-linking, and hence different mechanical (nano-rheological) properties, maybe envisaged from droplet to droplet, especially when comparing droplets from different batches. Investigations on

different individual droplets have confirmed this variability to be small. That is, from droplet to droplet there is a quantitative variation in the "deformability" and viscoelastic response. With this in mind, the variation of F_{crit} from 15 subsequent force measurements on a single droplet was determined to be 550 ± 30 μN/m. Furthermore the variation in F_{crit} determined from droplets from different emulsion batches prepared under the same conditions was less than ±10%; this variation is significantly smaller than the variation in F_{crit} between droplets of different cross-linking levels and comparable to the error in calculating the spring constant of the cantilever. It should be noted in all subsequent discussion of F_{crit}, values of F_{crit} are those of the average value determined from at least two, generally several, droplets.

4.2.1.2 Droplet Relaxation, Force Curve Hysteresis and Viscoelasticity

The hysteresis in Figure 4.11, i.e. where the force upon retraction is less than that on approach, is likely to be a result of viscoelastic behaviour. Plastic (permanent) deformation is ruled out by reproducing the same force-separation relationship in subsequent loading-unloading cycles. Plastic deformation would result in irreversible deformation within the droplet, resulting in the droplet appearing more rigid and thus altering F_{crit} on subsequent measurements.[133] Viscoelastic droplets relax back to their original shape over a given time, thus subsequent force plots are indistinguishable. Previously, force curve hysteresis arising from viscoelastic effects has been reported n AFM studies of polymer films,[147] polymer microspheres[116] and biological cells.[178-180] For viscoelastic bodies, force curve hysteresis arises when the drive velocity is comparable to the rate of relaxation as shown schematically in Figure 4.12. Under these conditions, at a given nominal separation the actual separation on retraction will be greater than on approach. Thus it follows that at infinitely slow drive velocities (loading and unloading) negligible force curve hysteresis would be expected.[21,22]

Hysteresis may also occur due to contact angle hysteresis if the contact area between the glass substrate and the PDMS droplet increases upon loading.[68,72,82] However, the large contact angle, discussed in section 4.1.3, and the lack of adhesion observed in force measurements implies the PDMS does not readily wet hydrophilic glass suggesting these effects are likely to be negligible.

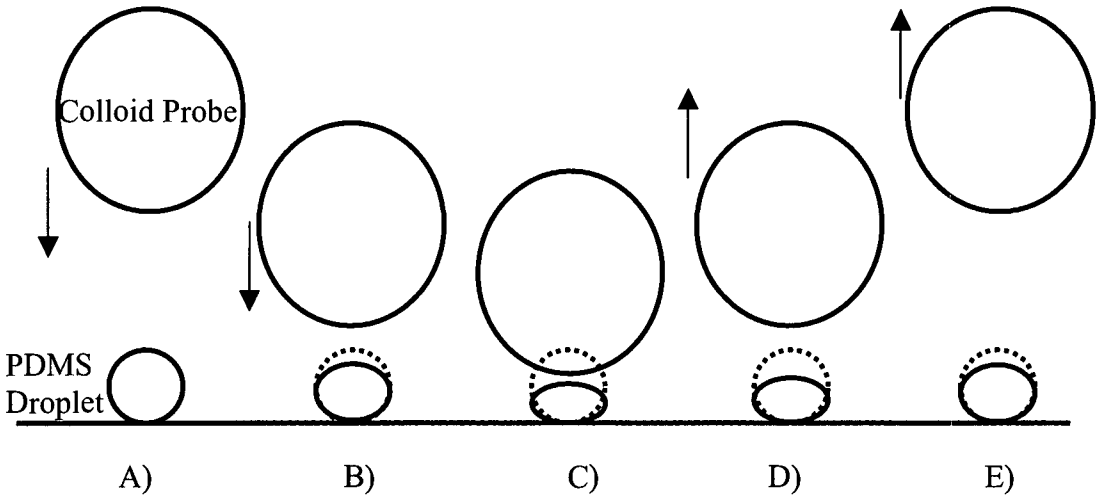


Figure 4.12 Schematic representation of the viscoelastic response during a colloid probe investigation. A) Colloid probe is approaching with surface forces $< F_{crit}$ and droplet remains undeformed. B) Colloid probe is approaching with surface forces $> F_{crit}$ and droplet begins to deform. C) Colloid probe is momentarily stationary between loading and unloading cycle with a negative nominal separation. D) Colloid probe is retracting, with the same nominal separation as in B. The PDMS Droplet begins to relax back to its original separation. E) Colloid probe is retracting with the same nominal separation as in A. Droplet has not completely recovered and has a different actual separation, despite the same nominal separation.

Figure 4.13 shows a series of force versus nominal separation plots for a highly cross-linked PDMS droplet and a silica probe determined at different drive velocities over the same trajectory. The viscoelastic response of a cross-linked PDMS droplet is demonstrated by the approach-rate-dependent force curve hysteresis. It is clear from the significant hysteresis observed that, for drive velocities in the range 0.25 to 4.0 μm/s, the droplet relaxation time is comparable to the time scale of the loading - unloading cycle. The area inside the hysteresis loop of the force versus nominal separation plot reflects the energy dissipation on retraction. In the case of the deformation investigation in Figure 4.13 the energy dissipated, estimated by integration of experimental data, is 5.7×10^{-18} J at 0.25 μm/s, 6.2×10^{-18} J at 1.0 μm/s, and 8.2×10^{-18} J at 4.0 μm/s. Upon deforming the highly cross-linked droplet, energy is stored elastically and dissipated viscously. Therefore, at relatively fast drive velocities, more energy is stored and droplets appear stiffer, then upon retraction more energy is dissipated and thus more hysteresis is observed. This behaviour is akin to a typical viscoelastic body, e.g. as described by the Kelvin-Voigt model. With this in mind, it is postulated that as the drive velocity is further increased the elastic modulus

will dominate the viscous modulus and the droplet will act more like a spring and the level of hysteresis will decrease. In practice, such drive velocities are outside the range of the current AFM instrument and the droplet exhibits viscoelastic hysteresis over all frequencies investigated.

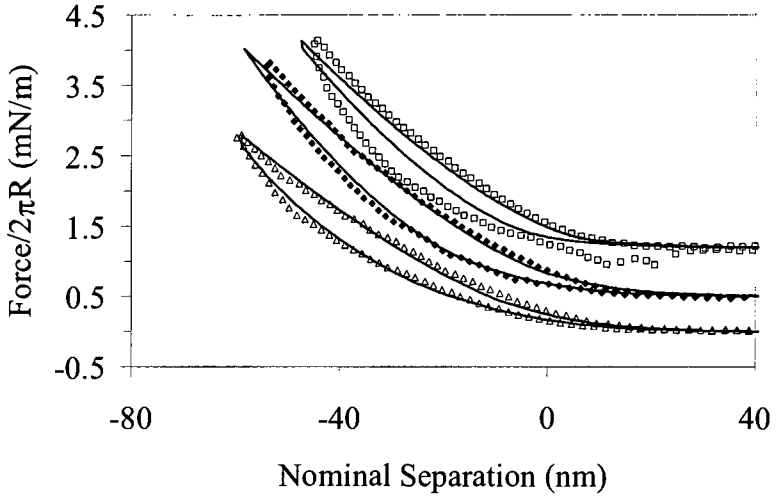


Figure 4.13 Interaction forces (approach and retract) versus nominal separation between a glass probe (R = 3.5 μm) and a droplet from emulsion A (R = 0.3 μm) in a background electrolyte solution of 1×10^{-3} M KNO_3 at pH 9.5 and at drive velocities: 0.25 μm/s (△) 1.0 μm/s (◆) 4.0 μm/s (□). The solid black lines show theoretical force curves using the following nano-rheological parameters: E_0 1.2 MPa, E_∞ 0.8 MPa, τ 0.12 s (see section 4.2.1.3.). For clarity 1.0 μm/s and 4.0 μm/s data has been offset by 0.5mN/m and 1 mN/m respectively.

In further exploring the viscoelastic response of a highly cross-linked PDMS droplet the influence of the maximum applied load on force versus nominal separation plots was determined (Figure 4.14). Variation in the applied load was achieved at constant drive amplitude by altering the point at which the piezo crystal starts the drive. In this manner the approach rate remains constant, which would not be the case if the drive amplitude were varied. That is, the influence of the applied load is investigated without changing the approach rate. The energy dissipation at maximum applied loads of 2.1, 3.2 and 6.0 mN/m was 2.6×10^{-18}, 6.2×10^{-18} and 14.4×10^{-18} J, respectively. These findings confirm the viscoelastic nature of these cross-linked droplets.

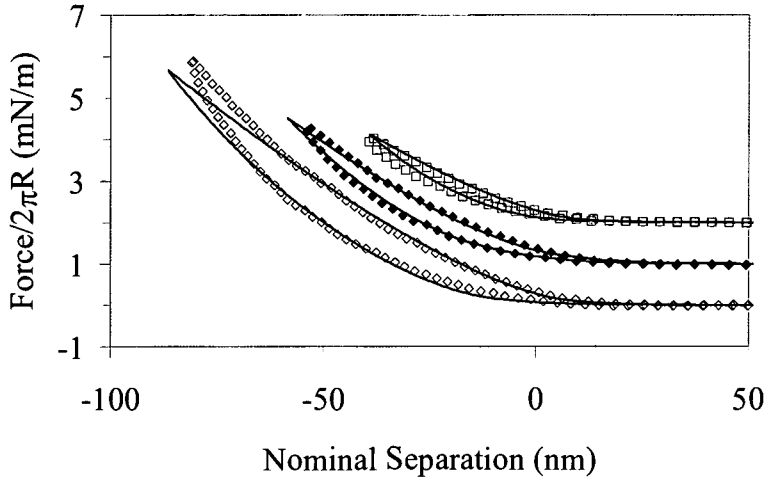


Figure 4.14 Interaction forces (approach and retract) versus nominal separation between a glass probe (R = 3.5 μm) and a droplet from emulsion A (R = 0.3 μm) in a background electrolyte solution of 1×10^{-3} M KNO_3 at pH 9.5 and at maximum loading forces of 2.1 (□), 3.2 (◆) and 6.2 (◆). The solid black lines show theoretical force curves using the following nano-rheological parameters: E_0 1.2 MPa, E_∞ 0.8 MPa, τ 0.12 s (see section 4.2.1.3). For clarity force measurements have been offset by 1.7 mN/m (□) and 1.0 mN/m (◇)

4.2.1.3 Viscoelastic Theory for the Determination of Nano-rheological Properties

It was demonstrated in Figure 4.11 that droplets interact prior to contact and thus comparisons with traditional contact theories such as JKR theory are inappropriate. Throughout this thesis, deformation of viscoelastic droplets has been described using Attard's theory[21,22] for the deformation of viscoelastic particles. This approach considers that viscoelastic particles can be described by long term (E_∞) and short term (E_0) elastic limits (defined in section 2.2.1) and a characteristic relaxation time (τ). For each droplet type nano-rheological parameters were determined by calculating a series of different theoretical force plots for a set of parameter values, then by systematic variation of the parameters, the nano-rheological parameters were taken to be those which best described a selection of four different experimental force plots (see section 3.2.5.5). Figure 4.13, shows experimentally and theoretically determined interaction forces between glass probe and a droplet from emulsion A at different drive velocities. Theoretical fits are in good agreement with determined interactions at drive velocities of 1 and 0.25, μm/s but underestimate the observed hysteresis observed at 4 μm/s. It is believed that the extent of hysteresis is influenced by the small adhesion observed in this particular experiment. No such discrepancies were observed for other droplets.

For this droplet from emulsion A the values for E_0, E_∞ and τ were determined to be 1.2 x 10^6 Nm^{-2}, 0.8 x 10^6 Nm^{-2} and 0.12s, respectively. Differences in nano-rheological parameters owing to batch variations were quantified for all droplets studied and determined to be ±10%. However, in section 4.1.1, the determined elastic modulus (G') for the bulk material from these droplets varied between 5×10^4 and 8×10^4 Nm^{-2}, which is an order of magnitude smaller than the values for E_0 and E_∞. Reasons for this difference include:

- G' was determined from dynamic stress application to a compressed bed of cross-linked droplets rather than a true bulk sample. Slippage between droplets during measurement may result in an under-estimation of G'.
- Interfacial properties of the droplets may also contribute to the determined nano-rheological parameters as deformation of small droplets increases the surface area / volume ratio to a much greater extent than deformation of bulk material

Values for E_0 and E_∞ are in good agreement with reported values for E of commercially available, highly cross-linked PDMS i.e. (1.7×10^6 to 0.4×10^6 Nm^{-2}).[67-73] These studies assume the PDMS to be elastic, and determine a single elasticity parameter, E (defined above), by pressing PDMS lenses against a flat surface. Genieser et al[181] quantified the viscoelasticity of cross-linked PDMS using a lateral force microscope and reported an elastic modulus of 0.6×10^6 Nm^{-2} with the viscous modulus becoming significant at ~3 Hz, which is of the same order as a 0.12s relaxation time. Clearly the material rheological properties of PDMS samples is highly dependent on the exact composition and extent of cross-linking (as exemplified in sections 4.1.1 and in 4.2.3.1), however the agreement between the determined elasticity parameters and literature values is encouraging. It is also encouraging that, in agreement with the experimental observations, the viscoelastic theory predicts force curve hysteresis, whereas traditional elastic theories do not. The theory also predicts the approach rate and loading force dependency of the force curve hysteresis. Whilst Figure 4.13 and 4.14 show good agreement between theory and determined interactions at low loads, Figure 4.14 shows some deviation at larger loads. This deviation is a general phenomenon, observed for all cross-linked droplets at high loads and is likely to be due to a combination of two effects. Firstly, at larger loads,

the force measurement may be influenced by the substrate underneath the droplet. Deruelle et al[67] report an apparently larger elastic modulus when the deformation of a polymer ribbon was significant (~10% or larger) in comparison with its thickness. This amount of deformation compares well with a nominal separation of ≈-60 nm for 600nm droplets, at which deviation from theory is first observed. Secondly, the cross-linking within the droplet may be heterogeneous and thus its deformation may not be described by a single viscoelastic element. That is, since MTES has a lower solubility than DEDMS, it may nucleate faster[156] during droplet preparation, This would result in a more densely cross-linked, and thus more rigid, core. Observations of inhomogeneous cross-linking have been reported in studies of polymer films.[182] These effects could be overcome with a more sophisticated model, incorporating more elastic moduli and relaxation times. However, this is beyond the scope of the current research.

4.2.2 Liquid Droplets of Newtonian PDMS

4.2.2.1 Interaction Forces, Deformation and Relaxation

Figure 4.15 shows a typical interaction force plot for a glass probe approaching a droplet from emulsion E (30% cross-linker, Newtonian PDMS) in a background solution of 1mM KNO_3 and at pH 9.5. In agreement with equivalent interactions for a

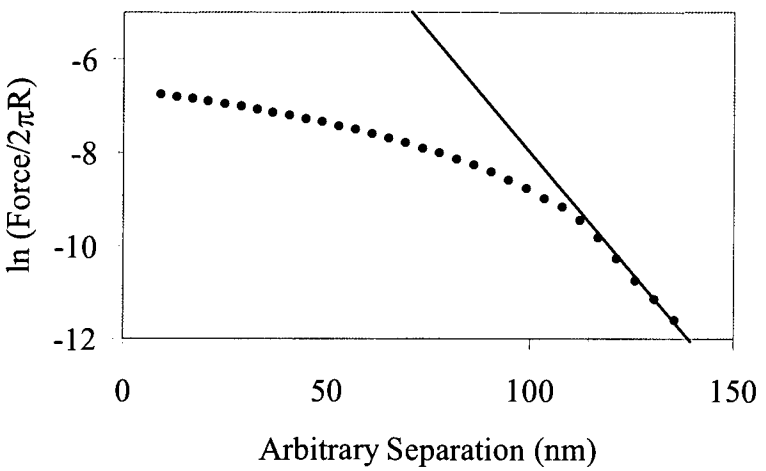


Figure 4.15 Log of the approach force versus arbitrary separation curves for a glass probe (R = 3.5 μm) interacting with a droplet from emulsion E (R = 0.25 μm) in a background electrolyte solution of 1×10^{-3} M KNO_3 at pH 9.5. Solid line represents the Poisson - Boltzmann equation with a Debye length of 9.6 nm.

highly cross-linked droplet (see Figure 4.9) the forces are repulsive, increase monotonically and at large separations show behaviour predicted by the PB equation. For the liquid-like droplet, F_{crit}, was significantly reduced in comparison with the cross-linked (viscoelastic) droplet i.e. 75 μN/m compared with 550 μN/m. In comparison, Hartley et al[15] reported F_{crit} of ~21 μN/m for interactions between a silica particle and a 300 μm decane droplet in 10^{-3} M $NaNO_3$ solution. Droplets composed of Newtonian fluids have no elastic modulus to resist deformation, thus F_{crit} of liquid droplets is smaller and likely to be more dependent on the Laplace pressure. The Laplace pressure is defined as the difference in pressure between the inside (P_{inside}) and outside ($P_{outside}$) of a droplet or bubble with respect to the interfacial tension and droplet radius, $P_{inside} - P_{outside} = 2\gamma/R$. This suggests that differences in F_{crit} are a result of different radii, and predicts a dependence on interfacial tension, discussed further in section 4.2.4.2.

Figure 4.16 shows the determined force from Figure 4.15 replotted against nominal separation with the associated force upon retraction also included. The interaction shows no hysteresis between loading and unloading, implying no dissipation of energy over the time scale of the deformation experiment. Additionally, no drive velocity dependence over the range of drive velocities capable by the AFM (0.1 - 30 μm/s) was observed. Similar observations have also been reported for a silica sphere interacting with a 300 μm n-decane droplet,[16] but contradict observations for a 19.7 μm polystyrene-divinylbenzene sphere interacting with a 500 μm n-hexadecane droplet.[17] In the latter case, velocity dependence was attributed to hydrodynamic forces; however, in this instance equation 2.7 gives an insignificant hydrodynamic force in comparison to the electrical double layer force. In general, drive velocity dependence and hysteresis (not resulting from adhesion or engulfment) are characteristics of viscoelastic bodies where the relaxation time of the droplet is comparable to the time scale of the experiment, and thus not expected for force interactions involving liquid droplets.

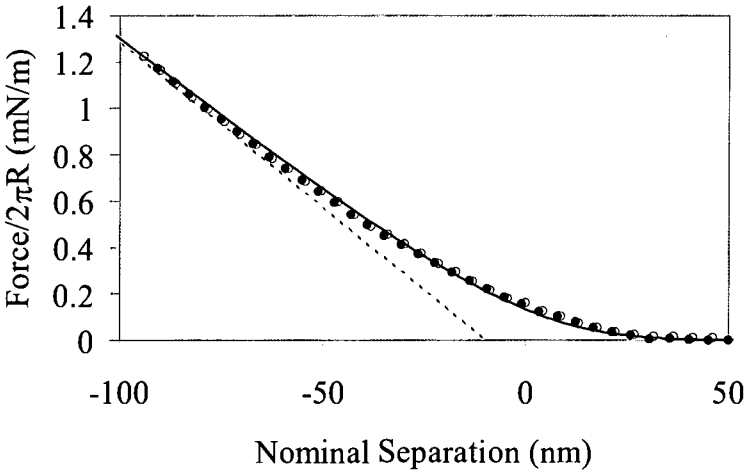


Figure 4.16 Interaction forces (approach (●) and retract (○)) versus nominal separation between a glass probe (R = 3.5 μm) and a droplet from emulsion E (R = 0.25 μm) in a background electrolyte solution of 1×10^{-3} M KNO_3 at pH 9.5. Solid line shows theoretical fit as outlined in section 3.2.5.5, dotted line shows the approach outlined by Ducker[10], in both cases $k_{drop} = 47$ mNm^{-1}

4.2.2.2 Spring Constant Determination

The interaction forces in Figure 4.16 shows a region of linear compliance (dotted line), which does not correspond to rigid body compliance. That is the determined force increases linearly with separation. The majority of reported colloid probe AFM investigations and theoretical treatments[18,19,90-93] on particle – bubble[10-12] and particle – droplet[14-16,154] interactions report this phenomenon. Whilst, these studies focus on interactions involving droplets (and bubbles) with considerably larger radii than in the current study, the agreement with literature is encouraging. Figure 4.16 demonstrates that, where the force is linear with respect to separation, then interactions can be characterised using Hooke's law. Ducker et al,[10] and other subsequent authors[11,12] used equation 3.3 (dotted line) to determine the spring constant of the droplet or bubble within this linear region. However, using this analysis one is limited to describing the linear region of a force plot. The approach used to describe linear behaviour in this thesis, outlined in section 3.2.5.5, describes the entirety of the force plot including the region where surface forces are significantly influencing the data. Encouragingly, both approaches result in equivalent values for the spring constant without discrepancy. For the force - separation relationship shown in Figure 4.16 the determined spring constant is 47 mN/m.

4.2.3 The Influence of Bulk Rheology, pH and Radius on Droplet Deformation

4.2.3.1 The Influence of Bulk Rheology on Interaction Forces

Typical interactions of a glass sphere approaching PDMS droplets with various levels of cross-linking (30 – 50%) in a background solution of 1mM KNO_3 at pH 9.5 are presented in Figure 4.17. It was demonstrated in section 4.1.1 that this range of cross-linking results in viscoelastic droplets with G' varying from ~8×10^4 to ~8×10^3 Nm^{-2} and viscous droplets with η varying from 0.6 to 2.6 $Nm^{-2}s$. Despite extensive variation in the bulk rheology, interaction forces are entirely repulsive, increase monotonically, with a force region at large separations where no deformation occurs. This observation implies that the analysis approach used to determine the zero of separation in 4.2.1.1 is applicable to all determined forces-separation relationships for emulsion droplet samples in Figure 4.17. Closer inspection of Figure 4.17 shows that the deviation from the PB equation is less pronounced for the more cross-linked droplets. F_{crit} and G' for the bulk PDMS material is plotted against the extent of cross-linking in Figure 4.18. F_{crit} increases exponentially with the level of cross-linking and a general linear correlation between the elastic modulus and F_{crit} can be identified. However plotting F_{crit} against the elastic modulus, see inset, reveals values do not pass

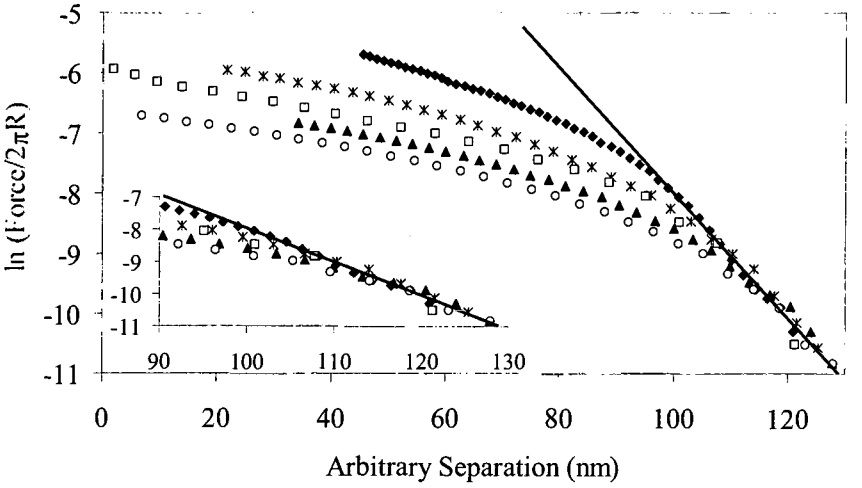


Figure 4.17 Approach force versus arbitrary separation curves for a glass probe (R = 3.5 μm) interacting with a droplet from emulsion A (◆), B (*), C (□), D (▲), E (○) in a background electrolyte solution of 1×10^{-3} M KNO_3 at pH 9.5. Solid line represents the Poisson - Boltzmann equation with a Debye length of 9.6 nm. Inset shows an enlarged region where forces decay at the same rate predicted by Poisson - Boltzmann equation.

through the origin, suggesting that F_{crit} is not solely dependent on the elastic modulus. It is shown below, 4.2.4 and 4.2.5, that F_{crit} and thus droplet deformability are also dependent on interfacial effects.

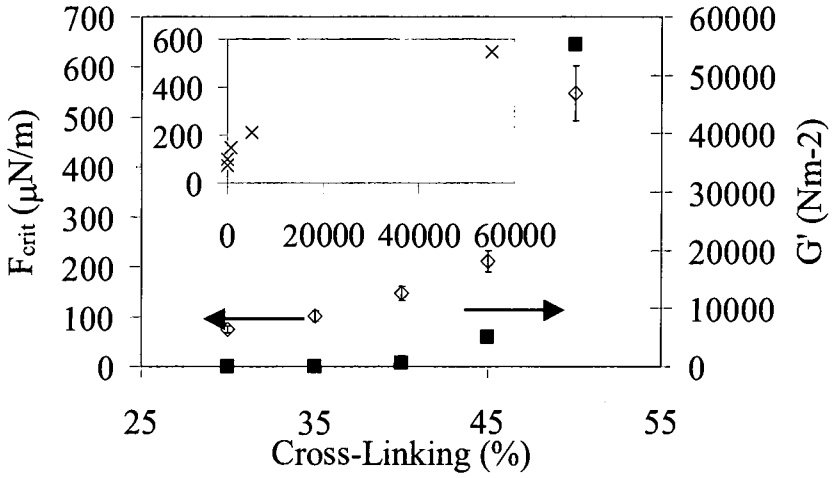


Figure 4.18 F_{crit} (◇) for droplet and elastic modulus for bulk PDMS material (determined at 1 Hz, 10 Nm^{-2}), (■) versus droplet cross-linking concentration. Inset replots F_{crit} against elastic modulus

The determined forces in Figure 4.17 are replotted against nominal separation with the associated force upon retraction in Figure 4.19. Examining the interaction forces reveals that the different cross-linking levels result in interactions forces that vary by an order of magnitude. Furthermore, droplets from emulsions A, B and C exhibit viscoelastic behaviour i.e. force curve hysteresis and rate and loading force dependence, as outlined in 4.2.1, whereas droplets from emulsions D and E exhibit the Hookean behaviour outlined in section 4.2.2. It is interesting to note that the viscoelastic rheology of bulk samples of PDMS from emulsions A, B and C is reflected in the relevant force separation plots. The instantaneous relaxation of droplets from emulsions D and E results from the Newtonian rheology of the PDMS allowing the shape of the droplet to be governed by the internal (Laplace) and external pressures without time dependence.

Figure 4.19 also includes theoretical viscoelastic fits from Attard's theory using the nano-rheological parameters shown in Table 4.3. In each instance, where the amount of deformation was small, interactions were well described by the theoretical force plots. The range at which viscoelastic theoretical fits accurately described interaction

forces varied with cross-linking, i.e. interactions pertaining to droplet A deviate from theory at a nominal separation of ~ -60 nm, whereas interactions pertaining to droplet C agree with theory up to a separation of ~ -100 nm.

Table 4.3 Nano rheological parameters and spring constants used to describe interactions for PDMS droplets.

Emulsion & cross-linking	E_0 (Nm^{-2})	E_∞ (Nm^{-2})	τ (s)	G' (Nm^{-2})	$k_{droplet}$ (mN/m)
A (50%)	1.2×10^6	0.8×10^6	0.12	5.5×10^4	290
B (45%)	0.6×10^6	0.45×10^6	0.07	5.0×10^3	143
C (40%)	0.35×10^6	0.3×10^6	0.05	7.0×10^2	87
D (35%)	-	-	0	-	59
E (30%)	-	-	0	-	47

In general values for E_0 and E_∞ overestimate the determined bulk G' values by over an order of magnitude but are in good agreement with reported E values for a variety of cross-linked PDMS samples where time dependence wasn't assumed[67-73]. Possible reasons for this were outlined in 4.2.1.3, i.e. as a result of slippage during rheological

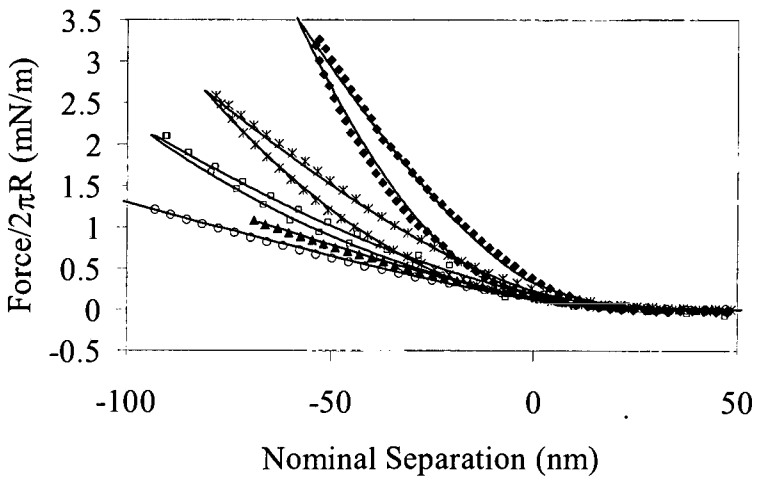


Figure 4.19 Force (approach and retraction) versus nominal separation for the interaction of a glass probe and a droplet from emulsion A (◆), B (✳), C (□), D (▲), E (○) in a background electrolyte solution of 1×10^{-3} M KNO_3 at pH 9.5. Solid black lines show theoretical force curve fits calculated using the nano-rheological parameters in Table 4.3 (next page).

measurement within the sample and interfacial effects.

For the highly cross-linked droplets from emulsion samples A, B and C the values for E_0 and E_∞ increase with increased cross-linking. The variation of the nano-rheological parameters of the droplets with respect to the cross-linking level may be readily rationalised. Upon increasing the degree of cross-linking the value for E_∞, which relates to the elastic modulus, increases from 0.35 to 1.2 MNm^{-2}, which correlates favourably with the proportional difference in load between droplets at nominal separations of –25 and –50 nm. Furthermore, the values of E_0 and E_∞ increase disproportionately, i.e. as the E_0:E_∞ ratio increases, both the relaxation time and the extent of force curve hysteresis are increased (for a perfectly elastic sphere, $E_0 = E_\infty$, and no time-dependence is observed). This behaviour is equivalent to a viscoelastic body, where the relaxation time is controlled by the relative values of the viscous and elastic moduli. This also correlates well with larger relative differences between elastic and viscous moduli with increasing cross-linking.

Hysteresis and rate dependence are observed when the interaction time, t, is of a similar magnitude to τ. Typically, the approach and retract cycles were varied from 4 to 0.25 s, however, the actual time droplets were within a proximity where interactions are significant is likely to be less than a third of this time. Thus the determined τ values in the range of 0.05 and 0.5 s are reasonable. Furthermore, the lower τ-value for droplets from emulsion B in comparison with droplets from emulsion A, results in droplets from emulsion B showing elastic behaviour at increased drive velocities; this notion is supported by the smaller amount of hysteresis (energy dissipation) observed for droplets from emulsion B (5.3×10^{-18} J) in comparison with droplets from emulsion A (6.2×10^{-18} J).

Interactions pertaining to droplets from emulsions D and E (Figure 4.19) are well described in terms of Hookean springs with spring constants of 59 and 47 mN/m, respectively. Whilst it is believed that the Laplace pressure, and thus interfacial tension, largely influences the deformation of liquid droplets, differences in the spring constants may also result from viscosity differences (2.6 compared to 0.6 $Nm^{-2}s$ for droplets from emulsion D and E respectively). For comparison, spring constants of droplets from emulsions A, B and C are shown in Table 4.3 (for these viscoelastic droplets the spring constants were approximated from force-separation relationships on approach). The determined spring constants are also plotted against F_{crit} in Figure 4.20. The observed linearity in this figure suggests the F_{crit} has been determined consistently throughout. That is, given that all interactions are reasonably well described by Hooke's law, the spring constant will be proportional to F_{crit} if the amount of deformation at this force is equivalent.

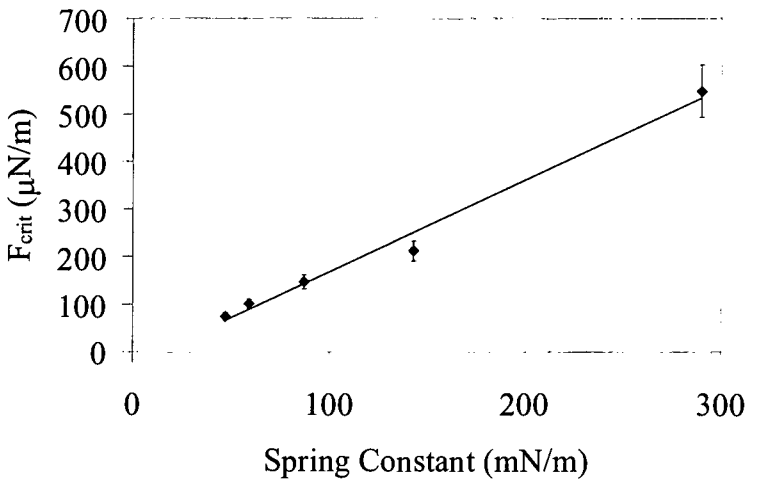


Figure 4.20 F_{crit} plotted against determined droplet spring constant.

In summation, the interactions of a droplet in a loading – unloading cycle are influenced by the droplet's bulk rheology. That is, where the bulk rheology of the droplet's material is viscoelastic, drive velocity dependence and force curve hysteresis are observed. Additionally, there is a general correlation between the nano-rheology, spring constant, F_{crit} and the bulk rheolgy, i.e. droplets are less readily deformed as the bulk elastic modulus is increased.

4.2.3.2 The Influence of pH and Surface Potential on Interactions Forces

The influence of pH on the interactions of a glass probe approaching both a cross-linked droplet (emulsion A) and a liquid-like droplet (emulsion E) are shown in Figure 4.21a and 4.21b respectively. Over this pH range, interactions remain repulsive and the determined force increases monotonically. Furthermore the decay of forces at large separations continues to show the characteristic behaviour associated with the PB equation. Interactions presented in both figures are considerably coincident. That is the solution pH has no significant influence over F_{crit}, or the extent of the deviation from the PB equation. However, the pH does influence the surface potential of both surfaces and thus the magnitude of the double layer force; therefore the same force will be measured at different separations.

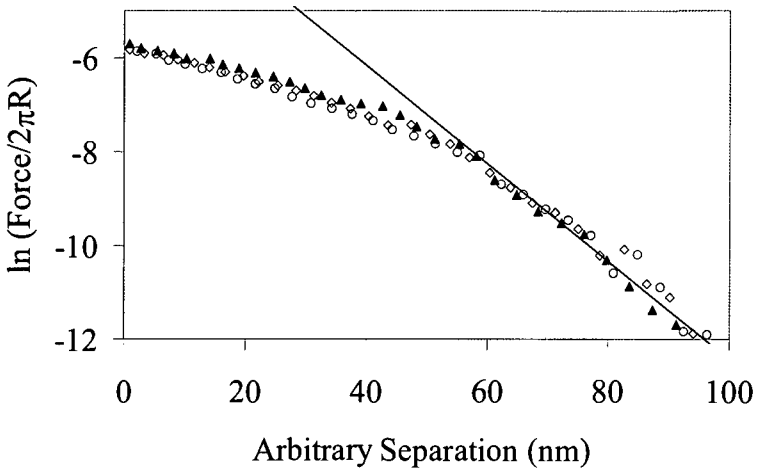


Figure 4.21a Log of the approach force versus arbitrary separation curves for a glass probe (R = 3.5 μm) interacting with a droplet from emulsion A (R = 0.3 μm), in a background electrolyte solution of 1×10^{-3} M KNO_3 at pH 9.5 (◇), pH 7 (▲) and pH 4.5 (○). Solid line represents the Poisson - Boltzmann equation with a Debye length of 9.6 nm.

In Figure 4.22a the force-separation relationships from Figure 4.21a are replotted against nominal separation along with the associated force upon retraction. Comparing the energy dissipation during deformation cycles, i.e. area within the hysteresis loops of unnormalised force-separation relationships, reveals only small relative differences over the pH range investigated (4.2×10^{-18} J at pH 9.5, 5.2×10^{-18} J at pH 7 and 4.8×10^{-18} J at pH 4.5); these are most likely a result of subtle variations in applied load. Figure 4.22a also includes theoretical fits to force – separation relationships using Attard's theory[21,22]. Under each pH investigated the theoretical

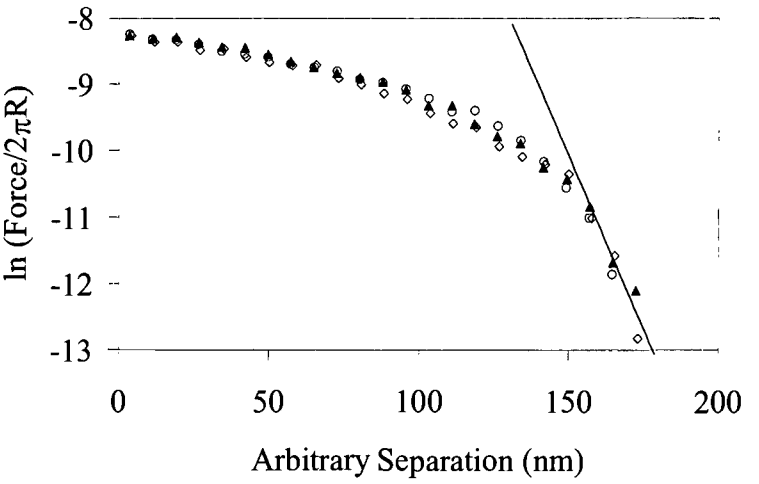


Figure 4.21b Log force versus arbitrary separation curves for a glass probe (R = 3.5 μm) approaching a droplet from emulsion E (R = 1.5 μm), in a background electrolyte solution of 1×10^{-3} M KNO_3 at pH 9.5 (◇), pH 7 (▲) and pH 4.5 (○). Solid line represents the Poisson - Boltzmann equation with a Debye length of 9.6 nm.

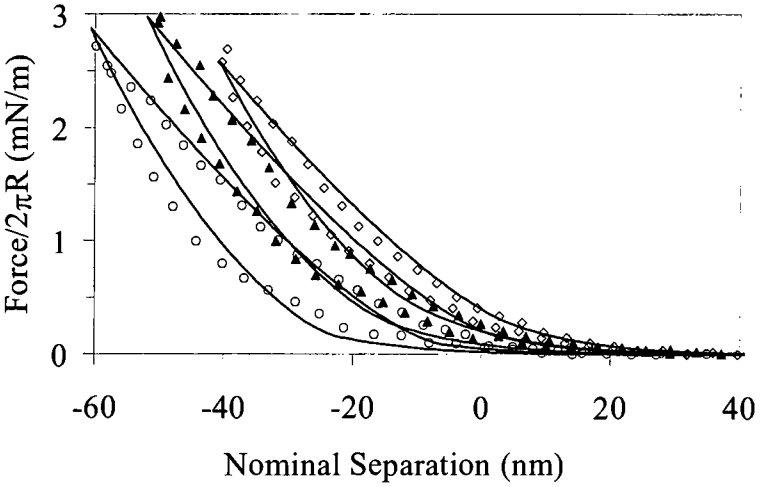


Figure 4.22a Interaction forces (approach and retract) versus nominal separation between a glass probe (R = 3.5 μm) and a droplet from emulsion A (R = 0.3 μm) at pH 9.5 (◇), pH 7.0 (▲), 4.5 (○) with a background electrolyte solution of 1×10^{-3} M KNO_3. Solid black lines represent theoretical viscoelastic fits with nano-rheological parameters: E_0 1.3 MPa, E_∞ 0.8 MPa, τ = 0.12 s (see text).

force curves were generated using the same nano-rheological parameters (E_0 = 1.3 MPa E_∞ = 0.8 MPa τ = 0.12 s), with the surface potentials equal to the zeta-potentials at the relevant pH, and small changes in the trajectory to account for the variation in applied loads. Determined interaction forces are well described by the same nano-rheological parameters suggesting that the droplet deformation and relaxation is independent of the pH and thus the surface potential. Likewise, the deformation and

relaxation of liquid-like droplets is also independent of the pH. Interactions from Figure 4.21b are replotted against nominal separation Figure 4.22b. In each case determined forces were entirely reversible and showed no drive velocity dependence. Furthermore all interactions were well described by a Hookean spring with a spring constant of 13 mN/m, (note R = 1.5 μm) confirming predictions that the deformability of liquid droplets is independent of the surface potential[19]

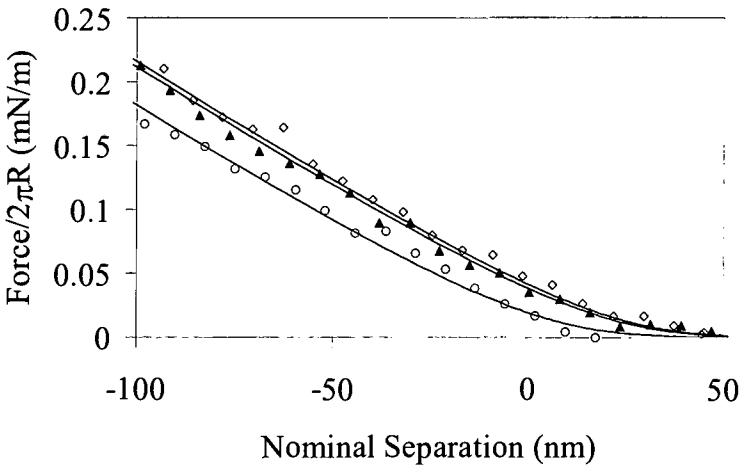


Figure 4.22b Interaction forces versus nominal separation between a glass probe (R = 3.5 μm) and a droplet from emulsion E (R = 1.5 μm) at pH 9.5 (◇), pH 7.0 (▲), 4.5 (○) with a background electrolyte solution of 1×10^{-3} M KNO_3. Solid black lines represent theoretical Hookean fits with k_{drop} = 13 mNm^{-1}

4.2.3.3 The Influence of Droplet Size on Droplet Deformation

It was proposed earlier that liquid droplets are entirely supported by their internal Laplace pressure. This implies that the amount of deformation under a specified applied load will be dependent on the droplet size. Droplets from emulsion E are entirely viscous and thus, with time are susceptible to coalescence if repulsive forces are reduced, i.e. droplets may be prepared with a range of sizes by reducing the pH of the emulsion to the isoelectric point. Specifically sized droplets were then selected for AFM investigation. Interaction forces for a glass sphere approaching droplets of different size from emulsion E are plotted against arbitrary separation in Figure 4.23. Interactions exhibited equivalent behaviour characteristic of the smaller liquid-like PDMS droplets e.g. (Figures 4.15 and 4.16) with PB behaviour observed at large separations. Figure 4.23 also demonstrates interaction forces and F_{crit} decrease as the droplet's radius increases. This behaviour is further investigated in Figure 4.24 where

the calculated spring constant of 30% cross-linked PDMS droplets (emulsion E) from a series of different sized droplets is plotted against the inverse of the droplet radius.

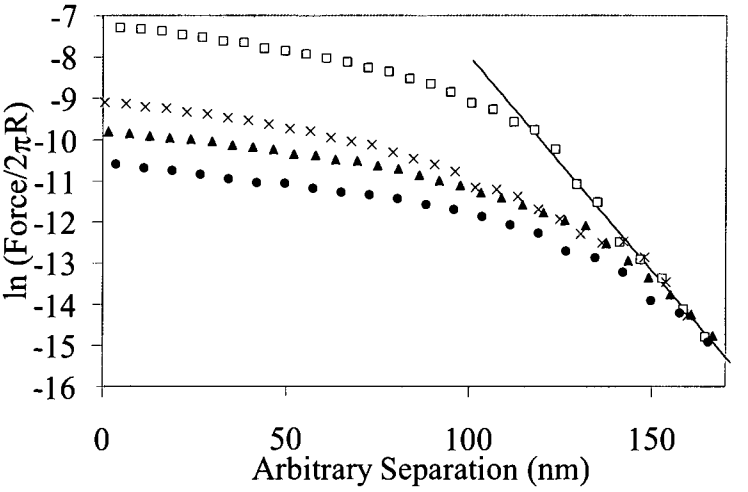


Figure 4.23 Log of the approach force versus arbitrary separation curves determined for a glass probe (R = 3.5 μm) interacting with droplets from emulsion E R = 0.5 μm (□), 3.2 μm (×), 7.5 μm (▲), 11.6 μm (•), in a background electrolyte solution of 1×10^{-3} M KNO_3 at pH 9.5. Solid line represents the Poisson - Boltzmann equation with a Debye length of 9.6 nm.

The figure demonstrates a dependence on Laplace pressure, highlighted by the close proportionality between the inverse of the radius and the determined spring constant. The scatter in the data in Figure 4.24 is likely to be a result of uncertainty in droplet size, estimated from in-situ optical microscopy and AFM imaging, rather than uncertainty in the spring constant. Previously, both theoretical[90,92] and experimental studies[10,15,86] of macroscopic droplets, and air bubbles, reported spring constants similar to the interfacial tension. Spring constants plotted in Figure 4.24 show that the spring constant of large droplets is considerably smaller than the interfacial tension. Badros[93] reported that spring constants are strongly dependent on the contact angle and that a minimum in the droplet spring constant occurs at relatively large contact angles (eg 160°), which compares well with the contact angle of 150° determined for PDMS droplets on hydrophilic glass AFM substrates here.

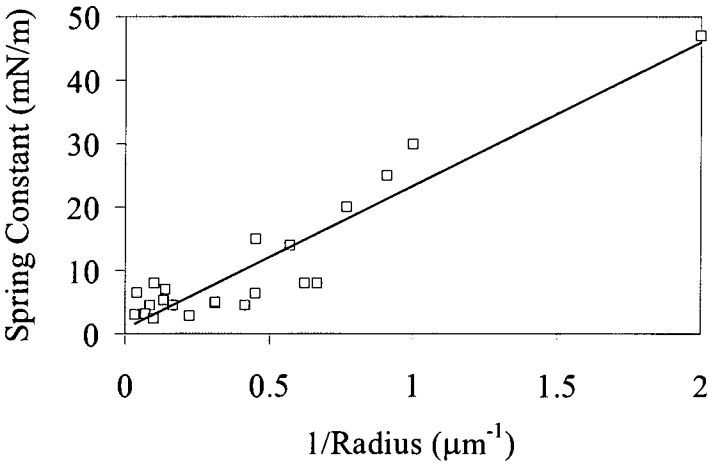


Figure 4.24 The spring constant of droplet E (30% cross-linked) plotted against the reciprocal of droplet radius.

4.2.4 Interactions Forces and Deformation in the Presence of SDS

4.2.4.1 Influence of SDS on Droplet of Varied Cross-Linking.

Figure 4.25 demonstrates the influence of adsorbed sodium dodecyl sulphate (SDS) for a glass probe interacting with droplets from emulsions A, C and E. Interaction forces were determined at pH 9.5 in a 1mM KNO_3, 1mM SDS, solution and compare well with interactions determined from the same droplets in the absence of SDS in Figure 4.17, i.e. forces are of the similar magnitude, monotonic and repulsive, with PB behaviour observed at large separations (here the calculated Debye length (κ^{-1}) is 6.7 nm). Comparing values for F_{crit}, prior and subsequent to the adsorption of SDS, indicates that the presence of SDS has no significant influence on F_{crit} for extensively cross-linked droplets (emulsion A). However, F_{crit} was reduced from 150 to 130 μN/m and from 75 to 39 μN/m for droplets from emulsions C and E, respectively. It was shown in section 4.1, that the presence of SDS increases the zeta-potential of PDMS droplets, and the interfacial tension decreases from 18 mN/m to 10 mN/m. The observed reduction in F_{crit} is considered to be a result of the reduced interfacial tension and not a result of zeta-potential variation. This is justified, as the force-separation behaviour did not change with surface potential in section 4.2.3.2. The observed decrease in F_{crit} resulting from the presence of SDS for droplets from emulsion C suggests that the Laplace pressure influences deformation even though the droplet is still substantially cross-linked. Interaction forces from Figure 4.25 are replotted against nominal separation along with the associated force upon retraction in

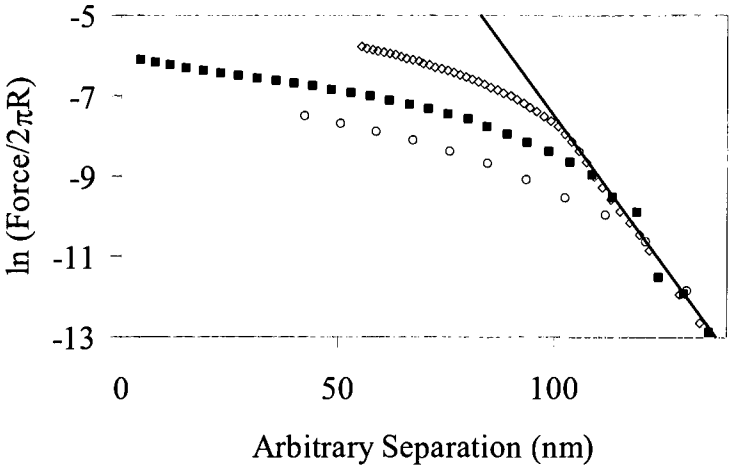


Figure 4.25 Log approach force versus arbitrary separation curves for a glass probe (R = 3.5 μm) interacting with a droplet from emulsion A (◇), C (■) and E (○) in a background electrolyte solution of 1×10^{-3} M KNO_3 and 1×10^{-3} M SDS at pH 9.5. Solid line represents the Poisson - Boltzmann equation with a Debye length of 6.7 nm.

Figure 4.26. Additionally, Figure 4.26 compares determined forces with interactions from Figure 4.19 where interaction forces were determined in the absence of SDS. Qualitative comparisons between interactions determined in the presence and absence of SDS can be misleading, i.e. the presence of SDS reduces the Debye length resulting in shorter ranged double layer forces that increase more rapidly with decreasing separation. Thus it follows that, the deformability is best evaluated by the nano-rheological parameters as shown in Table 4.4.

Table 4.4 Nano-rheological parameters for PDMS of droplets in the presence and the absence of SDS

Emulsion	E_0 (Nm^{-2})	E_∞ (Nm^{-2})	τ (s)	*Spring constant* (mNm^{-1})
A	1.2×10^6	0.8×10^6	0.12	290
with SDS	1.2×10^6	0.8×10^6	0.12	290
C	0.35×10^6	0.3×10^6	0.05	87
with SDS	0.33×10^6	0.28×10^6	0.05	79
E				47
with SDS				27

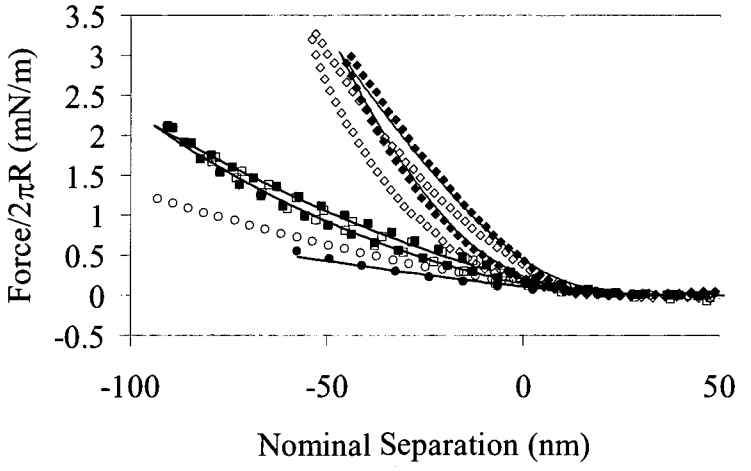


Figure 4.26 Approach and retraction force versus nominal separation curves for a glass probe (R = 3.5 μm) interacting with a droplet from emulsion A (◆), C (■), E (●) in a background electrolyte solution of 1×10^{-3} M KNO_3 and 1×10^{-3} M SDS at pH 9.5. Empty symbols show force data obtained from the same droplets in a background electrolyte solution of 1×10^{-3} M KNO_3 at pH 9.5. The solid black lines are the viscoelastic and Hookean fits using parameters in Table 4.4.

For 50% cross-linked droplets (emulsion A) the values of E_0, E_∞, τ and the spring constant remain unchanged in the presence of SDS. In contrast, the presence of SDS reduced E_0, E_∞ and the spring constant by ~10% for emulsion C, and decreased the spring constant of droplets from emulsion E by >40%. These observed changes in the nano-rheology, spring constants and F_{crit} values suggest that droplet deformation is controlled by an interplay between the Laplace pressure and the elastic modulus. Droplets from emulsion A are not influenced by the presence of surfactant since the influence of the Laplace pressure is minimal in comparison to the relatively large elastic modulus. Droplets from emulsion C are apparently influenced by both the Laplace pressure and the bulk rheology. Droplets from emulsion E, posses no bulk elastic modulus and thus are entirely supported by the Laplace pressure, thus a reduction in the interfacial tension significantly reduces droplet deformability.

4.2.4.2 Influence of SDS Concentration on the Deformability of Liquid-Like Droplets

Figure 4.27 compares interaction forces between a glass probe and a droplet (R = 7.5 μm) from emulsion E in the absence and presence of SDS. Interactions were determined in a background electrolyte solution of 10^{-3} M KNO_3 at pH 9.5 with SDS concentrations of 0.1, 1 and 10 mM. Interactions exhibit behaviour typical of other liquid-like droplet investigations, i.e. see Figure 4.15 and 4.17, with PB behaviour observed at large separations irrespective of the surfactant concentration. Additionally, the value of F_{crit} decreases with an increasing concentration of SDS. Interaction forces in Figure 4.27 are replotted against nominal separation with spring constant fits in Figure 4.28. Comparing interactions in Figure 4.28 reveals weaker forces, and thus more deformation, with increasing concentrations of the SDS. Figure 4.29 quantifies this concentration effect in terms of the interfacial tension. These interactions demonstrate that the spring constant of a droplet is approximately proportional to the interfacial tension, a result often reported for macroscopic droplets[15,16,18,19,90-92] further confirming that the deformation of liquid droplets is directly related to the Laplace pressure.

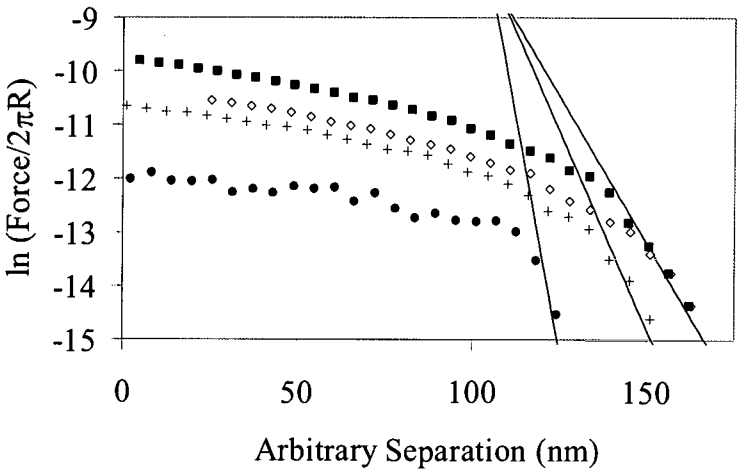


Figure 4.27 Log approach force versus arbitrary separation for the interaction of a glass probe (R = 3.5 μm) and a droplet from emulsion E (R = 7.5 μm) in a background electrolyte solution of 1 × 10^{-3} M KNO_3 at pH 9.5 in the absence of SDS (■) in the presence of 1 × 10^{-4} M SDS (◇), 1 × 10^{-3} M SDS (×), 1 × 10^{-2} M SDS (●). Solid line represents the Poisson - Boltzmann equations with Debye lengths (from right to left) of 9.6, 6.7 and 2.9 nm.

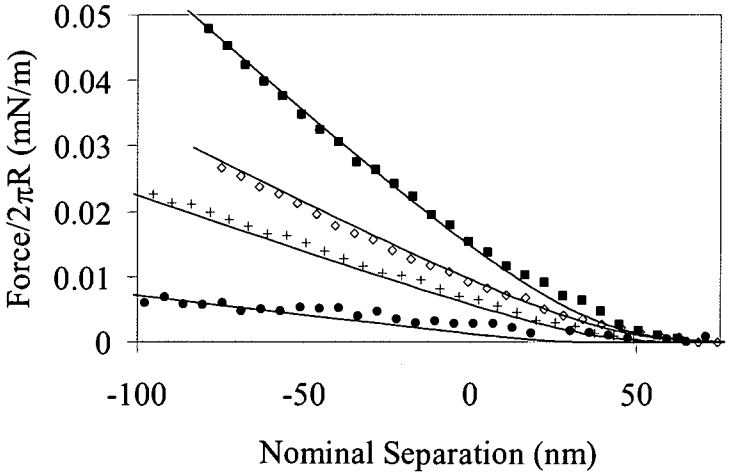


Figure 4.28 Force versus nominal separation curves determined for a glass probe (R = 3.5 μm) and a droplet from emulsion E (R = 10 μm) in a background electrolyte solution of 1×10^{-3} M KNO_3 at pH 9.5 in the absence of SDS (■) in the presence of 1×10^{-4} M SDS (◇), 1×10^{-3} M SDS (×) and 1×10^{-2} M SDS (●). Solid line represents the Hookean spring fits, with spring constants of 11, 6, 4.5 and 1.5 mN/m in height descending order.

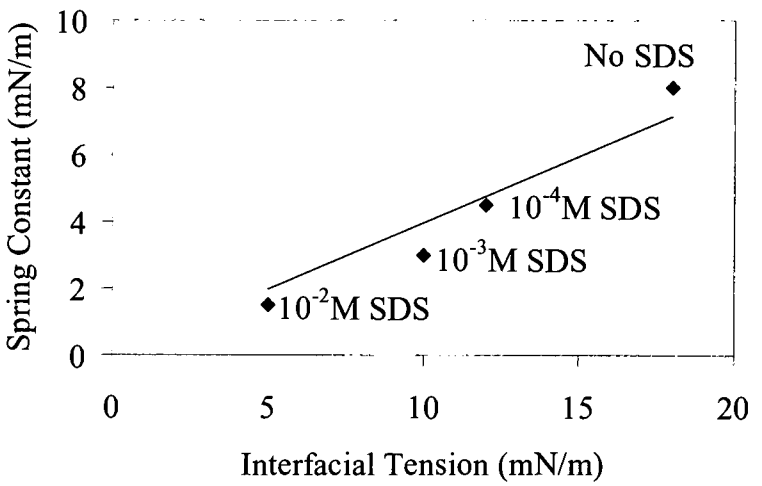


Figure 4.29 Droplet spring constants from force data in Figure 4.28 plotted against the interfacial tension with associated SDS concentrations.

4.2.5 Interaction Forces of Droplets with Adsorbed Nano-Particles

4.2.5.1 Influence of Adsorbed Hydrophilic Nano-Particles on Droplets with Varied Cross-Linking

Hydrophilic silica nano-particles were adsorbed on to PDMS droplets *in-situ* by introducing a 0.5 weight % of nano-particles, 1.0×10^{-2} M KNO_3, pH 9, solution into the AFM fluid cell and allowing 18 hours for adsorption to take place. After equilibration, the background solution was then replaced with a 1.0×10^{-3} M KNO_3 solution at pH 9.5 and then further equilibrated for 45 minutes before determining the interaction forces. Based on previous work,[171] particles are believed to adsorb in a Langmuir fashion with the estimated surface coverage being 0.8 of an equivalent hexagonally close packed monolayer. SEM micrographs of PDMS droplets with adsorbed hydrophilic silica nano-particles under similar conditions are shown in Figure 4.30. These micrographs demonstrate an adsorbed particles assemble at the interface as aggregates, approximately 50 nm in diameter, with close to complete monolayer coverage. Once dispersed in water, silica nano-particles form 50nm aggregates that subsequently adsorb to the PDMS droplet interface. This aggregate does affect the adsorption of nano-particles, as larger size of aggregates, results in larger energy barriers for coagulation.[177] However, it is not known whether adsorption of individual particles, as opposed to small aggregates will effect the droplet deformation.

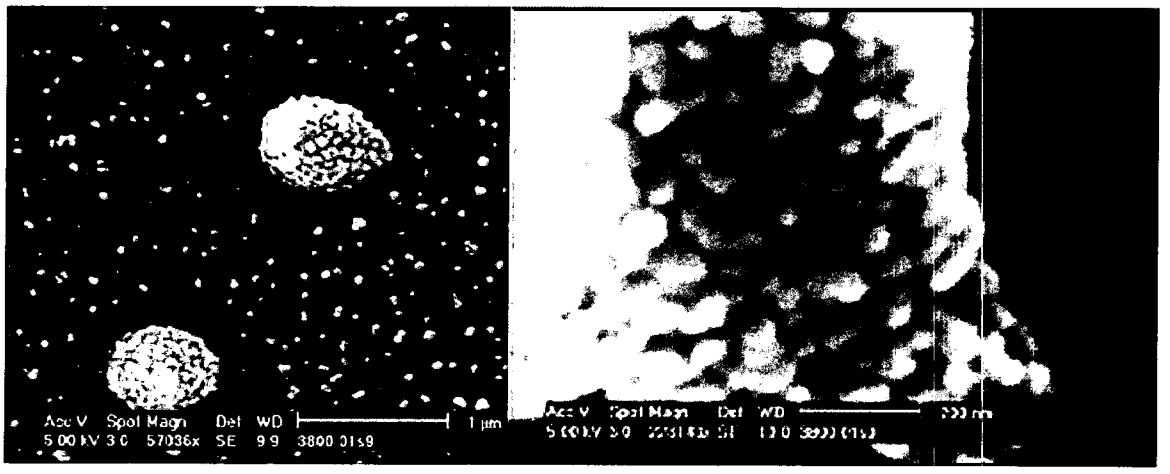


Figure 4.30 Freeze fracture SEM micrographs of non cross-linked PDMS droplets with a plateau coverage of silica particles at two levels of magnification. Images reproduced from reference 181.

Figure 4.31 compares the interactions of a glass probe approaching droplets from emulsions A, C and E with adsorbed, hydrophilic silica nano-particles. Interactions are similar to those determined without adsorbed nano-particles (Figure 4.17), i.e. interaction forces are of similar magnitude and exhibits PB behaviour at relatively large separations. Interestingly, the change in F_{crit} for droplets was within small separations thus suggesting that particle-laden droplets are more rigid. Figure 4.32 also includes theoretical fits to the determined interactions using nano-rheological parameters shown in Table 4.5, these values highlight that the decease in deformation is more pronounced for droplets with less cross-linking. These changes compare well with the observation of greater reductions in the nano-rheological parameters with decreased cross-linking for the adsorption of SDS discussed in section 4.2.4.1. Previously the adsorption of particles has been reported to increase the interfacial elasticity .[46-48] An increase in interfacial elasticity is consistent with the observed changes in force, that is, an decrease in deformation due to an increase in interfacial elasticity is expected to be more pronounced in more deformable droplets.

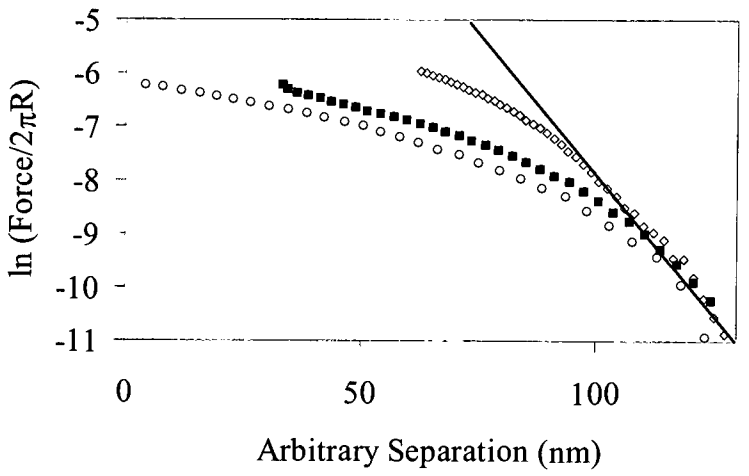


Figure 4.31 Log force versus arbitrary separation curves determined for a glass probe (R = 3.5 μm) approaching a droplet from emulsion A (◇), C (■), E (○) in a background electrolyte solution of 1×10^{-3} M KNO_3 at pH 9.5 in the presence of nano-particles adsorbed at 10^{-2} KNO_3. Solid line represents the Poisson - Boltzmann equation with a Debye length of 9.6.

Table 4.5 Nano-rheological parameters for droplets with (and without) adsorbed hydrophilic silica nano-particles

Emulsion	E_0 (Nm^{-2})	E_∞ (Nm^{-2})	τ (s)	*Spring constant* (mNm^{-1})
A	1.2×10^6	0.8×10^6	0.12	290
With nano -particles	1.4×10^6	1.0×10^6	0.14	348
C	0.35×10^6	0.3×10^6	0.05	87
With nano -particles	0.5×10^6	0.44×10^6	0.05	104
E	-	-	0	47
With nano -particles	-	-	0	73

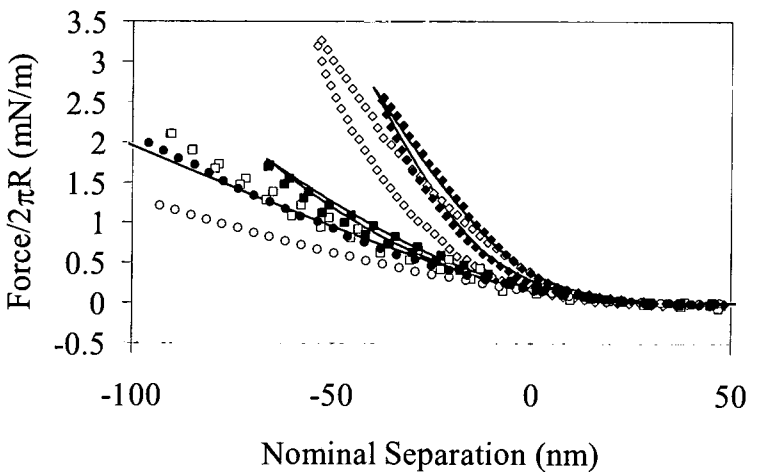


Figure 4.32 Interaction force versus arbitrary separation curves between a glass probe (R = 3.5 μm) and a droplet from emulsion A (◆), C (■), E (●) in a background electrolyte solution of 1×10^{-3} M KNO_3 at pH 9.5 in the presence of nano-particles adsorbed at 10^{-2} KNO_3. Empty symbols shows force data for droplets determined in a background electrolyte solution of 1×10^{-3} M KNO_3 at pH 9.5 in the absence of any adsorbed particles. Solid lines represent viscoelastic and Hookean fits with the values given in table 4.5

4.2.5.2 Influence of Hydrophobic Particles on Liquid-Like PDMS Droplets

The effect of nano-particle surface coverage on the PDMS droplet interface is further investigated by adsorbing hydrophobic silica nano-particles to a relatively large (R = 25 μm) PDMS 30% cross-linked droplet. Various nano-particle surface coverages were achieved by adsorbing nano-particles at different concentrations of KNO_3 (10^{-3} to 10^{-1} M). Increasing the electrolyte concentration reduces surface forces between particles, which results in more densely packed layers and/or multilayer surface coverage.[172,183] Figure 4.33 shows a nano-particle adsorption (surface coverage) versus salt concentration isotherm for hydrophobic nano-particles and PDMS droplets constructed from data within reference 172. The isotherm shows that increasing the electrolyte concentration results in increased nano-particle coverage. The datum point relating to 10^{-1} M KNO^3 relates to multilayer coverage > 4 equivalent monolayers. The exact coverage is unknown, and is a result of the electrolyte concentration exceeding the critical coagulation concentration. Figure 4.34 illustrates that the adsorption of hydrophobic silica nano-particles to PDMS droplets results in dense multilayer coverage with a high degree of interfacial structure, under the same conditions the adsorption of hydrophilic silica nano-particles resulted in monolayer coverage with no nano-particle aggregation. This suggests the adsorption free energy is more negative for hydrophobic particles

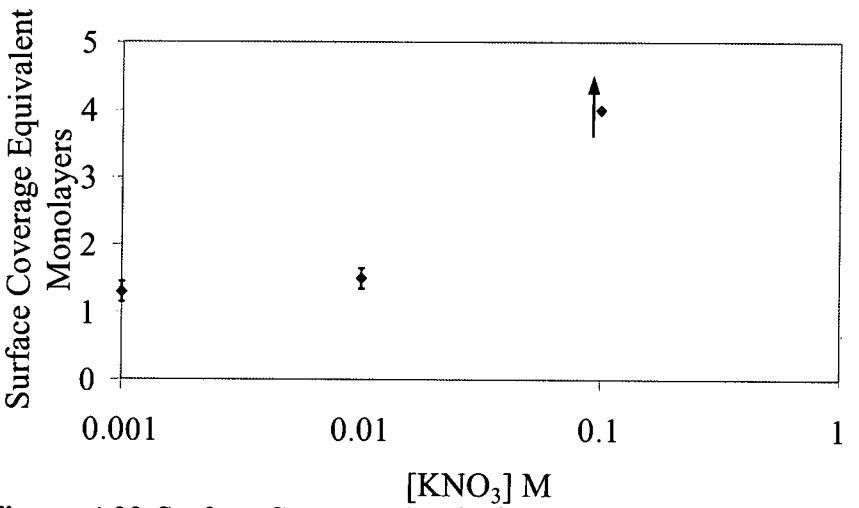


Figure 4.33 Surface Coverage (equivalent monolayer) of hydrophobic nano-particles at the PDMS droplet – water interface plotted against the salt concentration at which particles were adsorbed. Data taken from reference 182.

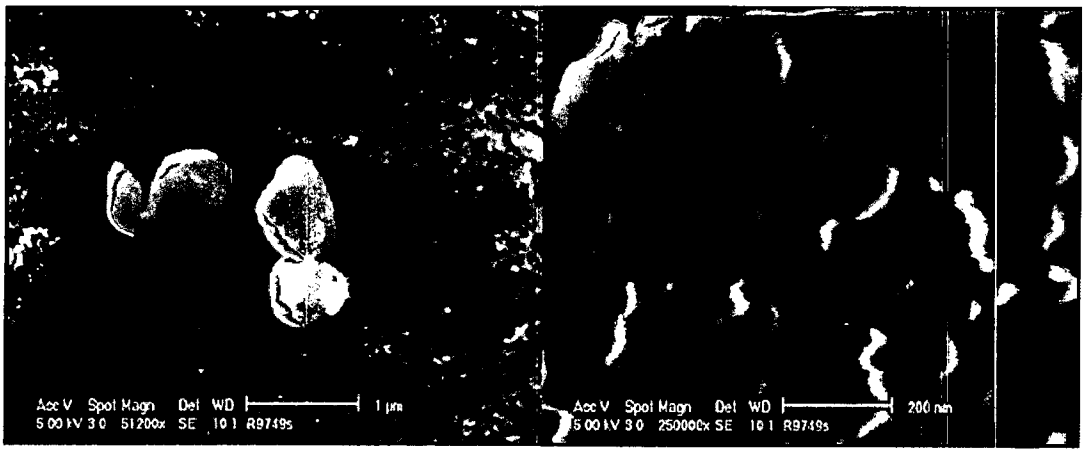


Figure 4.34 Freeze-fracture-SEM images of non cross-linked PDMS droplets with a multilayer coverage of hydrophobic silica adsorbed at pH=9 and in the presence of 10^{-2} M NaCl. Images reproduced from reference 182

Figure 4.35 shows the interaction between a glass probe approaching a PDMS droplet (R = 25 µm) from emulsion E, with adsorbed hydrophobic nano-particles at varying surface coverage. In each instance, particles were adsorbed over 18 hours, with forces determined in a 1.0×10^{-3} M KNO_3 solution at pH 9.5 after a 45 minutes equilibration time. Upon the inclusion and adsorbed of hydrophobic nano-particles at the droplet interface interactions remain repulsive, increases monotonically. It could be argued

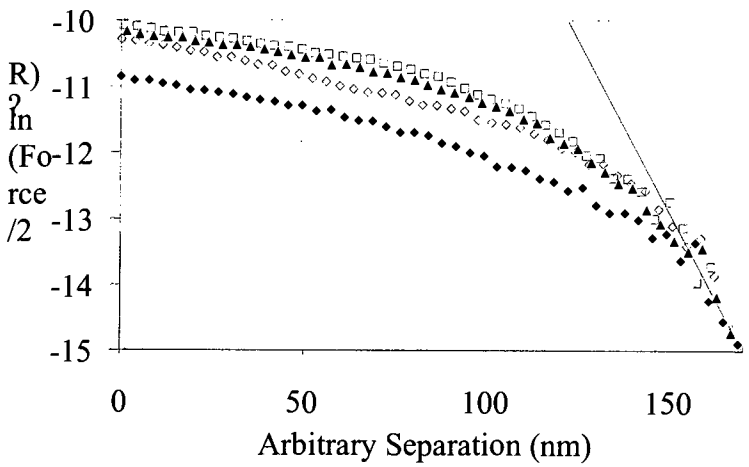


Figure 4.35 Approach force versus arbitrary separation curves determined for a glass probe (R = 3.5 µm) interacting with a relatively large (R = 25 µm) PDMS droplet from emulsion E in a background electrolyte solution of 1.0×10^{-3} M KNO_3 at pH 9.5 in the absence of adsorbed nano-particles (◆) nano-particles adsorbed in a 10^{-3} M KNO_3 solution (◇), nano-particles adsorbed at 10^{-2} KNO_3 solution (▲) and nano-particles adsorbed at 10^{-1} KNO_3 solution (□). Solid black lines show Poisson - Boltzmann behaviour

that PB behaviour is not observed unequivocally. However, if the zero of separation had not been calculated correctly then interactions would disagree with calculated Hookean fits. That is, the Hookean fits used throughout this thesis will give the same zero nominal separation, independent of the droplet spring constant. Thus it follows, where deformation can be described by a Hookean spring, then the zero of separation can be determined by laterally shifting force curves such that it coincides theoretical calculations. In doing this one must simultaneously fit the spring constant. A similar concept has been used in recent literature to determine the zero separations for much larger n-deance droplets.[184] In Figure 4.36 the determined force is replotted against nominal separation along with theoretical Hookean spring constant fits. In each case, interactions were entirely reversible and showed no rate dependence, whilst Hookean fits validate that nominal separations have been determined correctly. An increased force due to reduced deformation is consistent with reports of increased interfacial elasticity with increasing surface coverage.[46-48] In Figure 4.37 the determined spring constants are plotted against the surface coverage of adsorbed nano-particles. The spring constant increases with surface coverage, it is not thought that the variation is a result of interfacial tension, but rather interfacial elasticity. That is, the variation in determined spring constant for a droplet with approximately one equivalent monolayer and multilayer coverage is large considering that the interfacial tension is not expected to vary greatly. The presence of nano-particles is however, known to significantly alter the interfacial elasticity with vary coverages.

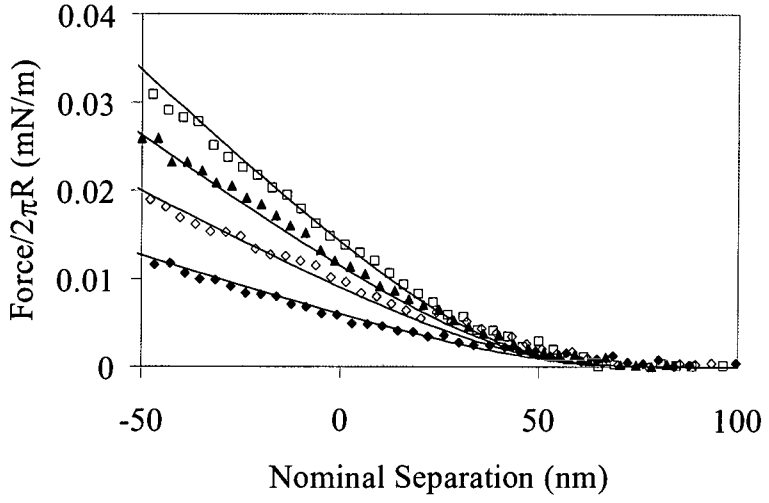


Figure 4.36 Force versus nominal separation curves determined for a glass probe (R = 3.5 μm) and a relatively large (R = 25 μm) PDMS droplet from emulsion E in a background electrolyte solution of 1.0×10^{-3} M KNO_3 at pH 9.5 in the absence of adsorbed nano-particles (◆) nano-particles adsorbed in a 10^{-3} M KNO_3 solution (◇), nano-particles adsorbed at 10^{-2} KNO_3 solution (▲) and nano-particles adsorbed at 10^{-1} KNO_3 solution (□). Solid black lines show theoretical 'Hookean' force plots for springs constants of 9, 7, 5 and 3 mN/m in height descending order.

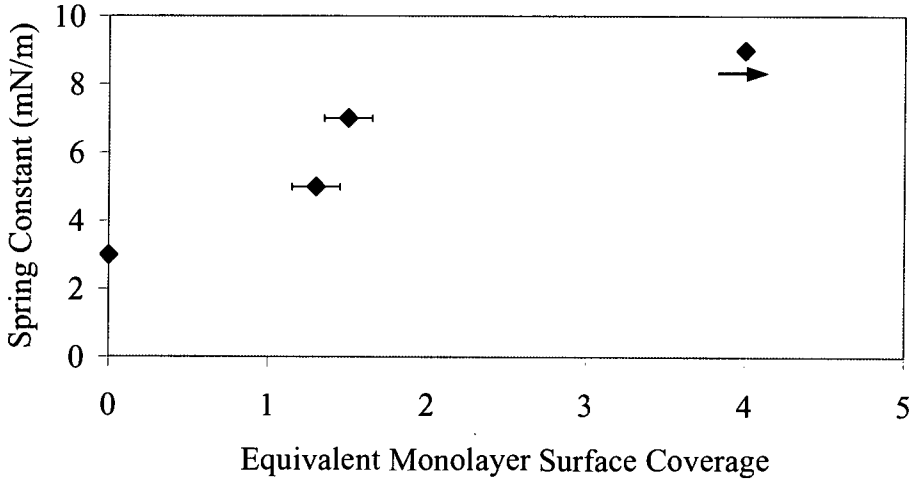


Figure 4.37 Determined PDMS droplets spring constant plotted against equivalent monolayer surface coverage of hydrophobic nano-particles

These findings with respect to the influence of adsorbed nano-particles on interaction and deformation of droplets have implications when considering the stability of particle stabilised (Pickering) emulsions.

5. Conclusions and Perspectives

The repulsive forces between a colloid probe and a variety of colloidal sized PDMS droplets in electrolyte solution have been determined using AFM. Interactions were well described by the combination of an electrical double layer force and droplet deformation. Upon approach the interactions were repulsive and increased monotonically. At large separations the repulsive forces are well characterised by the electrical double layer interactions of rigid particles. This apparent rigid body behaviour is observed up to a critical load, denoted here as F_{crit}. This value strongly depends on the amount of cross-lining, interfacial tension and droplet size. That is, F_{crit} decreases with decreasing cross-linking, interfacial tension and increasing droplet size. In this study F_{crit} was resolvable for highly deformable 30% cross-linked droplets as large as 50 μm (diameter). When loading forces exceed F_{crit} i.e. at smaller separations, interaction forces vary from those predicted for rigid bodies. With the observation of rigid body behaviour and independently determined zeta-potentials the zero of separation can be established by laterally shifting data to coincide with predict electrical double layer forces. Once the zero nominal separations has been determined one can calculate the extent of deformation. This approach has been used throughout this thesis for droplets with a wide range of deformability.

By systematically varying the level of cross-linking within the PDMS droplets and by adsorbing surfactant or nano-particles at the droplet-water interface, the influences of material properties, droplet size, interfacial tension and interfacial elasticity on droplet interaction forces and deformability were isolated. Highly cross-linked droplets are viscoelastic exhibiting force curve hysteresis with loading force and drive velocity dependence. Over the range of drive velocities investigated (0.25 to $4\mu ms^{-1}$) interactions were fitted with and well described by the theoretical model of Attard. To the authors knowledge this is the only soft contact model that allows accounts for the time dependence and hysteresis observed in viscoelastic systems. This model describes interactions with short term and long term elasticity parameters and a characteristic relaxation time. The long term elasticity parameter is equivalent to the conventional elasticity parameter where no time dependence is assumed. The short term elasticity parameter relates the increase in rigidity owing to viscous effects. When cross-linking was greater than 40% the determined values of the elasticity parameters ranged between 10^5 and 10^6 Nm^{-2} which compares well with literature

values for PDMS. Whilst there is no immediately apparent relationship between the relaxation time used in the model and that used in convention rheology, the two are thought to be comparable. Determined relaxation times seem reasonable, varying between 0.05 to 0.5 s. Despite the good agreement with predicted values, values failed to relate well to the determined bulk elastic modulus, most likely a result of droplets stability against coagulation. The adsorption of surfactant and nano-particles to these droplets resulted in minimal, if any, changes in fitted parameters. This suggests that, bulk material properties rather than interfacial effects controlled their deformation.

Droplets with low levels of cross-linking behaved distinctively different with highly cross-linked droplets. That is, there existed a linear relationship between the force and separation and a distinct lack of hysteresis and time dependence. These low level cross-linked droplets studied here could be described by a simple Hookean spring analysis, but were too small to apply any fully comprehensive published analysis. Clearly the development of such analysis would provide interesting insights and new research possibilities. Despite this, the Hookean spring analysis used here does allow quantitative comparison between droplets and including viscoelastic droplets at a chosen drive velocity. The determined spring constants of a small 30% cross-linked droplets, R = 0.25 μm, were an order of magnitude smaller than that of 50% cross-linked droplets with the same radius. Calculated spring constants of liquid droplets are linearly proportional to the surface tension and the reciprocal of the droplet radius (over a size range of 0.25 – 25 μm), suggesting that the Laplace pressure controls droplet deformation. Furthermore droplet deformation can be controlled by the adsorption of nano-particles (diameter ~ 50 nm), with greater surface coverages resulting in more rigid droplets, this effect is more pronounced for hydrophobic than hydrophilic nano-particles.

The large contrast in droplet deformation behaviour, i.e. bulk rheology dominated behaviour of highly cross-linked droplets, and interfacial behaviour dominating moderately cross-linked liquid droplets, is well demonstrated using the PDMS droplet system and thus the approach used within this thesis could be easily applied for inter droplet interactions as well as bio-colloids, foams and microcapsule interactions.

These investigations undertaken in this study lead to additional interesting research possibilities including:

- Examining the role of droplet deformability on adhesion.
- Investigating interaction forces with varying concentrations of electrolyte, in particular near the critical coagulation concentration.
- Influence of adsorbed polymeric layers on the interaction forces and deformation of droplets.
- Investigating the force required to adhere two PDMS droplets (symmetrical interactions), with comparisons to colloid stability studies.

References:

1. Ducker, W.A., Senden, T.J., Pashley, R.M., *Nature*, **1991**, *353*, p239
2. Rutland, M.W., Senden, T.J., *Langmuir*, **1993**, *9*, p412
3. Fieler, A., Jenkins, P., Ralston, J., *Phys. Chem. Chem. Phys.*, **2000**, *2*, p5678
4. Lee, S.-W., Sigmund, M.W., *J. Colloid Interface Sci.*, **2001**, *243*, p365
5. Carambassis, A., Jonker, L.C., Attard, P., Rutland, M.W., *Phys. Rev. Lett.*, **1998**, *80*, p5357
6. Zauscher, S., Klingenberg, D.J., *J. Colloid Interface Sci.*, **2001**, *119*, p497
7. Milling, A., Biggs, S., *J. Colloid Interface Sci.*, **1995**, *170*, p604
8. Danov, K.D., Denkov, N.D., Petsev, D.N., Ivanov, I.B., Borwankar, R., *Langmuir*, **1993**, *9*, p1731
9. Ducker, W.A., Senden, T.J., Pashley, R.M., *Langmuir*, **1992**, *8*, p1831
10. Ducker, W.A., Xu, Z., Israelachvili, J.N., *Langmuir*, **1994**, *10*, p3279
11. Fielden, M.L., Hayes, R.A., Ralston, J., *Langmuir*, **1996**, *12*, p3721
12. Preuss, M., Butt H.-J., *Langmuir*, **1998**, *14*, p3164
13. Vakarelski, I., Toritani, A., Nakayama, M., Higashitani, K., *Langmuir*, **2003**, *19*, p110
14. Mulvaney, P., Perera, J.M., Biggs, S., Griesser, F., Stevens, G.W., *J. Colloid Interface Sci.*, **1996**, *183*, p614
15. Hartley, P.G., Griesser, F., Mulvaney, P., Stevens, G.W., *Langmuir*, **1999**, *15*, p7882
16. Nespolo, S.A., Chan, D.Y.C., Grieser, F., Hartley, P.G., Stevens, G.W., *Langmuir*, **2003**, *19*, p2124
17. Aston, D.E., Berg, J.C., *J. Colloid Interface Sci.*, **2001**, *235*, p162
18. Chan, D.Y.C., Dagastine, R.R., White, L.R., *J. Colloid Interface Sci.*, **2001**, *236*, p141
19. Dagastine, R.R., White, L.R., *J. Colloid Interface Sci.*, **2002**, *247*, p310
20. Barnes, T.J., *PhD thesis, University of South Australia*, **2003**
21. Attard, P., *Phys. Rev. E*, **2001**, *63*, 061604
22. Attard, P., *Langmuir*, **2001**, *17*, p4322
23. Hunter, R.J., "*Foundations of Colloid Science*", 2nd ed., Oxford University Press, Oxford

24. Israelachvili, J.N. "*Intermolecular and Surface Forces*", 2nd ed., Academinc Press, London
25. Butt, H-J., Graf, K., Kappl, M., "*Physics and Chemistry of Interfaces*", Wiley-VCH Weinheim
26. Cappella, B., Dietler, G., *Surf. Sci. Reports*, **1999**, *34*, p1
27. Claesson, P.M., Ederth, T., Bergeron, V., Rutland, M.W., *Advances Colloid Interface Sci.*, **1996**, *67*, p119
28. Horn, R.G., *J. Am. Ceram. Soc.*, **1990**, *73*, p1117
29. Chan, D.Y.C., Pashley, R.M., White, L.R., *J. Colloid Interface Sci.*, **1980**, *77*, p283
30. McCormack, D., Carnie, S.L., Chan D.Y.C., *J. Colloid Interface Sci.*, **1995**, *169*, p177
31. Attard, P., *J. Phys. Chem.*, **1995**, *99*, p14174
32. Gregory, J., *J. Colloid Interface Sci.*, **1975**, *51*, p44
33. Hogg, R., Healy, T.W., Fuerstenau, D.W., *Faraday Trans.*, **1966**, *62*, p1638
34. Hamaker, H.C., *Physica*, **1937**, *4*, p1058
35. Lifshitz, E.M. *Soviet Phys.*, 1956, 2, p73; This original article is written in Russian, however the contents are well reviewed in: Israelachvili, J.N., *Quart. Rev. Biophys.*, **1974**, *6*, p341
36. Blake, T.D., Kitchener, J.A., *J. Chem. Soc., Faraday Trans. 1*, **1972**, *68*, p1435
37. Israelachivili, J.N., Pashley, R.M., *J. Colloid Interface Sci.*, **1984**, *98*, p500
38. Lee, C.Y., McCammon, J.A., Rossky, P.J., *J. Chem. Phys.*, **1984**, *80*, p4448
39. Prodgornik, R., *J. Chem. Phys.*, **1989**, *91*, p5840
40. Attard, P., *J. Phys. Chem.*, **1989**, *93*, p6441
41. Parker, J.L., Claesson, P.M., Attard, P., *J. Phys. Chem.*, **1994**, *98*, p468
42. Meagher, L., Craig, V.S.J., *Langmuir*, **1994**, *10*, p2736
43. Rabinovich, Ya.I., Yoon, R.-H., *Colloids Surf.*, **1994**, *93*, p263
44. Tyrrell, J.W.G., Attard, P., *Phys. Rev. Lett.*, **2001**, *87*, 176104
45. Steitz, R., Gutberlet, T., Hauss, T., Klösgen, B., Krastev, R., Schemmel, S., Somonsen, A.C., Findenegg, G.H., *Langmuir*, **2003**, *19*, p2409
46. Tambe, D.E., Sharma, M.M., *J. Colloid Interface Sci.*, **1993**, *157*, p244
47. Tambe, D.E., Sharma, M.M., *J. Colloid Interface Sci.*, **1994**, *162*, p1
48. Tambe, D.E., Sharma, M.M., *J. Colloid Interface Sci.*, **1995**, *171*, p456

49. de Gennes P.G., *Adv. Colloid Interface Sci.*, **1987**, *27*, p989
50. Esumi, K., "*Polymer interfaces and emulsions* " Marcel Dekker, New York 1999
51. Asakura. S., Oosawa, F., *J. Polym Sci.*, **1958**, *33*, p183
52. Attard, P., *J. Chem. Phys.*, **1989**, *91*, p3083
53. Richetti, P., Kékicheff, P., *Phys. Rev. Lett.*, **1992**, *68*, p1951
54. Biggs, S., Burns, J.L., Yan, Y., Jameson, G.J., Jenkins, P., *Langmuir*, **2000**, *16*, p9242
55. Milling, A.J., Kendall, K., *Langmuir*, **2000**, *16*, p5106
56. Chan, D.Y.C., Horn, R.G., *J. Chem. Phys.*, **1985**, *83*, p5311
57. Craig, V.S.J., Neto, C., *Langmuir*, **2001**, *17*, p6018
58. Pashley, R.M., Israelachvili J.N., *J. Colloid Interface Sci*, **1984**, *101*, p511
59. Chapel, J.P., *Langmuir*, **1994**, *10*, p4237
60. Colic, M., Fisher, M.L., Franks, G.V., *Langmuir*, **1998**, *14*, p6107
61. Johnson, K.L., Kendall, K., Roberts, A.D., *Proc. Roy. Soc. Lond. A.*, **1971**, *324*, p301
62. Tabor, D., *J. Colloid Interface Sci.*, **1977**, *58*, p2
63. Derjaguin, B.V., Muller, V.M., Toporov, Y.P., *J. Colloid Interface Sci.*, **1975**, *314*, p58
64. Horn, R.G., Israelachvili, J.N., Pribac, F., *J. Colloid Interface Sci.*, **1987**, *115*, p480
65. Vakarelski, I., Toritani, A., Nakayama, M., Higashitani, K., *Langmuir*, **2003**, *19*, p110
66. Chaudhury, M.K., Whitesides, G.M., *Langmuir*, **1991**, *7*, p1013
67. Deruelle, M., Hervet, H., Jandeau, G., Léger, L., *J. Adhesion Sci. Technol.*, **1998**, *12*, p225
68. Chaudhury, M.K., Owen, M.J., *Langmuir*, **1993**, *9*, p29
69. Chaudhury, M.K., Weaver, T., Hui, C.Y., Kramer, E.J., J. Appl. Phys., **1996**, *80*, p30
70. Chaudhury, M.K., Owen, M.J., *J. Phys. Chem.*, **1993**, *97*, p5722
71. Deruelle, M., Léger, L., Tirrell, M., *Macromolecules*, **1995**, *28*, p7419
72. Tirrell, M., *Langmuir*, **1996**, 12, p4548
73. Rundlöf, M., Karlsson, M., Wågberg, L., Poptoshev, E., Rutland, M., Claesson, P., *J. Colloid Interface Sci.*, **2000**, *230*, p441

74. Briscoe, B.J., Liu, K.K., Williams, D.R., *J. Colloid Interface Sci.*, **1998**, *200*, p256
75. Maugis, D., Barquins, M., *J. Phys. D. Appl. Phys.*, **1978**, *11*, p1989
76. Flanigan, C.M., Shull, K.R., *Langmuir*, **1999**, *15*, p4966
77. Burnham, N.A., Colton, R.J., *J. Vac. Sci. Technol. A*, **1989**, *7*, p2906
78. Hughes, B.D., White, L.R., *Quart. J. Mech. Appl. Math.*, **1979**, *32*, p445
79. Parker, J.L., Attard, P., *J. Phys. Chem.*, **1992**, *96*, 10398
80. Muller, V.M., Yushchenko, V.S., Derjaguin, B.V., *J. Colloid Interf. Sci.* **1980**, *77*, p91
81. Attard, P., Parker, J.L., *Phys. Rev. A*, **1992**, *46*, p7959
82. Attard, P., *J. Phys. Chem. B*, **2000**, *104*, p10635
83. Vinogradova, O.I., Feuillebois, F., *Langmuir*, **2002**, *18*, p5132
84. Connor, J.N., Horn, R.G., *Langmuir*, **2001**, *17*, p7194
85. Connor, J.N., Horn, R.G., *Faraday Discuss.*, **2003**, *123*, p193
86. Horn, R.G., Bachmann, D.J., Connor, J.N., Miklavcic, S.J., *J. Phys.: Condens. Matter.*, **1996**, *8*, p9483
87. Connor, J.N., Horn, R.G., Miklavcic, S.J., *Uzbek J. Phys.*, **1999**, *1*, p99
88. Miklavcic, S.J., Horn, R.G., Bachmann, D.J., *J. Phys. Chem.*, **1995**, *99*, p16362
89. Bachmann, D.J., Miklavcic, S.J., *Langmuir*, **1996**, *12*, p4197
90. Attard, P., Miklavcic, S.J., *Langmuir*, **2001**, *17*, p8217
91. Attard, P., Miklavcic, S.J., *J. Colloid Interface Sci.*, **2002**, *247*, p255
92. Attard, P., Miklavcic, S.J., *Langmuir*, **2003**, *19*, p2532
93. Bardos, D.C., *Surf. Sci.*, **2002**, *517*, p157
94. Petsev, D.N., Denkov, N.D., Kralchevsky, P.A., *J. Colloid Interface Sci.*, **1995**, *176*, p201
95. Derjaguin, B.V., *Kolloid Journal*, **1934**, *69*, p155
96. White, L.R. *J. Colloid Interface Sci.*, **1983**, 95, p286
97. Israelachvili, J.N., Adams, G.E., *J. Chem. Soc. Faraday Trans. 1*, **1978**, *74*, p975
98. Tabor, D., Winterton, R. H. S., *Proc. Roy. Soc. A.*, **1969**, *312*, 435
99. Pashley, R.M., *J. Colloid Interface Sci.*, **1981**, *83*, p531
100. Ruths, M., Granick, S., *Langmuir*, **1998**, *14*, p1804

101. Luengo, G., Pan, J., Heuberger, M., Israelachivili. J., *Langmuir*, **1998**, *14*, p3873
102. Zorin, Z.M., Churaev, N.V., Esipova, N.E., Sergeeva, I.P., Sobolev, V.D., Gasanov, E.K., *J. Colloid Interface Sci.*, **1992**, *152*, p170
103. Churaev, N.V., Ershov, A.P., Esipova, N.E., Iskandarjan, G.A., Madjarova, E.A., Sergeeva, I.P., Sobolev, V.D., Svitova T.F., Zakharova, M.A., Zorin, Z.M., Poirier, J.-E., *Col. and Surf A: Physiochemical and Engineering Aspects*, **1994**, *91*, p97
104. Aronson, M.P., Petko, M.F., Princen, H.M., *J. Colloid Interface Sci.*, **1978**, *65*, p296
105. Scheludko, A., Exerowa, D., *Kolloid-Z.*, **1957**, *155*, p39
106. Mysels, K.J., *Disc.Faraday Soc.*, **1966**, *42*, p42
107. Exerowa, D., Scheludko, A., *Chim. Phys.*, **1971**, *24*, p47
108. Velev, O.D., Constantinides, G.N., Avraam, D.G., Payatakes, A.C., Borwankar, R.P., *J. Colloid Interface Sci.*, **1995**, *175*, 68
109. Bergeron, V., Radke, C.J., *Langmuir*, **1992**, *8*, p3020
110. Cascão Pereira, L.G., Johnsson, C., Radke, C.J., Blanch, H.W., *Langmuir*, **2003**, *19*, p7503
111. Angarska, J.K., Dimitrova, B.S., Danov, K.D., Kralchevsky, P.A., Anaanthapadmanabhan, K.P., Lips, A., *Langmuir*, **2004**, *20*, p1799
112. Parker, J.L., Stewart, A.M., *Progr. Colloid Polym. Sci.*, **1992**, *88*, p162
113. Parker, J.L., *Langmuir* , **1992**, *8*, p551
114. Ederth, T., Tamada, K., Claesson, P.M., Valiokas, R., Colorado, Jr, R., Graupe, M., Shmakova, O.E., Lee. T.R., *J. Colloid Interface Sci.*, **2001**, *235*, p391
115. Ederth, T., Claesson, P., Liedberg, B., *Langmuir*, **1998**, *14*, p4782
116. Schmitt F.-J., Ederth, T., Weidenhammer, P., Claesson. P., Jacobasch, H.-J., *J. Adhesion Sci. Tech.*, **1999**, *13*, p79
117. Fröberg, J.C., Ederth, T., *J. Colloid Interface Sci.*, **1999**, *210*, p215
118. Attard, P., Schulz, J., Rutland, M.W., *Rev. Sci. Instrum.* **1998**, *69*, p3852
119. Roberston, S.K., Bike, S., *Langmuir*, **1998**, *14*, p928
120. Flicker, S.G., Tipa, J.L., Bike, S.G., *J. Col. Interf, Sci.*, **1993**, *158*, p317
121. Prieve, D.C., Frej, N.A., *Langmuir*, **1990**, *6*, p396

122. Robertson, S.K., Uhrick, A.F., Bike, S.G., *J. Colloid Interface Sci.*, **1998**, *202*, p208
123. Sober, D.L., Walz, J.Y., *Langmuir*, **1995**, *11*, p2352
124. Prieve, D.C., *Adv. Colloid Interface Sci.*, **1999**, *16*, p9274
125. Bevan, M.A., Prieve, D.C., *J. Chem. Phys.*, **2000**, *113*, p1228
126. Binnig, G., Quate, C.F., Gerber, Ch., *Phys. Rev. Lett.*, **1986**, *56*, p930
127. Smith, D.P.E., Binnig, G., Quate, C.F., *Appl. Phys. Lett.*, **1986**, *49*, p1166
128. Hartman, U., *Phys. Rev. B.*, **1991**, *43*, p2404
129. Toikka, G., Hayes, R.A., *J. Colloid Interface Sci.*, **1997**, *191*, p102
130. Larson, I., Drummond, C.J., Chan, D.Y.C., Grieser, F., *Langmuir*, **1997**, *13*, p2109
131. Tsao, Y.-H. Evans, D.F. Wennerström, H., *Science*, **1993**, *262*, p547
132. Burnham, N.A., Colton, R.J., Pollocks, H.M., *Nanotechnology*, **1993**, *4*, p64
133. Burham, N.A., Dominguez, D.D., Mowery, R.L., Colton, R.J., *Phys. Rev. lett.* **1990**, *64*, p1931
134. Toikka, G., Hayes, R.A., Ralston, J., *J. Colloid Interface Sci.*, **1996**, *180*, p329
135. Biggs, S., Spinks, G., *J. Adhesion. Sci. Technol.*, **1998**, *12*, p461
136. Reitsma, M., Craig, V.S.J., Biggs, S., *J. Adhesion*, **2000**, *74*, p125
137. Butt, H.-J., Kappl, M., Mueller, H., Raiteri, R., Meyer, W., Rühe, J., *Langmuir*, **1999**, *15*, p2559
138. Seog, J., Dean, D., Plaas, A.H.K., Wong-Palms, S., Grodzinsky, A.J. Ortiz, C., *Macromolecules*, **2002**, *35*, p5601
139. Kidoaki, S., Matsuda, T., *Col and Surf B: Biointerfaces*, **2002**, *23*, p153
140. Feiler, A., Larson, I., Jenkins, P., Attard, P., *Langmuir*, **2000**, *16*, p10269
141. Bogdanovic, G., Tiberg, F. Rutland, M.W., *Langmuir*, **2001**, *17*, p5911
142. Toikka, G., Spinks, G.M., Brown, H.R., *J. Adhesion*, **1999**, *74*, p317
143. Domke, J., Radmacher, M., *Langmuir*, **1998**, *14*, p3320
144. Considine, R.F., Drummond, C.J., Dixon, D.R., *Langmuir*, **2001**, *17*, p6325
145. Nakajima, K., Yamaguchi, H., Lee, J.-C., Kageshima, M., Ikehara, T., Nishi, T., *Jpn. J. Appl, Phys.*, **1997**, *36*, p3850
146. Tao, N.J., Lindsay, S.M., Lees, S., *Biophys. J.*, **1992**, *63*, p1165
147. Reynaud, C., Sommer, F., Quet, C., El Bounia, N., Duc, T.M., *Surface and Interf. Anal.*, **2000**, *30*, p185

148. Braithwaite, G.J.C., Luckham, P.F., Howe, A.M., *J. Colloid Interface Sci.*, **1999**, *213*, p525

149. Weisenhorn, A., Khorsandi, M., Kasas, S., Gotzos, V., Butt, H.-J., *Nanotechnology*. **1993**, *4*, p106.

150. Burnham, N., Dominguez, D., Mowery, R., Colton, R., *Phys. Rev. Let.*, **1990**, *64*, p1931.

151. Weisenhorn, A., Maivald, P., Butt, H.-J., Hansma, P., *Phys. Rev. B.*, **1992**, *45*, p11226

152. Snyder, B., Aston, D., Berg, J., *Langmuir*. **1997**, *13*, p590

153. Considine, R., Hayes, R., Horn. R., *Langmuir*. **1999**, *15*, p1657

154. Bhatt, D., Newmn, J., Radke, C.J., *Langmuir*, **2001**, *17*, p116

155. Technical Bulletin Pigments. *Degussa-Huls* **1994,** *18*, *5*

156. Yan, N., Maham, Y., Masliyah, J.H., Gray, M.R., Mather, A.E., *J. Colloid Interface Sci.*, **2000**, *228*, p1

157. Obey, T.M., Vincent, B., *J. Colloid Interface Sci.*, **1994**, *163*, p454

158. Goller, M.I., Obey, T.M., Teare, D.O.H., Vincent, B., Wegener, M.R. *Colloids and Surf. A:*, **1997**, *123*, p183

159. Thomas, J.C., *Proceedings of SPIE-The International Society for Optical Engineering 1430(Photon Correl. Spectrosc.: Multicompon. Syst.)*, **1991**, *1430*, p2

160. Barnes, T.J., and Prestidge, C.A., *Langmuir*, **2000**, *16*, p4116

161. Ware, B.E., *Adv. Colloid Interface Sci.* **1974**, *4*, p1

162. Miller, J.F., Shätzel, K., Vincent, B., *J. Colloid Interface Sci.*, **1990**, *143*, p532

163. Harkins, W.D., Brown, F.E., *J. Amer. Chem. Soc.* **1919**, *41*, p499

164. Wilkinson, M.C., Aronson, M.P., *Journal of the Chemical Society, Faraday Transactions 1*, **1973**, *69*, p474

165. Cleveland, J.P., Manne, S., Bocek, D., Hansma, P. K., *Rev. Sci. Instr.*, **1993**, *64*, p403

166. Burnham, N.A., Chen, X., Hodges, C.S., Matei, G.A., Thoreson, E.J., Roberts, C.J., Davies, M.C., Tendler, S.J.B., *Nanotech.*, **2003**, *14*, p1

167. Zang, H., PhD Thesis, University of South Australia, **2003**

168. Fleming, B.D., Wanless, E.J., *Microscopy and Microanalysis*, **2000**, *6*, p104

169. Grabbe, A., Horn, R.G., *J. Colloid Interface Sci.*, **1993**, *157*, p375

170. French, R.H., *J. Am. Ceram. Soc.*, **2000**, 83, p2117

171. Simovic, S., Prestidge, C.A., *Langmuir*, **2003**, *19*, p3785
172. Simovic, S., Prestidge, C.A., *Langmuir*, **2003**, *19*, p8364
173. Falender, J.R., Yeh, G.S.Y., Mark, J.E., *J. Chem. Phys.*, **1989**, *70*, p5324
174. Ferry, J.H., 'Viscoelastic Properties of Polymer' 3rd ed., J. Wiley, New York
175. Hartley P.G., Larson, I, Scales, P.J., *Langmuir*, **1997**, *13*, p2207
176. Binks, B.P., Dong, J., *J. Chem. Soc., Faraday Trans.*, **1998**, *94*, p401
177. Simovic, S. PhD Thesis, University of South Australia, to be published 2004
178. A-Hassan, E., Heinz, W.F., Antonik, M.D., D'Costa, N.P., Nageswaran, S., Schoenenberger, C.-A., Hoh, J.H., *Biophys. J.*, **1998**, *74*, p1564
179. Wu, H.W., Kuhn, T., Moy, V.T., *Scanning*, **1998**, *20*, p389
180. Dvorak, J.A., Nagao, E., *Exp. Cell. Res.*, **1998**, *242*, p69
181. Genieser L.H., Hendriks, K.C.P., Baaijens, F.T.P., Meijer, H.E.H., *J. Rheol.*, **2000**, *44*, p1003
182. Yim, H., Kent, M., McNamara, W.F., Ivkov, R., Satija, S., Majewski, J. *Macromolecules*, **1999**, *32*, p7932
183. Bogdanovic, G., Sennerfors, T., Zhmud, B., Tiberg, F., *J. Colloid Interface Sci.*, **2002**, *255*, p44
184. Dagastine, R.R., Prieve, D.C., White, L.R., *J. Colloid Interface Sci.*, **2004**, *269*, p84